INEEL/EXT-03-00870
Revision 1

NGNP Point Design – Results of the Initial Neutronics and Thermal-Hydraulic Assessments During FY-03

September 2003

Idaho National Engineering and Environmental Laboratory
Bechtel BWXT Idaho, LLC

INEEL/EXT-03-00870 Rev. 1

NGNP Preliminary Point Design – Results of the Initial Neutronics and Thermal-Hydraulic Assessments

Philip E. MacDonald

INEEL Prismatic Design:

James W. Sterbentz
Robert L. Sant
Paul D. Bayless
Richard R. Schultz

INEEL Pebble Bed Design:

Hans D. Gougar
Richard L. Moore
Abderrafi M. Ougouag
William K. Terry

September 2003

Idaho National Engineering and Environmental Laboratory
Idaho Falls, Idaho 83415

Prepared for the
U.S. Department of Energy
Office of Nuclear Energy, Science and Technology
Under DOE Idaho Operations Office
Contract DE-AC07-99ID13727

NGNP Point Design – Results of the Initial Neutronics and Thermal-Hydraulic Assessments During FY-03

Prepared by: Phillip E. MacDonald

Reviewed by: David Petti 9-23-03

Approved by: Tim H. Southworth 9-23-03

Acknowledgement

General Atomics submitted the Very High Temperature Gas-cooled Reactor (VHTR) concept to the Generation IV Roadmap for consideration. General Atomics' VHTR concept was based on its Gas Turbine – Modular Helium Reactor (GT-MHR) design. The Generation IV Roadmap Gas-Cooled Reactor Technical Working Group chose the VHTR as the representative high-temperature gas-cooled reactor concept for further development and demonstration. An alternative core design that could potentially be used is one that uses graphite fuel pebbles. The original information submittal to the Generation IV Roadmap about the VHTR was relatively brief. The INEEL subsequently carried out the NGNP point design work presented in this report for both the prismatic and pebble core designs to define the key parameters of these reactor concepts better. General Atomics is acknowledged for the provision of some additional technical information and analyses to more fully describe their VHTR submittal to the Generation IV Roadmap. The individuals at General Atomics that provided information included in this report are Alan M. Baxter, John M. Bolin, Malcolm P. LaBar, Matthew B. Richards, and Arkal S. Shenoy. The INEEL takes full responsibility for the results presented in this report.

Executive Summary

This report presents the preliminary preconceptual designs for two possible versions of the Next Generation Nuclear Plant (NGNP), one for a prismatic fuel type helium gas-cooled reactor and one for a pebble bed fuel helium gas reactor. Both designs are to meet three basic requirements: a coolant outlet temperature of 1000 °C, passive safety, and a total power output consistent with that expected for commercial high-temperature gas-cooled reactors. The two efforts are discussed separately below. The analytical results presented in this report are very promising, however, we wish to caution the reader that future, more detailed, design work will be needed to provide final answers to a number of key questions including the allowable power level, the inlet temperature, the power density, the optimum fuel form, and others. The point design work presented in this report provides a starting point for other evaluations, and directions for the detailed design, but not final answers.

Prismatic NGNP Design. The prismatic NGNP reactor is essentially a large graphite pile composed of hexagonal blocks. Approximately one-third of these blocks are fuel blocks arranged in an annular core with the remaining two-thirds of the blocks being graphite blocks arranged to form an inner and outer neutron reflector about the annulus. During transients, the graphite reflector mass acts as an important temporal heat sink and storage device to maintain fuel temperatures below values that may damage the fuel (i.e. temperatures above 1600 °C). The blocks are stationary during reactor operation, but at the end of each power cycle, every block can be replaced if needed, thus allowing for the ability to rebuild a new core pile at regular intervals and eliminate the material damage effects due to long-term neutron irradiation and high temperatures. The annularity of the core ensures inherent safety under transient conditions.

In the case of the fuel blocks, a fraction of the blocks will need to be replaced at regular intervals coinciding with the end of each power cycle. Actual numbers of fuel blocks replaced will depend on core reactivity, burnup requirements, and power cycle lengths, currently geared to be 18-24 months in duration in order to achieve parity with current commercial power plant fuel cycle lengths. The scope of the point design effort here, however, does not address the complex optimization issues associated with fuel management and the maximization of the uranium resource and minimization of the fuel cycle costs. This is a task reserved for FY-04. Uranium enrichments necessary to meet the projected cycle lengths are, however, estimated to be 10% for the initial core and 12-15% for subsequent reload fuel blocks.

The solid fuel and graphite blocks that compose the core provide an effective configuration to minimize neutron leakage and maximize neutron economy of the graphite pile configuration. This leads to the most compact core possible and together with the 108 straight-through cylindrical coolant channels drilled lengthwise in each fuel block allows for efficient heat transfer out of the annular core, minimal helium coolant pressure drop across the core, and a core power density on the order of 6.5 W/cc. Design approaches were identified which take advantage of the ability to control the coolant flow distribution in the prismatic core to achieve a total core power level of 600 MWt having a mixed mean core outlet coolant temperature of 1000ºC. Potentially higher prismatic core power levels (up to maybe 800 MWt) are also possible but require significantly more detailed design and analysis.

It should be noted that the prismatic NGNP is an evolutionary design with roots stemming from the Fort Saint Vrain high-temperature gas-cooled reactor design, but is directly based on the recent General Atomics Very High Temperature Gas-cooled Reactor (VHTR) submittal to the Generation IV Roadmap, which was based of their gas turbine-modular helium reactor (GT-MHR) design. Therefore, the design of the prismatic NGNP reactor has a broad experience and database to draw upon. Modifications of the GT-MHR design will be proposed in order to meet the NGNP design requirement of inherent safety and the NGNP design goal of a 1000 °C outlet helium gas temperature.

The initial INEEL neutronic evaluations corroborate the results of the previous General Atomics annular GT-MHR design. The initial core loading (first non-equilibrium cycle) achieves a 420-540 effective full power day (14-18 month) design burnup for the GT-MHR with an initial effective enrichment of 10.36 wt% U-235 uniformly distributed across the 3-ring annular core. The core also exhibits strongly negative Doppler effect and isothermal temperature coefficients of reactivity over the burnup cycle. In the event of rapid loss of the helium gas (7.12 MPa), there is negligible core reactivity change. And, water or steam ingress into the core coolant channels produces a small reactivity effect up to a water density of approximately 0.001 g/cc (18.1 Kg of H_20 in 18 million cc of coolant channels). Additional neutronic results in Section 3 further corroborate and benchmark our models relative to the GT-MHR design.

An important issue involving the performance of the fuel particles under normal operating conditions is the power peaking of the fuel rods at the annular core interfaces with the inner and outer graphite reflectors, but primarily at the inner reflector interface. Sustained reduction of this power peaking over the power cycles will improve the particle fuel performance. Fortunately for the prismatic NGNP design, there are a number of possible solutions that can effectively solve this problem. These solutions involve: (1) use of the allocated B_4C burnable poison rod locations in the fuel blocks, (2) graded particle packing fractions in the fuel rod Rows 1, 2, 3, and 4 nearest the interface, (3) graded fuel enrichments in these same Rows 1-4, (4) replacement of specific fuel rods with burnable poisons (e.g. B_4C), and (5) B_4C loaded in the graphite reflector blocks in Rings 5 and 9 near the reflector/core interfaces. The results of including B_4C burnable poison rods at the core/inner reflector interface, graded particle packing fractions in the fuel rods near the fuel/inner reflector interface, and graded enrichment in the fuel rods near the fuel/inner reflector interface are presented in this report.

Despite its larger physical size, a graphite-moderated, gas-cooled reactor is smaller neutronically than a light water reactor of the same power level, and hence is more stable against xenon-induced power oscillations. The power stability of the GT-MHR has been studied extensively, and calculations have demonstrated that the 10-block high, 600 MWt GT-MHR is stable in the axial, radial, and azimuthal directions against xenon oscillations. Studies on a 12-block high GT-MHR operating at 1250 MWt indicate that a 12-block high GT-MHR core operating up to 720 MWt should also be stable in the axial, radial, and azimuthal directions, but the stability of cores that are any longer is uncertain.

Parametric thermal-hydraulic design studies were performed using the POKE computer code. The primary purpose of these studies was to investigate design options for the prismatic NGNP that would allow (1) an outlet temperature of 1000 °C, (2) the lowest possible inlet temperature, and (3) the highest possible overall core power, while maintaining the peak fuel temperatures during normal operation at an acceptable level of about 1250 °C. (A general “rule of thumb” is that fuel performance and fission-product release in a high-temperature gas-cooled reactor will be acceptable if the peak fuel temperature remains below about 1250 °C.) The study began with an analysis of the current 600 MWt GT-MHR design operating with a coolant inlet temperature of 491 °C, an average coolant outlet temperature of 850 °C, a coolant flow rate of 320 kg/s, a bypass flow fraction of 0.2, and conventional column-by-column refueling. Two major design modifications were then evaluated: reducing the bypass flow and better controlling the inlet coolant flow distribution. Reducing the bypass flow fraction from 20 to 10% reduces peak fuel temperatures by about 50 °C and reduces coolant channel hot streaks by about 75 °C. Controlling the inlet flow distribution has an even more dramatic effect on reducing the maximum fuel temperatures and coolant hot streaks. The results indicate that a NGNP with these or other potential design modifications can have an outlet temperature of 1000 °C and fuel temperatures similar (same peak temperatures, slightly higher volumetric average temperatures) to the GT-MHR design. Also, controlling the flow distribution allows for reducing the coolant inlet temperature and coolant flow rate, such that the

operating temperature for the reactor vessel (490 °C) and the core pressure drop for the NGNP would be about the same as that for the reference GT-MHR.

Taller and higher power reactor cores were also evaluated with the POKE computer code. The power density was kept the same as that for the 10-block-high, 600-MWt core, since this parameter has a strong effect on core temperature response during accident conditions. Both 12-block-high (720 MWt) and 14-block-high (840 MWt) cores were evaluated. For the higher-powered cores, the coolant flow rate was increased in proportion to the power level, in order to maintain the same coolant temperature rise as the 600 MW_t core. It was determined that the higher-powered cores will operate with about the same fuel and graphite temperatures as the 600 MWt core.

A thermal-hydraulic model of the NGNP reactor vessel and reactor cavity has been developed at the INEEL for use with the RELAP5-3D/ATHENA computer code. The code was first benchmarked against previous high- and low-pressure conduction cooldown transient calculations performed at General Atomics for the GT-MHR. When the decay heat curve provided by General Atomics was used in the INEEL simulations of the GT-MHR high and low pressure conduction cooldown transients, peak fuel temperatures only slightly below the values reported by General Atomics were calculated. The small differences are attributed to the somewhat better convective heat transfer in the bypass regions calculated by RELAP. The code and model were then used to perform analyses of the transient response of the NGNP prismatic core design and determine the effects of core geometry on the peak reactor vessel and fuel temperatures.

Most important, sensitivity calculations were performed to determine the power that could be obtained for different core heights without exceeding a peak transient fuel temperature of 1600 °C. With a coolant inlet temperature of 490 °C and 10% nominal core bypass flow, it is estimated that the peak power for a 10-block high core is 686 MWt, for a 12-block high core is 786 MWt, and for a 14-block core is about 889 MWt. Cases were also run with no core bypass modeled, as this configuration yielded somewhat better agreement with the GT-MHR benchmark case for the low-pressure conduction cooldown transient. In these calculations, the estimated peak operating powers were 624 MWt for a 10-block core, 723 MWt for a 12-block core, and 833-MWt for a 14-block core. However, the mechanical stability of cores longer than 10 blocks high has not been studied. Fort Saint Vrain operating experience suggests that such long fuel block columns could potentially fluctuate laterally. The feasibility of laterally supporting the fuel columns between the column ends to prevent lateral column movement has not yet been determined.

Parametric analyses were also performed of the limiting temperature transient, the depressurized (low-pressure) conduction cooldown design basis event using the TAC2D computer code. The power and core temperature profiles from the POKE analysis were used as input to the TAC2D analysis. For the prismatic NGNP with 10 fuel blocks per column, TAC2D predicts that a reactor power of 621 MWt will limit the peak core temperature during a low-pressure conduction cooldown event to 1600 ºC. The peak vessel temperature found in this analysis was 529 ºC. The TAC2D results for the 12- and 14-block high cores show that the reactor thermal power can be increased to 686 and 754 MWt, respectively, while limiting the peak transient core temperature to 1600 ºC.

Computational fluid dynamics calculations are also underway to perform an initial evaluation of the temperature profile of the helium exiting the reactor via the hot duct. These calculations will ultimately show whether “hot streaking” (non-uniform high temperature regions) is present and its magnitude relative to the downstream equipment design specifications.

Pebble Bed NGNP. The pebble bed NGNP essentially consists of an annular vat filled with fuel spheres, or “pebbles,” that are dropped in at the top and removed at the bottom, so that they flow slowly through the core region. This design configuration introduces several unique advantages compared to batch

fueled reactor designs. Continuous online refueling reduces the frequency of required shutdowns. Also, the pebble bed reactor operates with very little excess reactivity, so that safety is enhanced substantially. The fuel enrichment is typically only 8%.

Pebble bed reactors of 300 MWt or less have been shown analytically to be passively safe, but the ability of a pebble bed NGNP of 600 MWt or higher to preserve passive safety had not previously been shown. The pebble bed NGNP design was developed along two parallel paths. On one path, two reactor modules of 300 MWt each supplied the desired power of 600 MWt. These modules are similar to the South African Pebble Bed Modular Reactor (PBMR), with the main differences being a slightly higher power output than the original PBMR design (268 MWt) and a higher coolant outlet temperature. In this design, a single power conversion unit receives hot helium from both reactor modules. On the other path, the feasibility of a single pebble-bed reactor module of 600 MWt was assessed. A sequence of candidate 600 MWt designs was analyzed, culminating in a configuration that meets the requirements for passive safety.

Both the 300 MWt and 600 MWt versions of the pebble bed NGNP introduce some significant innovations in pebble bed reactor design. The first of these is a pebble design tailored for the specific core configuration to give better fuel utilization and safer response to reactivity insertion events than in previous pebble bed reactors. The pebble design feature that is tailored to the specific reactor is the moderator-to-fuel ratio, which is adjusted by properly selecting the radius of the fueled zone within the pebble. This optimized pebble at least partially mitigates water ingress accidents from the neutronics standpoint; similar optimal moderation is not possible with batch-loaded reactors because the moderator-to-fuel ratio changes continuously in a batch loaded reactor as the fuel is burned. In contrast, the pebble bed reactor reaches a steady state distribution of burnup and fuel composition because of its continuous refueling. The improved fuel utilization provided by the optimized pebble leads to lower fuel costs, and it also permits the core with optimized pebbles to be smaller than a core with standard pebbles, so that reactor capital cost is reduced.

The design for the pebble bed NGNP also includes shutdown mechanisms that do not require any intervention by operators or automatic actuation; scram rods are only held out of the reactor as long as coolant flows properly and temperature remains within the prescribed range. Also, air ingress is prevented during accidents by nitrogen that is only kept out of the reactor vault when the pressure in the vault remains between prescribed limits. Nitrogen injected into the vault during accidents (when the vault pressure limits are exceeded) would also improve vault cooling. Also, a new system for examining pebbles removed from the core, developed elsewhere, will be applied to eliminate almost completely the inventory of pebbles awaiting recirculation.

Passive safety is the result of adequate heat removal in accident scenarios. The pebble bed NGNP is shown to possess ample thermal reactivity feedback to shut the reactor down with only a 100 °C temperature increase, for reactivity insertion events including water ingress accidents. Then the only heat removal required is the post-shutdown decay heat. Thermal analysis of the incrementally uprated 300 MWt design shows that conduction and radiation heat transfer are adequate to remove decay heat in a loss-of-coolant accident without exceeding prescribed temperature limits. To achieve the same passive safety in the 600 MWt design, the annular core was made somewhat narrower and taller (9.0 m versus 8.5 m in height). Most important, so that the core dimensions did not have to become much larger, the power density was significantly increased (4.92 versus 3.87 W/cm^3).

A number of important plant licensing issues were addressed in the pebble bed NGNP design project. Previous work analyzed the effects of changes in pebble packing, as might be caused by earthquakes. It was shown that thermal feedback effects can be expected to overcome the reactivity insertions from such changes in pebble packing. In the present work, an analysis was performed of the potential for hot spots to develop from random collections of high-power pebbles in regions of high thermal neutron flux. It was

found that such hot spots would lead to maximum peak temperatures unlikely to cause fuel damage even during a loss-of-coolant accident. The likelihood for such hot spots to form randomly is extremely low (with the worst cases having infinitesimally small probability of occurrence). As noted above, the optimized pebble design mitigates the potential for reactivity insertions caused by water ingress. Previous studies are cited to argue that air ingress will not lead to fuel damage. Nuclear-weapons proliferation issues have also been assessed in previous work; it was shown that the pebble-bed reactor is a very poor choice for proliferation.

In summary, two versions of an annular pebble bed NGNP have been developed, one using two modules of 300 MWt each, and the other using one module of 600 MWt. These reactors employ several innovative features to enhance safety, economy, and ease of licensing.

Blank Page

Contents

1. Introduction

In the coming decades, the United States, the other industrialized countries, and the entire world will need energy supplies and an upgraded energy infrastructure to meet growing demands for electric power and transportation fuels. The Generation IV Roadmap project identified reactor system concepts for producing electricity, which excelled at meeting the goals of superior economics, safety, sustainability, proliferation resistance, and physical security.[1] One of these reactor system concepts, the Very High Temperature Gas Cooled Reactor System (VHTR), is also uniquely suited for producing hydrogen without the consumption of fossil fuels or the emission of greenhouse gases. DOE has selected this system for the Next Generation Nuclear Power (NGNP) Project, a project to demonstrate emissions-free nuclear-assisted electricity and hydrogen production by 2015.

"Hydrogen holds the potential to provide a clean, reliable, and affordable energy supply that can enhance America's economy, environment, and security."[2] The U.S. hydrogen industry currently produces nine million tons of hydrogen per year[a] for use in chemicals production, petroleum refining, metals treating, and electrical applications, and the current use is experiencing rapid growth as more and more hydrogen is used to convert the lower-cost Western hemisphere heavy crude oils to gasoline. With a larger supply of hydrogen, the production of liquid fuels per barrel of oil could be increased by up to 15%, which would significantly reduce our imported crude oil.

Although hydrogen is the most abundant element in the universe, it does not naturally exist in large quantities or high concentrations on Earth. Steam methane reforming accounts for more than 95% of the current hydrogen production in the U.S. Unfortunately, steam methane reforming diverts valuable natural gas from home heating uses[b] and releases large quantities of carbon dioxide into the atmosphere. A much more environmentally friendly method of producing hydrogen would be to crack water at high temperatures using nuclear heat, and the current growth in hydrogen demand is already sufficient to justify the development of such methods. As efficient fuel cells are developed and the transportation sector is revolutionized,[c] the worldwide demand for hydrogen will eventually rival that for electricity. Given these additional needs, it is appropriate to start the development of nuclear energy systems designed for large-scale production of hydrogen.

1.1. Mission Objectives

- Demonstrate a full-scale prototype NGNP by the year 2015
- Demonstrate high-temperature Brayton Cycle electric power production at full scale
- Demonstrate nuclear-assisted production of hydrogen (with about 10 % of the heat)
- Demonstrate by test the exceptional safety capabilities of the advanced gas-cooled reactors
- Obtain an NRC License to construct and operate the NGNP, to provide a basis for future performance-based, risk-informed licensing
- Support the development, testing, and prototyping of hydrogen infrastructures such as refueling stations, the "Freedom Car" initiative, petrochemical extension, heavy crude oil or tar sands 'sweetening', and other industrial hydrogen applications

[a] Nine million tons of hydrogen per year is enough to fuel 20 to 30 million fuel cell cars, or enough to power 5 to 8 million homes.

[b] Hydrogen production currently uses 5% of the natural gas consumed in the United States.

[c] The first production fuel cell vehicles may be sold within a decade, and a hydrogen economy will be a significant enterprise within several decades.

1.2. Brief Project Description

The NGNP reference concept will be a helium-cooled, graphite moderated, thermal neutron spectrum reactor with a design goal outlet temperature of 1000 °C or higher. The reactor core could be either a prismatic graphite block type core or a pebble bed core; the final selection of a reference core concept will be made following completion of the preconceptual designs for each. The NGNP will produce both electricity and hydrogen. The process heat for hydrogen production will be transferred to the hydrogen plant through an intermediate heat exchanger (IHX). The reactor thermal power and core configuration will be designed to assure passive decay heat removal without fuel damage during hypothetical accidents. The fuel cycle will be a once-through very high burnup low-enriched uranium fuel cycle.

The basic technology for the NGNP has been established in former high-temperature gas-cooled reactor plants (DRAGON, Peach Bottom, AVR, THTR, Fort St. Vrain). In addition, the technologies for the NGNP are being advanced in the Gas Turbine-Modular Helium Reactor (GT-MHR) Project, and the South African state utility ESKOM sponsored project to develop the Pebble Bed Modular Reactor (PBMR). Furthermore, the Japanese HTTR and Chinese HTR-10 projects are demonstrating the feasibility of some of the planned NGNP components and materials. (The HTTR is expected to reach a maximum coolant outlet temperature of 950 °C.) Therefore, the NGNP project is focused on building a demonstration reactor, rather than simply confirming the basic feasibility of the concept.

One or more technologies will use heat from the high-temperature helium coolant to produce hydrogen. The first technology of interest is the thermochemical splitting of water into hydrogen and oxygen. There are a large number of thermochemical processes that could produce hydrogen, the most promising of which are sulfur-based and include the sulfur-iodine, hybrid sulfur-electrolysis, and sulfur-bromine processes (which operate in the 750 to 1000 °C range). The second technology of interest is thermally assisted electrolysis of water. The high efficiency Brayton cycle enabled by the NGNP may be used to generate the hydrogen from water by electrolysis. The efficiency of this process can be improved by heating the water to high-temperature steam before applying electrolysis.

The NGNP is the nearest term of the six reference Generation IV Roadmap reactor concepts.[1] It is envisioned that a deliberate and focused program of research and development in support of a disciplined design and construction project could make a demonstration NGNP, with a small-scale hydrogen production system, operational by 2015. The significant advantages of high fuel burnup, passive safety, low operating and maintenance cost, and potential modular construction were evident in the Generation IV submitted concepts. The final design of the demonstration NGNP will be constrained to maintain these advantages.

1.3. Purpose and Outline of this Report

This report presents the preliminary preconceptual point designs for two possible versions of the NGNP, a prismatic core NGNP and a pebble bed NGNP. The primary purpose of this work is to

1) Identify the bounding conditions for future reactor design (reactor vendor and/or architect engineer preconceptual design)
2) Identify the temperatures, pressures, and fluences needed for materials selection and qualification.
3) Establish reactor safety requirements (identify the conditions that should be considered for reactor safety/licensing).

4) Provide the background and identify the analytical tools, benchmarking exercises, and separate effects verification experiments needed for the INEEL's future design verification activities.

Section 2 presents more detailed descriptions of the GT-MHR and PBMR designs since these were our starting points for the NGNP designs. Section 3 presents the results of the preliminary neutronic design of the prismatic version of the NGNP. Section 4 presents the results of the thermal-hydraulic safety analyses of the prismatic version of the NGNP. Section 5 presents the neutronic and thermal-hydraulic design of the pebble bed version of the NGNP.

Both versions of the NGNP will supply helium coolant at a pressure vessel outlet temperature of 1000°C, in order for the hot helium to be usable for thermal-chemical or electrolysis splitting of water into hydrogen and oxygen. Both versions will be passively safe. And, both versions should supply at least 600 MWt of power. The last of these requirements is based on a desire to make the plant as economically competitive as possible.

This report is a revision of the report issued in July of 2003. Chapters 1 and 2 remain essentially the same as before. However, Chapter 3 has been revised starting with Section 3.4.10. Section 3.4.10 was expanded to include a discussion of three different temperature coefficients of reactivity: 1) isothermal, 2) fuel Doppler, and 3) moderator. Section 3.4.11 (fuel rod power peaking) was also expanded to discuss not only the reduction in fuel rod power peaking in the prismatic version of the NGNP expected when discrete burnable poison rods are loaded into the fuel bundle locations next to the inner reflector, but also the reduction in fuel rod power peaking expected when the fuel particle packing fraction and uranium enrichment in the fuel rods in the locations nearest the fuel/inner reflector interface are appropriately adjusted. Section 3.4.12 is a new section that presents the INEEL calculations of the decay heat expected after shutdown of a high-temperature gas-cooled reactor. Section 3.5 is also a new section that discusses the power stability of high-temperature gas-cooled reactor as a function of their length. This section, which was prepared at General Atomics, does not present new analyses, but rather reviews all of the past work on the subject at General Atomics.

Chapter 4 (thermal-hydraulic design of the prismatic version of the NGNP) has been almost entirely rewritten. We now present steady-state neutronic and thermal-hydraulic analyses from General Atomics that determine the allowable inlet and outlet temperatures of the NGNP. We also present revised low-pressure conduction cooldown (loss-of-coolant accident) calculations from both the INEEL and General Atomics that set the maximum allowable core power as a function of core height for the NGNP.

Chapter 5 has also been extensively revised and new optimization calculations are presented that indicate that a 700 MWt pebble bed version of the NGNP may be possible.

The analytical results presented in this report are very promising, however, we wish to caution the reader that future, more detailed, design work will be needed to provide final answers to a number of key questions including the allowable power level, the inlet temperature, the power density, the optimum fuel form, and others. The point design work presented in this report provides a starting point for other evaluations, and directions for the detailed design, but not final answers.

2. Reactor Description

As mentioned above, the NGNP will be an extension of previous high-temperature gas-cooled reactor plant designs, taking advantage of the prior engineering design and technology development work already completed. One of the most mature designs in the high-temperature gas reactor family is the 600 MWt GT-MHR design being developed in the joint NNSA-MINATOM (Russia) program for disposition of excess weapons-grade plutonium, and that is the design we have chosen to use as the starting point for our neutronic and thermal-hydraulic design work for the prismatic version of the NGNP.[3] It was initially developed as the U.S. DOE/General Atomics (GA) concept, and subsequently refined by the Russians through the preliminary design stage. Current activities include work on the final design and extensive research and development testing of various components. The GT-MHR plant is described in Section 2.1.

The ESKOM-developed PBMR design discussed in Section 2.2 provided the starting point for the 300 MWt pebble-bed NGNP point design described in Chapter 5. The inner reflector and fuel pebble design were modified to achieve improved fuel economy and safety with the higher coolant temperature. The 600 MWt pebble bed design has the same general characteristics but features a larger pressure vessel.

Some of the key differences between the current GT-MHR and/or PBMR designs and the NGNP are discussed in Section 2.3. The NGNP fuel is described in Section 2.4.

2.1. GT-MHR Plant Description

The key operating parameters for the GT-MHR are listed in Table 1 along with the operating parameters for the Fort St. Vrain high-temperature gas reactor, the largest and most recent gas-cooled reactor to operate in the U.S.[3]

Table 1. Key operating parameters for the GT-MHR and the Fort St. Vrain HTGR.

Condition or Feature	Fort St. Vrain HTGR	GT-MHR
Power Output [MW(t)]	841	600
Average power density (w/cm^3)	6.3	6.5
Coolant @ Pressure (MPa / psia)	Helium @ 4.83 / 700	Helium @ 7.12 / 1032
Moderator	Graphite	Graphite
Core Geometry	Cylindrical	Annular
Safety Design Philosophy	Active Safety Sys	Passive
Plant Design Life (Years)	30	60
Core outlet temperature (°C)	785	850
Core inlet temperature (°C)	406	488
Fuel – Coated Particle	HEU-Th/ ^{235}U (93% enriched)	LEU
Fuel Max Temp – Normal Operation (°C)	1260	1250
Fuel Max Temp – Emergency Conditions (°C)	NA - Active Safety System cools fuel.	1600

Figure 1 shows the GT-MHR reactor system and power conversion system within the reactor building. The plant is designed for a 60-year life with a capacity factor of at least 80%. Passive safety is achieved by designing for a core cool-down during a postulated loss-of-coolant accident that limits the peak fuel temperatures to 1600 °C. This is accomplished by conducting the decay heat radially through the core and pressure vessel and then radiating it to passive air-cooled panels in the reactor cavity building. High temperature concrete is not needed for the reactor building because of the cooling panels. There is also a non-safety shutdown cooling system (SCS) used only to remove decay heat during normal shutdowns, such as during refueling operations.

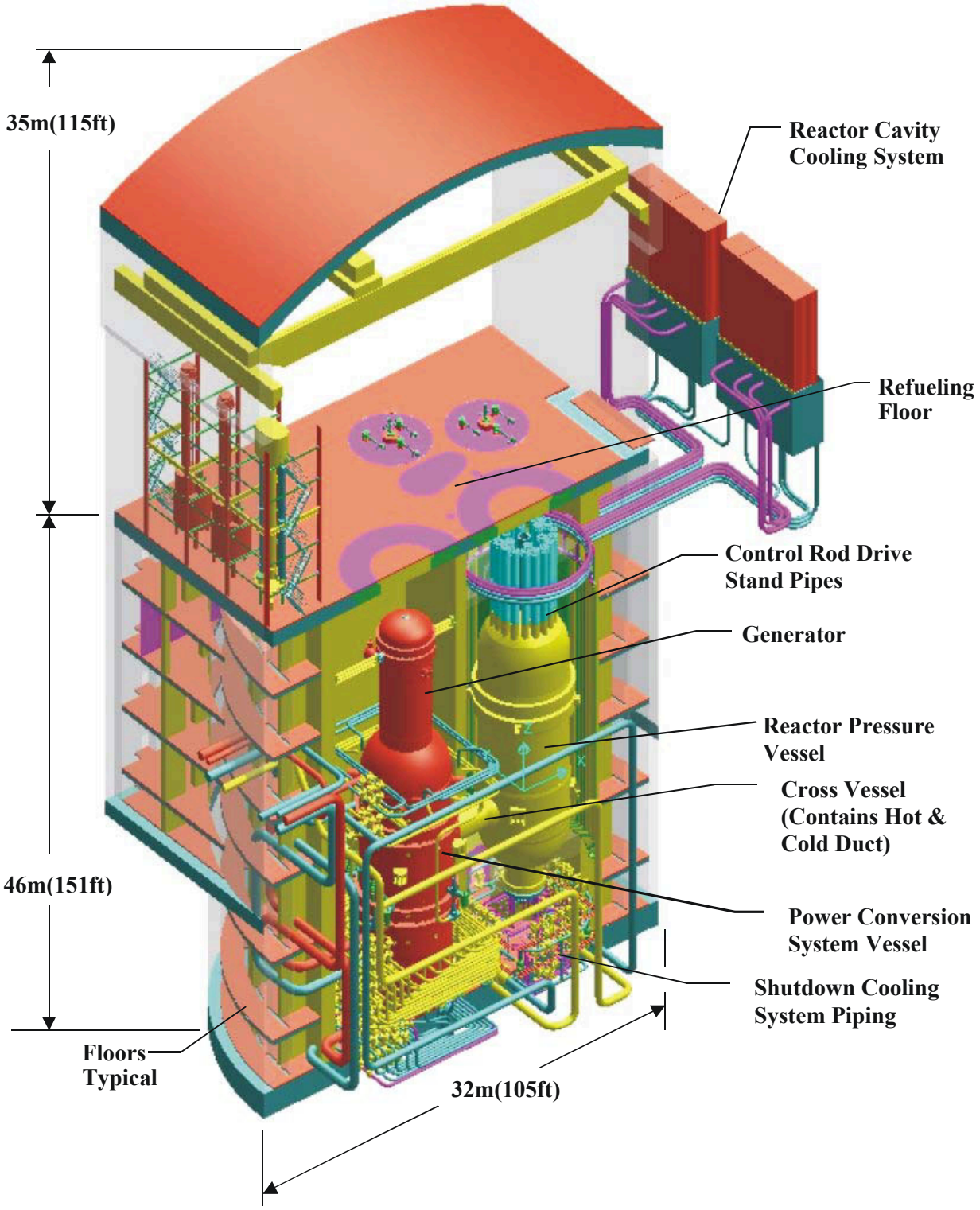

Figure 1. GT-MHR reactor building cutaway showing the arrangement of the reactor and power conversion systems.

The entire reactor confinement structure is underground. The reactor vessel and power conversion vessel are side-by-side and connected by a cross-vessel that is deliberately made as short as possible to minimize thermal expansion differences between the two large vessels. The core exit hot gas flows in the central channel (duct) located along the centerline of the cross-vessel to the turbine inlet. The reactor inlet gas flows in an annular channel between the center hot duct and the cross vessel to the reactor inlet. The power conversion vessel is set somewhat lower than the reactor pressure vessel to prevent natural circulation of hot gases into the power conversion vessel during a loss-of-flow accident (station blackout).

Figure 2 is a cutaway view of the reactor vessel showing more details of the inside of the core. The core consists of graphite blocks with an annular-fueled region surrounded by reflector elements. The fuel is TRISO coated fuel particles embedded in graphite compacts and placed in graphite prismatic blocks. The center of the core is a non-fueled graphite reflector. Normal operating maximum fuel temperatures do not exceed 1250 °C. The reflectors mitigate the high-energy fluxes, and boron pins placed in the outer reaches of the reflectors reduce thermal neutron fluxes on the metallic internals structures and reactor vessel.

From the cross-vessel, the reactor helium inlet coolant (~500 °C and ~7 MPa) flows upward in the annulus between the reactor pressure vessel and the metallic core barrel surrounding the side reflector. Hence it is a major determinant of the vessel operating temperature. The coolant then enters the upper plenum region volume, which contains the lower parts of the control rod housings. The reactor pressure vessel upper head is protected by fibrous "Kaowool" insulation blankets supported by high-temperature metallic plates. The insulation protects the head from hot plumes that could occur during a pressurized loss-of-forced-convection (P-LOFC) accident.

The inlet flow then passes down through the core's upper support elements, which are made of carbon-carbon composite material that must also withstand the hot gases in a long-term P-LOFC. The coolant then flows primarily into the coolant channel holes in the fuel elements. Some of the flow bypasses these channels, passing through the gaps between the fuel elements and reflector blocks. Thus the temperature rise of the coolant in the various flow paths through the core varies over a wide range. The coolant in the fuel element channels with the highest local power peaking is quite hot whereas the coolant in the relatively unheated gaps adjacent to the cooler reflectors remains near the inlet temperature. Since the average temperature rise through the core is ~350 °C, good mixing of the outlet coolant is needed to avoid excessive thermal stresses in the downstream components resulting from large temperature gradients and fluctuations, and to assure that the gas entering the turbine has a uniform mixed mean temperature of 850 °C. Various design options are available to mitigate the effects of these perturbations.

The reactor vessel operates at a maximum through-wall average temperature of 440°C during normal operation and reaches about 550 °C during a conduction cooldown event. The core's fuel elements and graphite reflectors, plus the control rods and housings and the shutdown ball channels are all non-metal, capable of withstanding the prescribed maximum core temperatures (~1600°C) or higher in the design-limiting loss-of-coolant accident.

The "Hot Duct" assembly is composed of a structural duct separating the core entrance gas from the core exit gas, and an insulation assembly on the inside surface of the structural duct to protect it from direct contact with the 850 °C core exit gas. The structural duct is subjected to the core pressure drop as an external pressure load on a cylinder. The insulation assemblies are designed to be remotely removed and replaced if needed during the 60-year plant life.

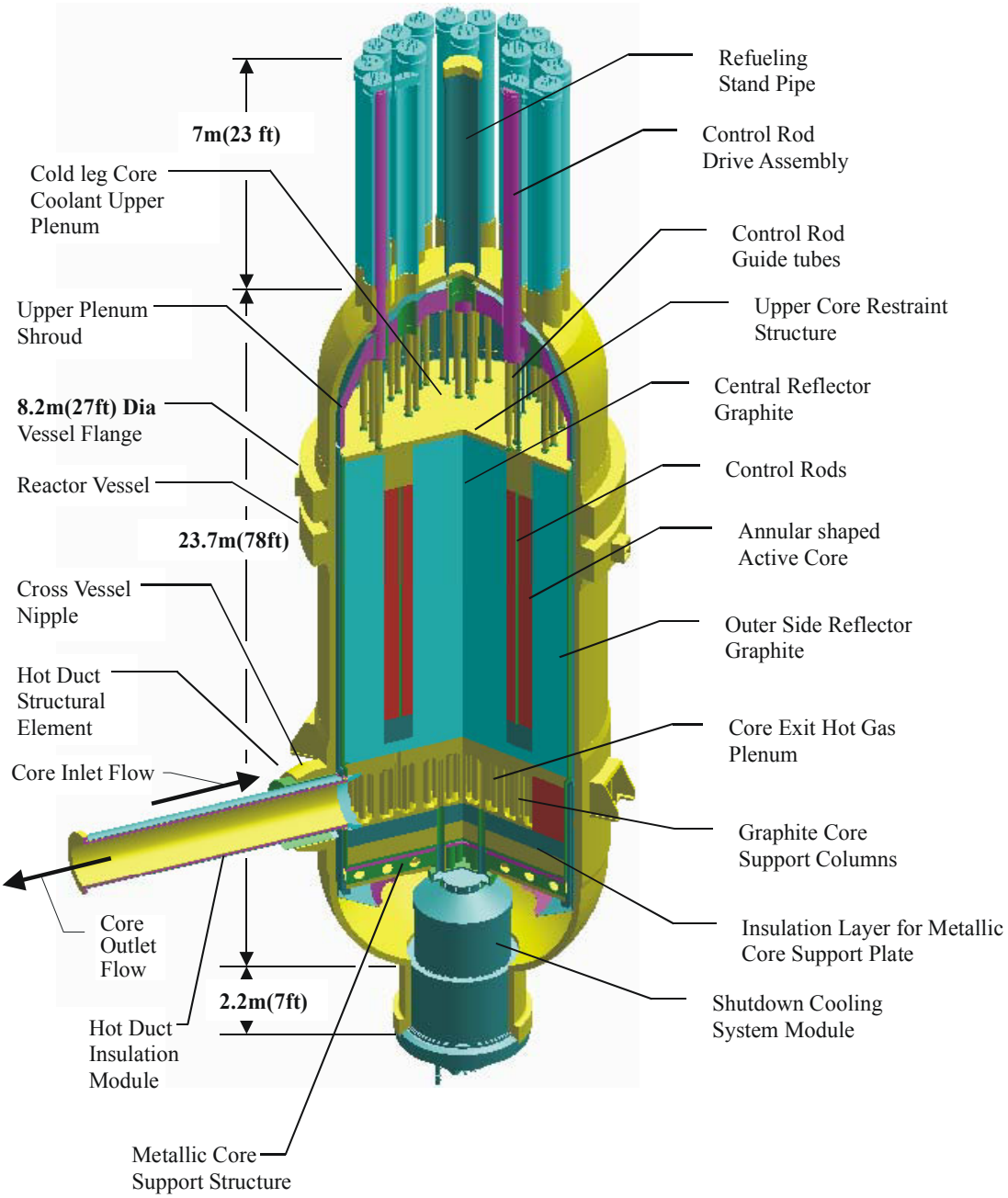

Figure 2. GT-MHR reactor system cutaway showing the metallic internals structures, core, control rod guide tubes, and shutdown cooling system.

Between the core exit plenum and the bottom metallic core support plate is an insulation layer ~1.2 meters thick. It is composed of a meter of nuclear graphite and 200 mm of carbon-carbon composite blocks. This combination of materials and thickness drops the temperature from 850 °C (core outlet temp) to ~510 °C on the top of the core support plate and ~490 °C on the bottom.

Below the bottom metallic core support is the SCS module shown in Figure 3, used to remove decay heat from the core during normal shutdowns. It is not a safety system. It contains a water-cooled heat exchanger and a motor driven circulator. It can be removed and replaced for maintenance. The high-temperature thermal insulation in the upper gas collector plenum will need to be upgraded to withstand the 1000 °C core outlet temperature of the NGNP.

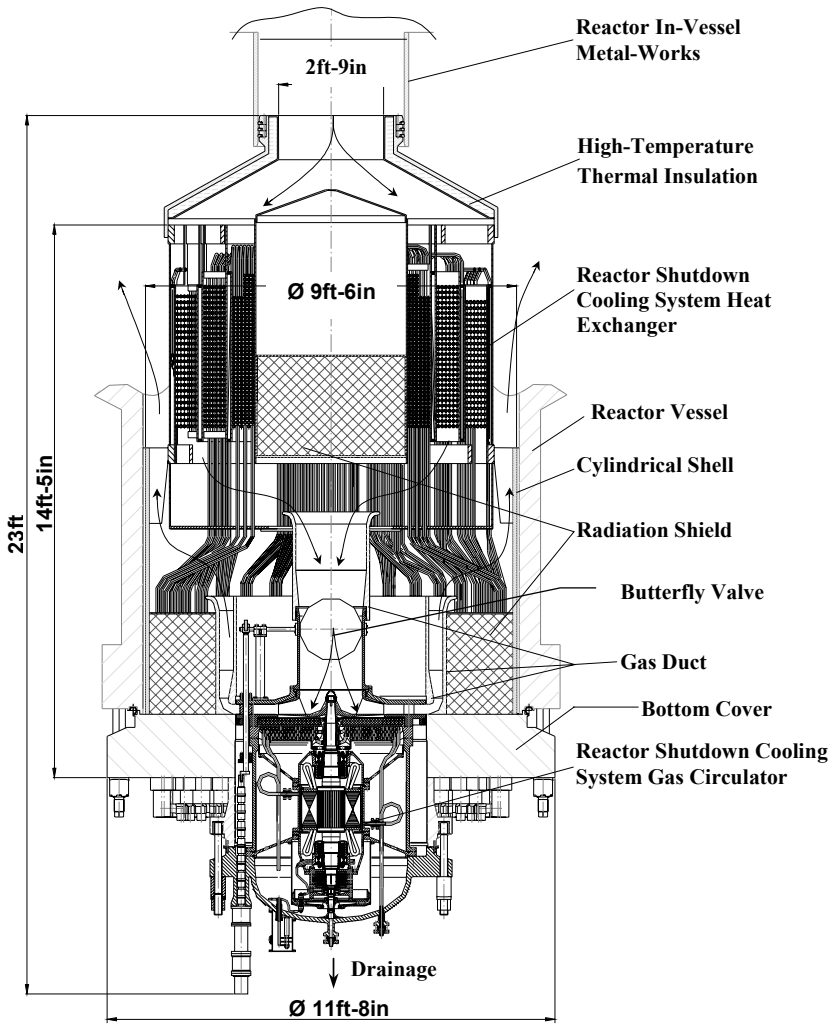

Figure 3. Cross-section of the GT-MHR shutdown cooling system.

The power conversion unit is shown in Figure 4. It is a direct (Brayton) cycle vertical single shaft axial flow gas turbine. The compressor is a two-stage compressor with a pre-cooler and an intercooler. Hot gas from the reactor enters the turbine from the hot duct. The turbine inlet volute is designed as an insulated structure like the hot duct. High temperatures are experienced by the turbine's first few stages, the turbine inlet structure, and the recuperators. All the other power conversion unit structures operate at relatively low temperatures. Gas exiting the turbine is passed through the recuperators to raise the core inlet coolant temperature to ~500 °C. The generator is contained within the primary helium coolant.

In the power conversion unit, the turbine blades and disks operate at temperatures that are similar to those of many modern air turbines that have no or only limited blade cooling. Some modern combustion turbines are operated with considerably higher inlet gas temperatures, but provisions are made to provide cooling to the blades and disks to maintain their material temperatures within acceptable ranges. The GT-MHR power conversion unit turbine has the potential benefit of being subjected to relatively clean, pure helium as opposed to the air and combustion products that a combustion turbine has to withstand. Therefore, the GT-MHR turbine lifetime could turn out to be longer than the average lifetime of 6 years for modern combustion turbines. Some components (e.g., the recuperators) must also withstand very rapid and severe temperature transients when the bypass valves operate to prevent generator runaway in a sudden loss of electrical load event.

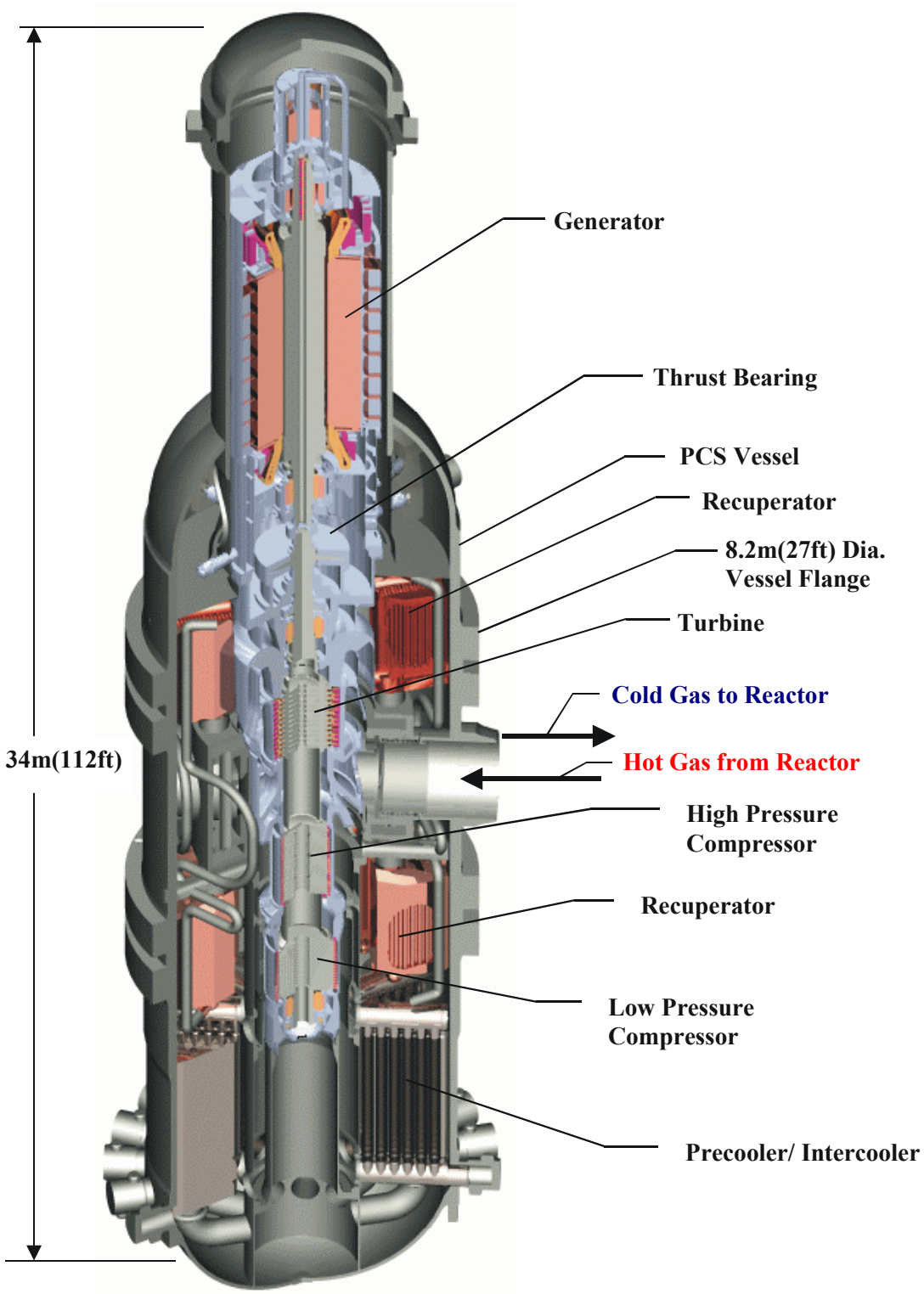

Figure 4. GT-MHR power conversion unit cutaway showing the turbomachinery: turbine, compressors, recuperators, intercooler/precooler, and generator.

2.2. Pebble Bed Reactors

Using the particle fuel concept invented in the U.S., R. Schulten proposed the alternative concept of the pebble-bed high-temperature gas-cooled reactor in the late 1950's. Design and construction began on the *AVR* (Arbeitsgemeinshaft Versuchs Reaktor) in Germany with initial criticality in 1967. The success of the AVR led to larger pebble-bed designs and the construction of the *THTR* (Thorium HochTemperatur Reaktor). This thorium-fueled power plant ran from 1986 until 1988 when, during a planned maintenance outage, some bolt heads from the hot duct cover plates were found inside the gas ducts. In isolation such a technical setback would not have prevented eventual restart but the combination of public safety concerns (Chernobyl was still a recent memory) and the growing strength of the PWR in Germany led to the decision not to restart. Photographs of the AVR (left) and THTR (right) are shown in Figure 5 (from Reference 4).

Figure 5. AVR and THTR.

In the mid-1980s, Frewer and Keller proposed a modular pebble-bed reactor concept (the *HTR-Modul-200*) that has formed the basis for subsequent PBR designs.[5] The modular pebble-bed core is a cylindrical vat constructed from graphite blocks that contains upwards of 450,000 pebbles. Some designs feature an inner reflector made of solid graphite or a bed of graphite pebbles. Each fuel pebble contains between 10,000 and 15,000 particles for a total, depending upon the design, of seven to nine grams of low-enriched uranium (LEU). The pebbles are randomly packed in the vessel with a packing density that varies between 0.61 and 0.64. Helium gas is blown in from the top and is forced through the packed bed to carry off heat. A sketch showing the HTR-Modul-200 plant layout is shown in Figure 6.

Reactor control is achieved with control rods inserted into the outer reflector. The small diameter of the modular pebble bed results in sufficient reactivity worth of these radial absorbers so that in-core poisoning is not necessary. A secondary shutdown system (KLAK) consisting of absorber balls blown into reflector channels is also available but these are not used for power shaping or ramping. Load following is also achievable through manipulation of the helium inventory of the primary loop.

In the cold shutdown mode, the reactivity is greater than at operating temperature. Calculations have not been performed for the pebble bed NGNP to determine the required (negative) reactivity insertion to hold the reactivity down in the cold shutdown mode. In early PBMR designs that proposed cylindrical (instead of annular) cores, it was not possible to insert enough negative reactivity with control rods in the outer reflector region if the core power was more than about 300 MWt. In the pebble bed NGNP, however, the

core is annular and the inner reflector is solid. This configuration will permit control rod insertion in the inner reflector, where the importance of thermal neutrons is greatest.

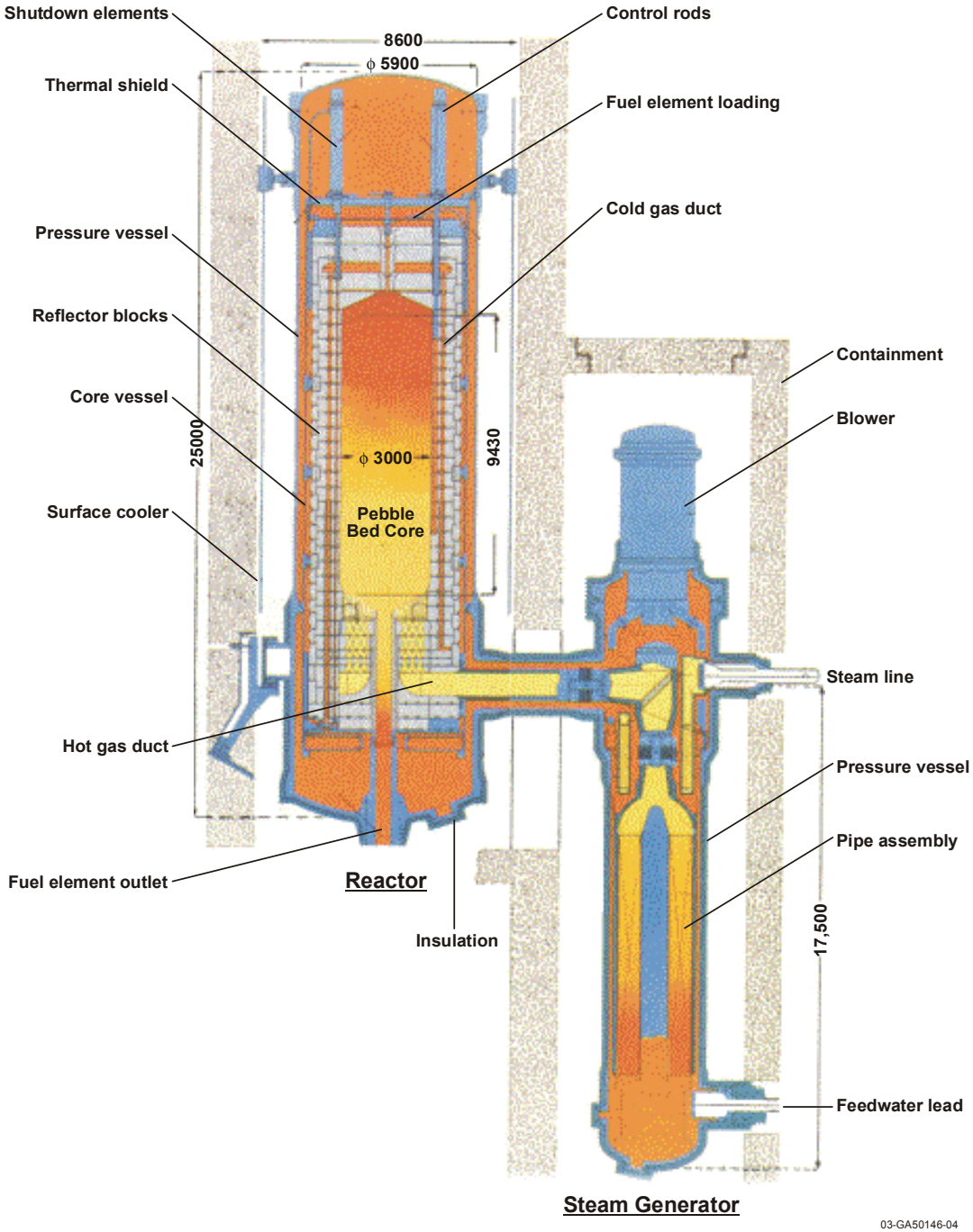

Figure 6. Plant layout for the HTR-Modul-200 high-temperature gas-cooled pebble bed reactor (Kraftwerk Union).[4]

The South African state utility ESKOM is engaged in an effort to develop the PBMR, a variant on the HTR-Modul-200. Figure 7 shows an isometric of the PBMR reactor pressure vessel and power conversion system.

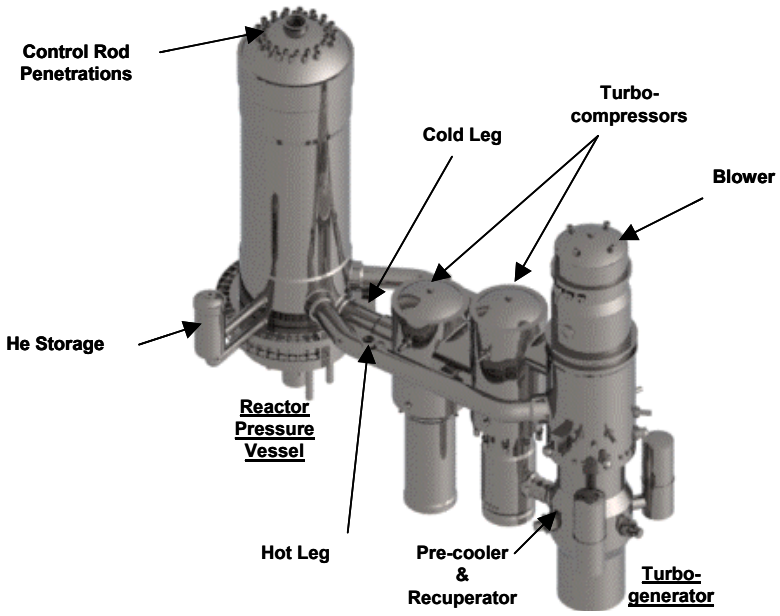

Figure 7. PBMR pressure vessel and power conversion system[d].

Table 2 contains a comparison of the more important core parameters in the HTR Modul-200 and the current PBMR design concept. The current PBMR design is rated at 400 MWt (160MWe) and features a solid inner reflector rather than one made of pebbles. This improves heat transfer in the core by limiting coolant flow through the inner reflector.

Table 2. Key parameters for two PBR designs.

	HTR-Modul-200	PBMR
Thermal Power (MWt)	200	400
Electric Power (MWe)		165
Core Diameter (m)	3.0	3.7
Core Height (m)	9.4	9.0
Inner Reflector Diameter (m)	None	~1.75m (solid graphite)
Mean Power Density (W/cm^3)	3.0	3.25
Number of Fuel Pebbles	360000	330000
System Pressure (MPa)	6	7.0
Helium Temperature (°C inlet/outlet)	250 / 700	500 / 900
Number of control rods	6	6
Number of Absorber ball systems	18	18
Average No. of Passes per Pebble	15	10
No. of Particles per Pebble	11200	15000
Heavy Metal Loading (g/pebble)	~7	~9
Enrichment	7%	8%
Discharge Burnup (MWd/kg)	80	80
Fuel Residence Time (days)	~1000	~850
Pressure Vessel Height (m)		22
Pressure Vessel Diameter (m)		8.2
Pressure Vessel Thickness (cm)		12-22

[d] Courtesy of the PBMR(Pty.), Ltd. (www.pbmr.co.za)

The PBMR uses the direct Brayton cycle power conversion system shown in Figure 8. Two turbocompressors and a turbogenerator are driven on their own shafts by the primary coolant. About 330,000 pebbles consisting of up to 9 grams of 8% LEU are packed into a core annulus and recirculated until they each reach a burnup of 80 MWD/kg after about 10 passes through the core. The PBMR modules shown in Figure 9 can be added incrementally to a generating station as the energy demands of the customer increases.

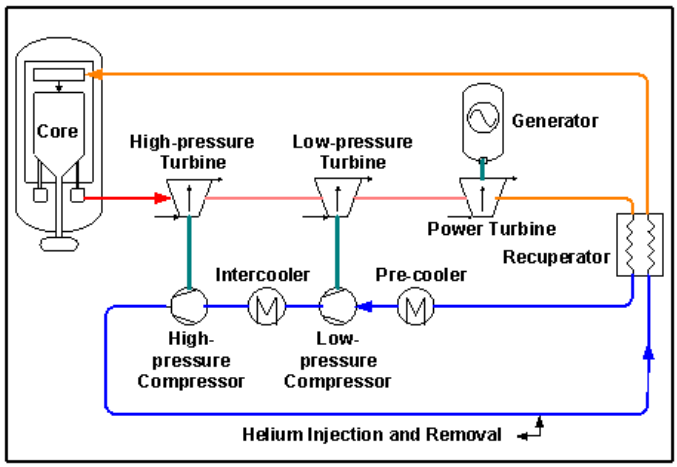

Figure 8. PBMR Power Conversion Cycle.

Recirculating fuel is a common feature of the German and South African designs. The fuel handling mechanism for such concepts is unique to the pebble bed and requires on-line burnup instrumentation at the point of discharge. The Germans demonstrated successful fueling operations, claiming that no more than 3% of the AVR outage time resulted from problems with the fuel handling system.[6] However, not all pebble-bed designs feature moving fuel. The Dutch firm NRG has designed a 40 MWt pebble-bed with stationary fuel, burnable poisons, and a higher enrichment (~20%). The core is designed for long-life (>10 years).[7]

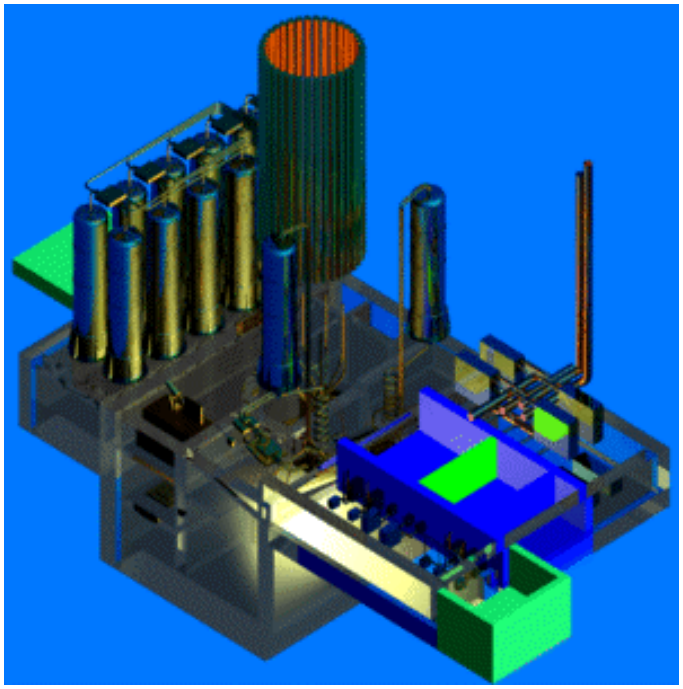

Figure 9. PBMR module.

2.3. NGNP Incremental Design Changes

The gas turbine version of the prismatic NGNP will probably be very similar to the current GT-MHR design; the differences between the NGNP and the current GT-MHR design will be mainly in the materials needed in the reactor and power conversion systems and in the details of the core neutronics and thermal-hydraulics. (Although, versions of the NGNP with somewhat higher cores and greater powers are also being considered.) Table 3 lays out the expected operating conditions and identifies the expected materials of construction and other important features of the prismatic version of the *demonstration* NGNP and provides direct comparisons with the GT-MHR and the Fort St. Vrain reactor designs. Note that the higher outlet temperature is achieved through thermal-hydraulic optimization of the core, not by means of a raise of the fuel operational and accident temperature limits.

Table 3. Comparison of NGNP operating conditions and features with GT-MHR and Fort St. Vrain.

Condition or Feature	Fort St. Vrain HTGR	GT-MHR	NGNP
Power Output [MW(t)]	841	600	600 to 800 (depends on core height)
Average power density (w/cm^3)	6.3	6.5	6.5
Coolant @ Pressure (MPa / psia)	Helium @ 4.83 / 700	Helium @ 7.12 / 1032	Helium @ 7.12 / 1032
Moderator	Graphite	Graphite	Graphite
Core Geometry	Cylindrical	Annular	Annular
Safety Design Philosophy	Active Safety Sys	Passive	Passive
Plant Design Life (Years)	30	60	60
Core outlet temperature (°C)	785	850	1000
Core inlet temperature (°C)	406	488	490
Fuel – Coated Particle	HEU-PyC/SiC Th/ ^{235}U (93% enriched)	LEU-PyC/SiC	a) LEU-PyC/SiC b) LEU-PyC/ZrC
Fuel Max Temp – Normal Operation (°C)	1260	1250	a) ~1250 (SiC coated) b) ~ 1400 (ZrC coated)
Fuel Max Temp – Emergency Conditions (°C)	Active safety system cools fuel.	1600	a) 1600 b) TBD
Fuel Element Design	Particles disbursed in carbon rods 0.5 in. dia x 1.95 in. long placed inside large graphite blocks.	Particles disbursed in carbon rods 0.5 in. dia x 1.95 in. long placed inside large graphite blocks.	Modified GT-MHR design to reduce fuel rod linear heat rate.
Control Rods	Inconel structure containing B_4C compacts.	Carbon-carbon/ Graphite Structure containing B_4C Compacts.	Carbon-carbon/ Graphite Structure containing B_4C Compacts.
Backup Reactivity Control System	B_4C pellets dropped in core	SiC coated B_4C balls dropped in core	SiC coated B_4C balls dropped in core.
Core Inlet Gas Plenum	-Metallic upper core support. -Metallic control rod guide tubes. -Ceramic fiber/metallic plate insulation. -Boronated graphite shielding.	-Carbon-carbon composite upper core support. -High-temp metallic control rod guide tubes. -Ceramic fiber/high-temp metallic plate insulation. -Boronated graphite shielding.	Modified GT-MHR design: -Carbon-carbon composite upper core support. -Carbon-carbon composite control rod guide tubes. -Ceramic fiber/hi-temp metallic plate insulation. -Boronated graphite shielding.
Core Outlet Gas Collector Plenum	Graphite structures with metal covered ceramic fiber and ceramic block insulation. Water-cooled pressure vessel liner.	Graphite structures with graphite and C/C composite insulation.	Requires some modification of the GT-MHR system with possibly more insulation.
Hot Gas Duct	Inconel plates over ceramic fiber insulation mats.	High-temp steel structure with nickel-base alloy sheets containing ceramic fiber mats.	Requires some modification of the GT-MHR system. Specifically, the cover plates may need to be a C/C composite material.
Reactor Internals structures	Medium-temp steel plate rolled into cylinder	High-temp steel sheets & plates fabricated into cylinders and plate.	The upper plenum and some of the other internals insulation material may need to be changed.
SCS heat exchanger entrance structures and tubes	Inconel plates over ceramic fiber insulation mats.	Nickel base alloy sheets containing ceramic fiber mats. High-temp steel tubes.	Requires high temperature insulation.

Condition or Feature	Fort St. Vrain HTGR	GT-MHR	NGNP
Primary Coolant Gas Circulator	Axial flow-Steam turbine drive: -9550 RPM -Press Rise = 0.097 Mpa/ 14 psi -Inlet temp = 395 °C/ 742 °F	Single shaft Axial flow Gas Turbine with 2 stage axial flow inter-cooled compressor: -Press Rise = 4.69 MPa/ 680 psi -Inlet temp = 26 °C/ 79 °F -Outlet temp = 110 °C/ 230 °F	Extend GT-MHR turbo-machine to 1000 °C turbine inlet temperature or, for hydrogen production, a motor driven axial flow circulator at core inlet conditions (in the vessel with the IHX)
Reactor Vessel	Pre-stressed Concrete Reactor Vessel Designed to ASME Code Div 2 for gas reactors.	2 ¼ CrMo, ASME Code Section III, Div 1 -Normal op Temp: 440 °C -Accident max temp: 500 °C for 400 hr, 540 °C for 50 hr	9Cr MoVNb or 2 ¼ CrMo, ASME Code Section III, Div 1, -Normal op Temp: 490 °C -Accident max temp: 560 °C for 400 hr (initial approximations).
Cross Vessel	NA	2 ¼ CrMo, ASME Code Section III, Div 1, (alternate material: 9CrMoVNb), -Normal op temp: 440 °C -Accident max temp: 440 °C	9CrMoVNb or 2 ¼ CrMo, ASME Code Section III, Div 1 -Normal op temp: 490 °C -Accident max temp: 500 °C (Initial approximations)
Power Conversion System Vessel	NA	2 ¼ CrMo, ASME Code Section III, Div 1, -Normal op temp: 150 °C -Accident max temp: 250 °C	9CrMoVNb or 2 ¼ CrMo, ASME Code Section III, Div 1, -Normal op Temp: 150 °C -Accident max temp: 300 °C

The major driver for the NGNP design is high temperature process heat for hydrogen production. Studies have shown that obtaining attractive hydrogen production efficiencies requires reactor outlet temperatures near 1000 °C, as shown in Figure 10. The core inlet temperature is currently estimated to be 490 °C. This results in a core temperature drop of 510 °C. Two major modifications of the GT-MHR design are needed to be able to reduce the core inlet temperature while still controlling the hot streak temperatures exiting the core: reducing the by pass flow and better controlling the inlet coolant flow distribution with orfices.

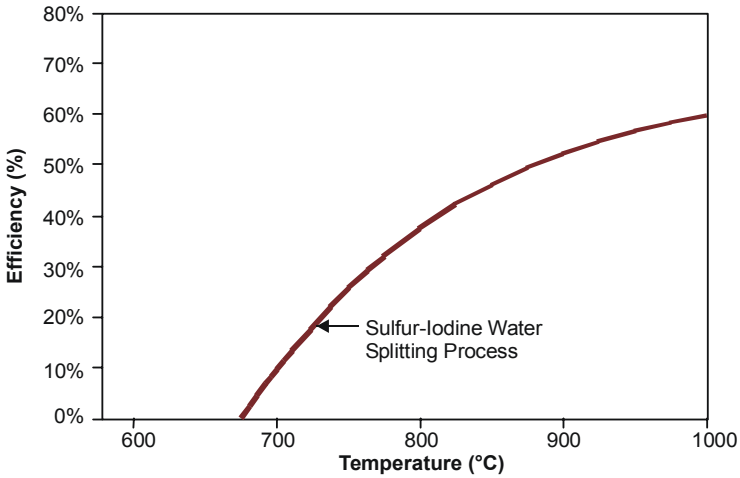

Figure 10. Hydrogen production process energy efficiency as a function of process heat input maximum temperature.

The demonstration NGNP plant configuration will be either a prismatic or pebble bed reactor system plus a power conversion unit similar to Figure 4 (essentially laid out as in Figure 1), except for the addition of a small stream of hot hydrogen that goes to a smaller IHX that acts as the heat source for a heat transfer circuit to the hydrogen plant. Figure 11 shows a rough sketch of this version of the plant on its INEEL site. Or, the demonstration NGNP plant configuration will be a reactor system plus a vessel with an IHX and primary reactor coolant system gas circulator, with the secondary of the IHX acting as a heat source for: a) a hydrogen production plant (that will use either a sulfur based thermo-chemical water-splitting or high-temperature electrolysis process); and b) a high-temperature gas turbine to produce electricity, which will probably be similar to that shown in Figure 4.

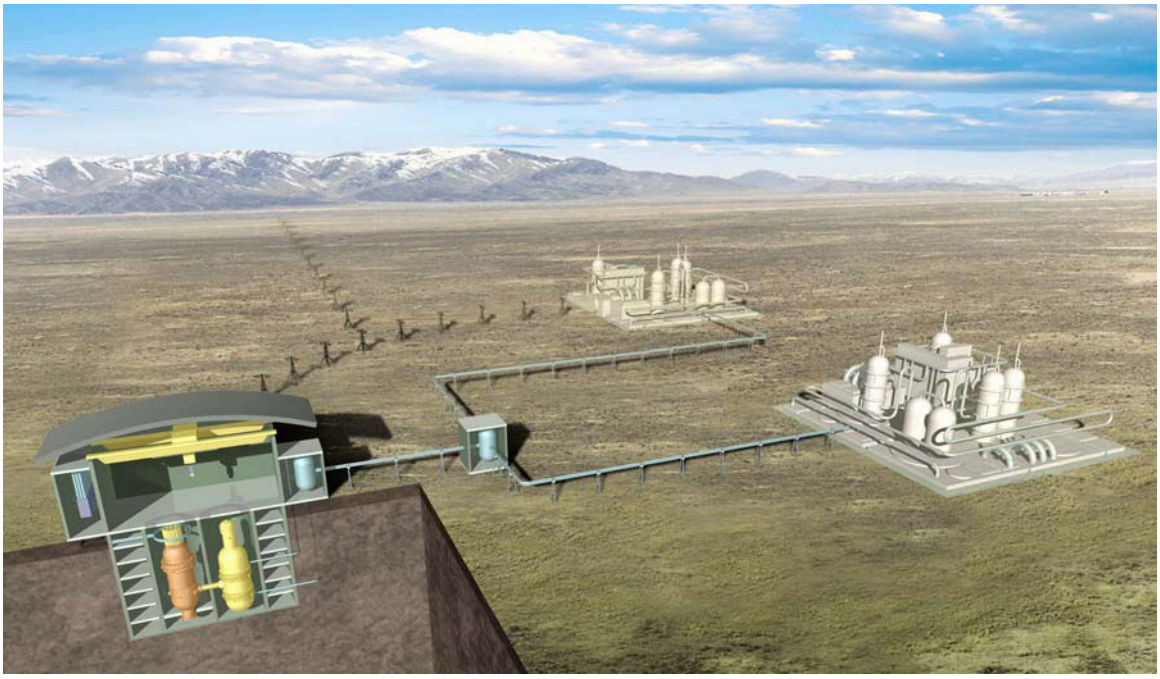

Figure 11. NGNP layout on the INEEL site.

To accommodate the reference core inlet temperature of 490 °C, medium temperature alloys are used for the metallic components and vessel. For those components bathed in the core exit gas, the design temperature increase from 850 to 1000 °C is significant. All GT-MHR or PBMR metallic materials at this temperature will have to be replaced with higher temperature alloys or non-metallic materials, such as carbon-carbon composites. Because of the 150 °C higher core outlet temperature, the outlet plenum temperatures would also need to have stricter requirements on temperature gradients and fluctuations because of the higher absolute temperatures. The upper plenum shroud inner surface materials will need to be changed, and possibly the control rod guide tubes will need to be changed as well if the P-LOFC accident plume temperatures go above 1000 °C.

The prismatic and pebble bed reactor cores have only graphite or carbon-carbon composite materials and will not be appreciably affected by the increased core out-let temperature. However these materials will need to be tested at slightly higher temperatures than those for the GT-MHR.

The IHX for the NGNP will have to be developed to handle 1000 °C temperatures. Some initial design studies have been performed for an IHX with 850 °C inlet temperature. Compact heat exchangers were found to be feasible. However, much engineering work remains for both an 850 and 1000 °C IHX. Depending on the function and design of the IHX secondary, large pressure differentials may occur with depressurization events. The IHX will probably not need to withstand rapid temperature transients such as those seen by the recuperators in the power conversion unit during sudden loss of generator load events.

Also, the gas turbine may need to be modified, and the inlet ducting and recuperator materials will need to be evaluated to find acceptable materials that can operate at the higher temperatures resulting from the increased core outlet temperature of 1000 °C. It is also possible that the turbine may require blade cooling and /or more disk cooling.

2.4. High Temperature Gas Reactor Fuel

The fuel for the NGNP builds upon the potential of the TRISO coated particle fuel design, as demonstrated in Germany and elsewhere. The TRISO coated particle is a spherical layered composite about 1 mm in diameter. It consists of a kernel of uranium oxycarbide (UCO) surrounded by a porous graphite buffer layer that absorbs radiation damage, allows space for fission gases produced during irradiation, and resists kernel migration at high temperature. Surrounding the buffer layer are a layer of dense pyrolytic carbon, a SiC layer, and a dense outer pyrolytic carbon layer. The pyrolytic carbon layers shrink under irradiation and provide compressive forces that act to protect the SiC layer, which is the primary pressure boundary for the micro-sphere. The inner pyrolytic carbon layer also protects the kernel from corrosive gases that are present during the deposition of the SiC layer. The SiC layer is the primary containment of fission products generated during irradiation and under accident conditions. Each micro-sphere acts as a mini pressure vessel, a feature that is intended to impart robustness to the gas reactor fuel system.

The baseline fuel kernel for the NGNP is low-enriched uranium oxycarbide (UCO). UCO was selected because the mixture of carbide and oxide components results in no free oxygen being released due to fission. As a result, no carbon monoxide is generated during irradiation and little kernel migration (i.e., amoeba effect) is expected. The oxycarbide fuel also ties up the lanthanide fission products as immobile oxides in the kernel, which gives the fuel added resiliency under accident conditions.

The current dimensions of the fuel and approximate densities of each layer are shown in Table 4. The kernel dimensions are based on the GT-MHR design. The buffer layer and the TRISO coating layer dimensions are the same as that used by the Germans in their successful gas reactor program in the 1970-80s.

Table 4. NGNP Coated Particle Fuel Parameters.

Parameter	Value
Kernel Composition	UCO
Kernel Diameter	350 microns
Kernel Density	$\geq$ 10.5 g/cc
Buffer Thickness	100 microns
Buffer Density	~ 1 g/cc
IPyC Thickness	40 microns
IPyC Density	~ 1.9 g/cc
SiC Thickness	35 microns
SiC Density	~ 3.2 g/cc
OPyC Thickness	40 microns
OPyC Density	~ 1.9 g/c

For the pebble bed version of a NGNP, the coated particles are over-coated with a graphitic powder and binders. These over-coated particles are then mixed with additional graphitic powder and binders and molded into a 5 cm sphere. An additional 0.5 cm fuel free zone is added to the sphere prior to isostatic pressing, machining, carbonization and heat-treating.

For the prismatic version of the NGNP, a similar process is envisioned where the over coated particles are mixed with graphitic powder and binders to form a cylindrical compact approximately 5 cm long and 1.25 cm in diameter. After final heat treatment, these compacts are inserted into specified holes in the graphite blocks. Figure 12 shows a cutaway schematic of a TRISO coated fuel particle and pictures of fuel particles, compacts, and fuel elements used in a high-temperature gas reactor with prismatic fuel (Fort St. Vrain). Figure 13 is a photograph of a TRISO coated fuel particle with part of the coating removed so that the fuel kernel is visible. Note the distinct layers of porous carbon buffer, high-density pyrocarbon, and silicon carbide.

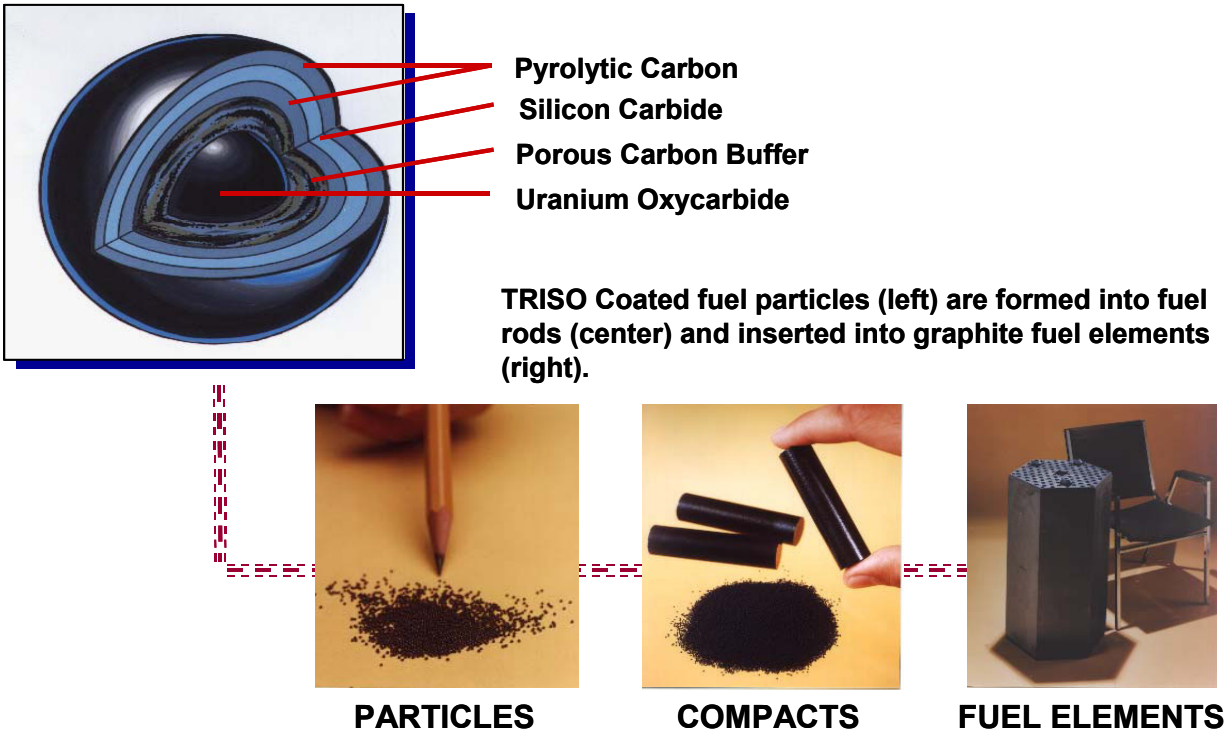

Figure 12. Cut away schematic of a TRISO coated fuel particle and pictures of prismatic fueled high-temperature gas reactor fuel particles, compacts, and fuel elements.

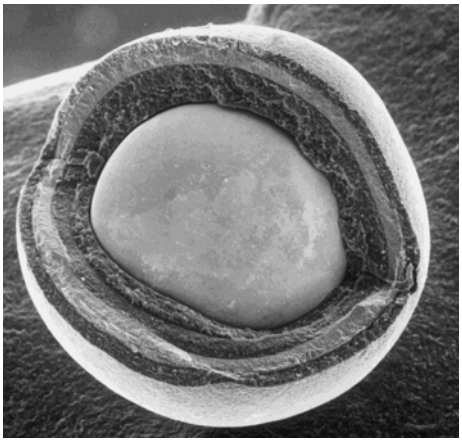

Figure 13. Photograph of a TRISO coated fuel particle with part of the coating removed.

3. NGNP Prismatic Core Point Design

3.1. Introduction

The NGNP reactor physics progress through the end of September 2003 for the prismatic point design is presented in this section. The eventual products of this work will include a basic core description, assignment of quantitative values to key core parameters, demonstration of core characteristics from neutronic calculations, and identification of design options that could be further explored in a conceptual design phase of the prismatic NGNP.

Although the NGNP design requirements are currently not fully defined, two design requirements are, however, rather firmly fixed. These include the need for inherent safety under all accident or transient conditions and a 1,000 °C outlet gas temperature. The first condition drives us immediately to an annular core configuration with substantial inner reflector graphite mass for absorption and temporal storage of thermal energy during the transients. The second requirement represents a significant increase in outlet gas temperature relative to other previously built and/or designed reactors. The higher gas temperatures drive up the graphite and fuel temperatures primarily in the active core region that in turn reduces the overall core reactivity. The reduced reactivity must then be overcome with an increase in enrichment and particle packing fraction in order to meet our power cycle length requirements, particularly since we expect that an 18-month fuel cycle will be necessary to make this concept economically viable.

In order to maximize our prismatic NGNP neutronic design effort, we have from the start drawn heavily on the General Atomics GT-MHR design.[3] Significant core physics, thermal-hydraulic, and fuel performance design analyses have already been performed by General Atomics in developing the GT-MHR design, and therefore that design is a logical and efficient starting point. It must be noted however that the GT-MHR design is not fully developed, nor necessarily optimized, particularly for the NGNP's higher temperature requirements. The first step in our approach was to build NGNP neutronic models based on the GT-MHR design and then to benchmark these models against the GT-MHR design analysis. Reproduction of the GT-MHR results using our neutronics models then gave us a level of confidence to further modify, analyze, and explore the design space using these models in conjunction with the two preliminary NGNP design requirements. Where the NGNP design requirements are undefined, parametric studies are being conducted to identify acceptable variable ranges. Ultimately, we will propose design modifications to the GT-MHR and demonstrate NGNP neutronic core characteristics that will define a viable NGNP design.

In this status report, we will address three main items: (1) the GT-MHR/NGNP core description, (2) the computer codes, and (3) the preliminary benchmarking neutronic results.

3.2. NGNP Core Description

Currently, the prismatic NGNP core description is based wholly on the General Atomics GT-MHR core description. The NGNP design requirements will eventually allow us to differentiate the two reactor core descriptions, but in the mean time preliminary NGNP design requirements have been proposed and put forward in order to aid in the NGNP core design and neutronic analysis. Table 5 below presents a few important preliminary core design parameters and shows the differences between the GT-MHR and the NGNP along with some core dimensional characteristics.

Table 5. Comparison of the GT-MHR and proposed NGNP core characteristics.

	GT-MHR	NGNP
Power ($MW_{(th)}$)	550-600	600-800
Average Power Density (W/cc)	6.5	6.5
Inlet Temp (°C)	488	490
Outlet Temp (°C)	850	1,000
Temp Differential (°C)	362	510
Coolant Flow Direction	Downward	Downward
Core Geometry	Annular	Annular
Inner Reflector Eff. Radius (m)	1.48	1.48
Active Core Eff. Radius (m)	2.41	2.41
Outer Reflector Eff. Radius (m)	3.33	3.33
Number of Fuel Columns	102	102
Number of Fuel Blocks per column	10	10 (600 MWt version)
Active Core Volume (m^3)	90.767	90.767 (600 MWt version)
Active Core Height (m)	7.93	7.93 (600 MWt version)
Fuel Element Geometry	Fort St. Vrain	Fort St. Vrain
Fuel Particle(s)	Fissile and Fertile	Fissile only
Enrichment	19.9 wt% U-235 0.711 wt% U-235	10.36 wt% U-235 (initial core) 15.5 wt% U-235 (re-load cores)
Capacity Factor	84%	>90%
Power Cycle Length	14-15.7 months	18-24 months

The NGNP overall core layout is shown in Figure 14 and currently is identical to the GT-MHR. The core consists of an inner graphite reflector (hexagonal rings 1-5), an active core (Rings 6, 7, and 8), outer replaceable graphite reflector (Rings 9 and 10), permanent side graphite reflector, and the core barrel (800H alloy or Hastalloy-X).

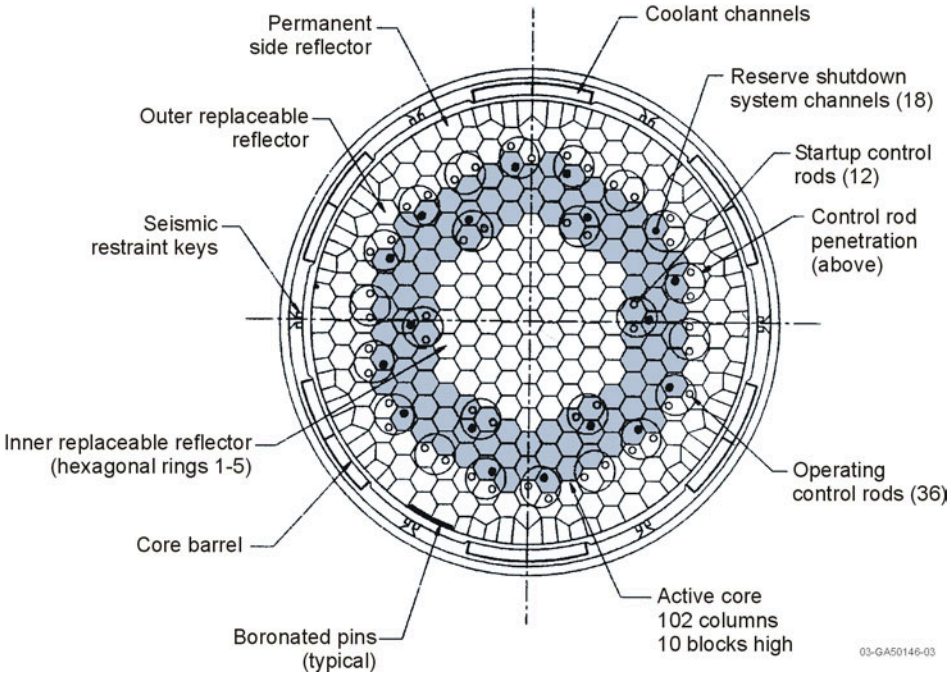

Figure 14. Cross sectional view of the GT-MHR and NGNP cores.

The active core is an annular configuration composed of 102 fuel columns. Each fuel column is a stack of fuel blocks ten high (600 MWt version) which translates into a total of 1,020 fuel blocks in the core. All preliminary neutronic evaluations utilize this core configuration. Modification to the core layout will be made based on future thermal-hydraulic design analyses. Reduction of the core diameter is a primary design consideration for alternative core layouts.

The GT-MHR fuel block is based on the Fort St. Vrain (FSV) fuel block design and also forms the basis for the NGNP design here. However, some redesign of the FSV fuel block is a definite possibility for future neutronic design analyses.

The GT-MHR fuel particle designs include two fuel particles: (1) fissile particles and (2) fertile particles.[3] The fissile particles have a uranium enrichment of 19.9 wt% U-235 and the fertile particles have enrichment typical of natural uranium (0.711 wt% U-235). The utility of a two-particle system allows for the mixing of these two particle types to easily achieve a desired effective enrichment. Effective enrichments may prove very useful in grading fuel rod rows near the reflector/active core interface to reduce fuel rod power peaking, and for optimizing block U-235 loading for core reloads. On the other hand, elimination of the fertile particle and using only a single fissile particle can greatly simplify the particle fabrication and testing requirements to license the fuel. The preliminary analysis herein focuses on just the single particle system or a single effective enrichment. For the initial core evaluated here, the effective enrichment is approximately 10.36 wt% U-235 with a packing fraction of 0.289. This effective enrichment is based on the General Atomics GT-MHR initial core loading with the two particle types.

3.3. Computer Codes And Models

The reactor physics computer codes MCNP, ORIGEN2, MOCUP and NJOY have been used exclusively to perform all neutronic analyses presented in this section of this report. Each is discussed briefly below.

The MCNP (Monte Carlo N-Particle) code[8,9] Version 4B and 4C (MCNP4B and MCNP4C) is a general purpose, continuous energy, generalized geometry, coupled neutron-photon-electron Monte Carlo transport code. The geometry capability allows for very explicit, three-dimensional representations of the reactor core and prismatic block details. With reflective boundary conditions applied to the six sides and on the top and bottom planes of the hexagonal fuel block models, lattice k-infinity values can be calculated. Partial and full core models can also be developed for core k-effective, control rod worth, and depletion calculations.

MCNP also has a powerful tally capability to calculate neutron fluxes and nuclear reaction rates averaged over any cell volume in a model. This allows the analyst to estimate flux spectral and spatial characteristics, fuel rod fission power, neutron fluence, radionuclide production rates, and neutron cross sections [fission, radiative capture, (n, 2n), (n, 3n), (n, p), (n, d), (n, t), and (n, α)]. The neutron cross-sections can then be used directly in a depletion calculation.

The continuous-energy neutron cross sections typically range from 10^{-5} to 20 MeV. The photon energy range is from 1 keV to 100 MeV, and the electron energy is from 1 keV to 1,000 MeV. A wide variety of nuclide cross-section and reaction data are available from the Evaluated Nuclear Data Files version 5 and 6, or ENDF/B-V and ENDF/B-VI. In addition, MCNP cross sections at high temperatures have been specially created for application to the NGNP.

Because the MCNP computer code is a Monte Carlo code, the calculated results are reported by the code with an associated statistical uncertainty or relative error. The relative errors translate into one-sigma statistical uncertainty values by multiplication of the relative error and the calculated result. Two-sigma and three-sigma confidence intervals are obtained by further multiplying the one-sigma values by a factor of two and three, respectively. The confidence levels associated with one-, two-, and three-sigma values are 68.3%, 95.4 %, and 99.7%, respectively. All statistical error values reported in this study are one-sigma values, unless otherwise stated. Error bars on calculated data are often smaller than the plotted symbol and therefore not visible.

The ORIGEN2 (Oak Ridge Isotope Generation) Version 2 and 2.1 code[10] is used to calculate the complex time-dependent and coupled behavior of both radioactive and stable isotopes under flux irradiation or power production time profiles. This includes the isotopic buildup due to production and destruction mechanisms, which include transmutation (radiative capture), fission, threshold particle reactions, and radioactive decay processes. The code mathematical basis uses the matrix exponential method to solve large numbers of coupled ordinary differential equations relating isotopic concentrations with a high degree of accuracy. This code has been used to perform depletion or burnup calculations for NGNP fuel blocks and partial core models.

ORIGEN2 input data includes core or block power (MWt) or irradiation flux (n/cm^2/sec), calculated one-group neutron reaction cross sections, and heavy metal loading. ORIGEN2 will output isotopic concentrations (moles, curies, grams), activities, and decay heats for over 1700 activation products, actinide and daughter products, and fission product isotopes. Decay and cross section libraries come with the standard code issue. One of these libraries is the high-temperature gas-cooled reactor cross-section library or the "htgrxslibd" library; this library is used as our base library, which is updated to reflect cross section changes during the course of a burnup calculation.

A special feature in the ORIGEN2 code allows the analyst to update or modify the standard cross section library with user-calculated cross sections, thereby allowing a depletion calculation to be reactor specific. ORIGEN2 performs a depletion calculation using effective one-group cross sections calculated, in our case, with MCNP calculated tally data.

The MOCUP (MCNP-ORIGEN2 Coupled Utility Program) code[11] is a system of external processors that links input and output files from the MCNP and ORIGEN2 codes in order to perform a time-dependent burnup or depletion calculation. MOCUP is composed of three processing modules, namely mcnpPRO, origenPRO, and compPRO. Each module performs a specific, sequential task during each burnup iteration. No modifications are required to the MCNP or ORIGEN2 codes in order to run the MOCUP code system.

The MOCUP code system performs a multitude of data manipulations, but only two main functions. These two functions include: (1) read MCNP flux and reaction rate output data, convert these data to one-group cross sections, and load them into the ORIGEN2 input file so they can update cross sections in the base library, and (2) read the ORIGEN2 isotopic concentration output punch file and create a new MCNP fuel composition. The new MCNP composition reflects the changes in heavy metal and fission product isotopic depletion or buildup as the result of burnup during the time step.

The NJOY nuclear data processing system[12] is a comprehensive computer code package for producing point-wise and multi-group neutron and photon cross sections from ENDF/B evaluated nuclear data. In order to understand the effects of temperature on NGNP core reactivity, it was necessary to develop additional heavy metal neutron cross section libraries at temperatures in the range of the NGNP under both normal and transient operation conditions. This required developing cross section data up to 2200 °C. The NJOY code (version 99.67) was run with the Evaluated Nuclear Data Files (ENDF/B-VI) and generated the cross sections in ACER format for use by the MCNP code.

Uranium and plutonium neutron cross section libraries at temperature for our usage now include the following:

(1) U-235, U-238 at 20, 124, 224, 324, 524, 624, 924, 1000, 1100, 1200, 1300, 1400, 1500, 1600, 1800, 2000, and 2200 °C, and
(2) Pu-239, Pu-240, Pu-241, and Pu-242 at 24, 314, 607, 901, 1488, 1880 °C.

An example of the Doppler-broadened U-235 absorption (radiative capture) neutron cross section is shown in Figures 15 and 16.

A number of MCNP computer models were developed for specific computational neutronic analyses. These models include detailed prismatic block and full core models. The block models include: (1) standard fuel blocks, (2) reserve-shutdown-system fuel blocks, (3) control rod fuel blocks, (4) graphite reflector blocks, and (5) graphite reflector blocks with control rods. Figures 17 and 18 show cross sectional views of the standard and reserve-shutdown-system MCNP fuel block models. The control rod fuel block is similar to the reserve-shutdown-system fuel block except that the large hole increases from 3.75 inches to 4.00 inches. These block models have reflective boundary conditions applied to the top and bottom and six hexagonal sides to create an infinite block array to represent the core.

Full core models have also been developed to support neutronic computational goals. These models are explicit one-sixth (1/6) core radial wedge models with reflective boundary conditions applied to the azimuthal planes to represent a full core. These 1/6-core models are further divided into two model groups based on axial definition. The first group has an axial height equal to the height of a single block. Reflective boundaries are then applied to the top and bottom of the axial planes to represent a core of infinite axial height. These models are specifically referred to herein as either single layer or "layer" models. The second group explicitly defines each of the axial layers of fuel and reflector blocks in explicit detail. These models are referred to herein as full core or "core" models.

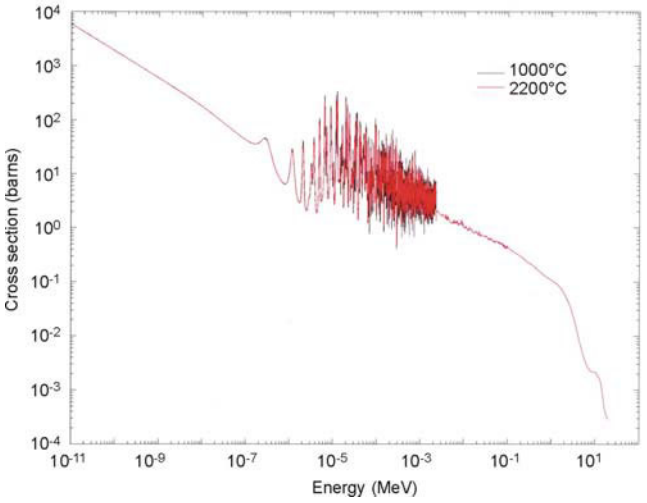

Figure 15. Absorption cross section for U-235 over the entire neutron energy range and shown at two temperatures (1,000 and 2,000°C).

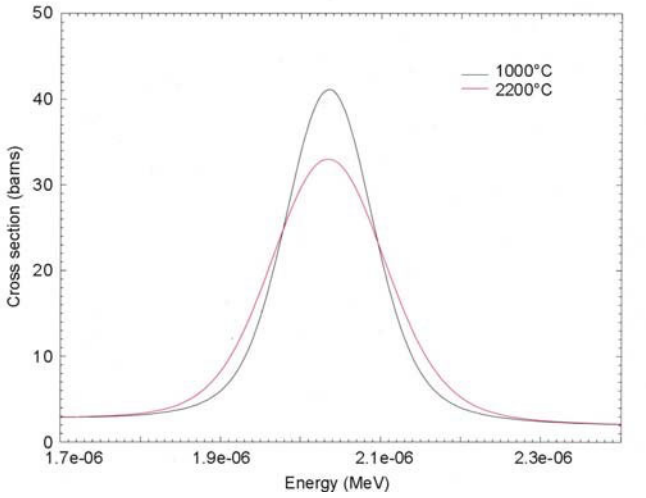

Figure 16. Low-lying thermal absorption resonance of U-235 around 2.05 eV showing the cross section effect of Doppler-broadening at the two temperatures (1,000 and 2,000°C).

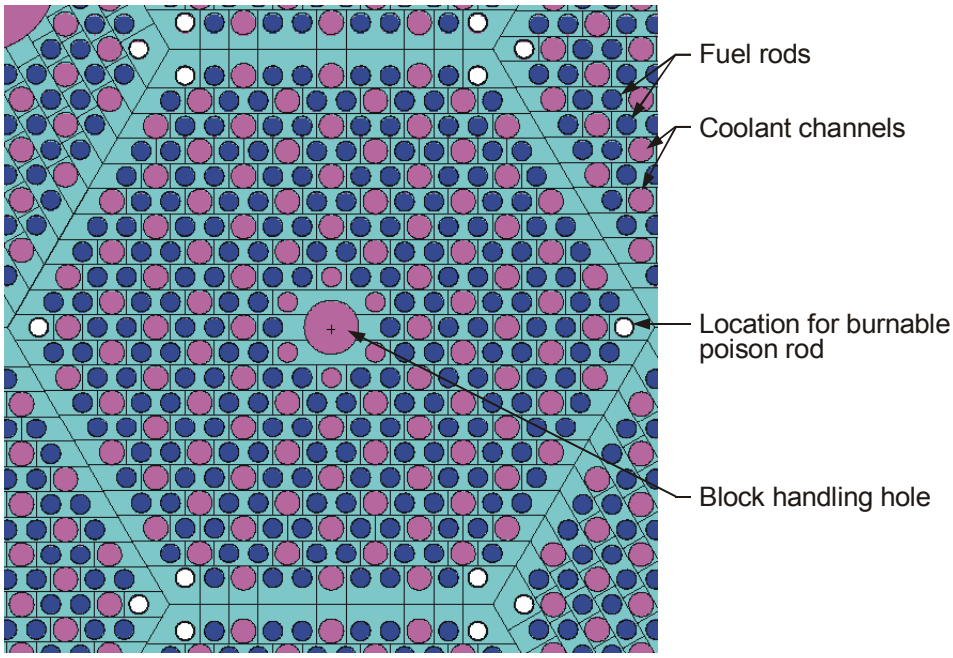

Figure 17. MCNP infinite lattice model showing a standard hexagonal fuel block. The six locations on the corners of the hexagonal block can be used to hold burnable poison rods.

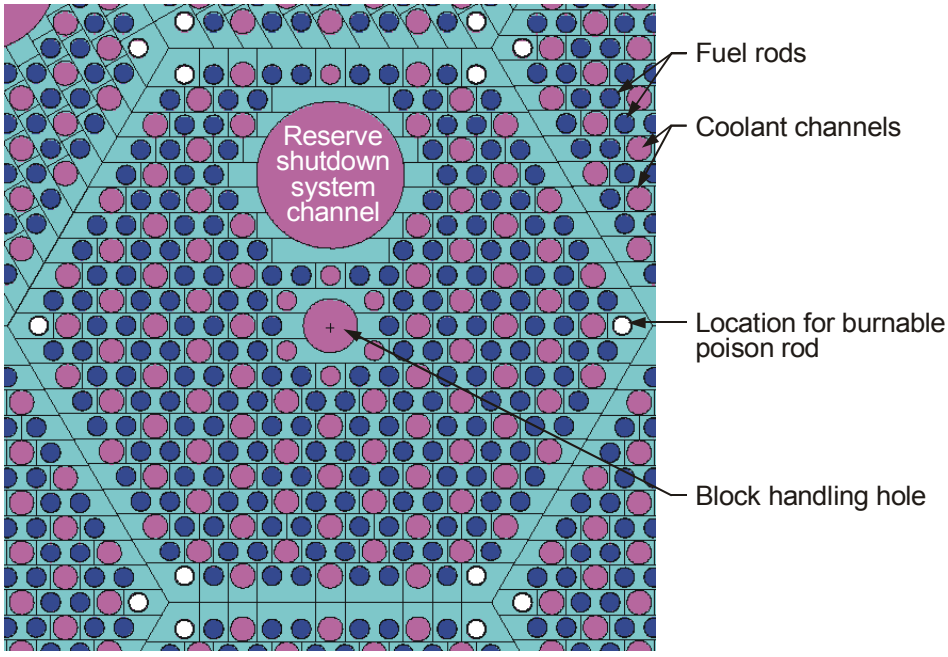

Figure 18. MCNP model of a reserve-shutdown-system fuel block. The control rod fuel block is similar to the reserve-shutdown-system fuel block except that the reserve-shutdown-system channel increases from 3.75 inches to 4.00 inches.

Both the single layer and full core models surprisingly predict very similar core k-effective values. The full core models are intended for estimating control rod worth as a function of axial position and number

of control rods in the core, while the more easily manipulated single layer models are intended for virtually all other core physics parameter calculations. Figure 19 is a cross sectional view of a 1/6-core model showing the inner graphite reflector, active core annulus (standard, reserve-shutdown-system, and control rod fuel blocks), and the outer graphite reflector, and core barrel.

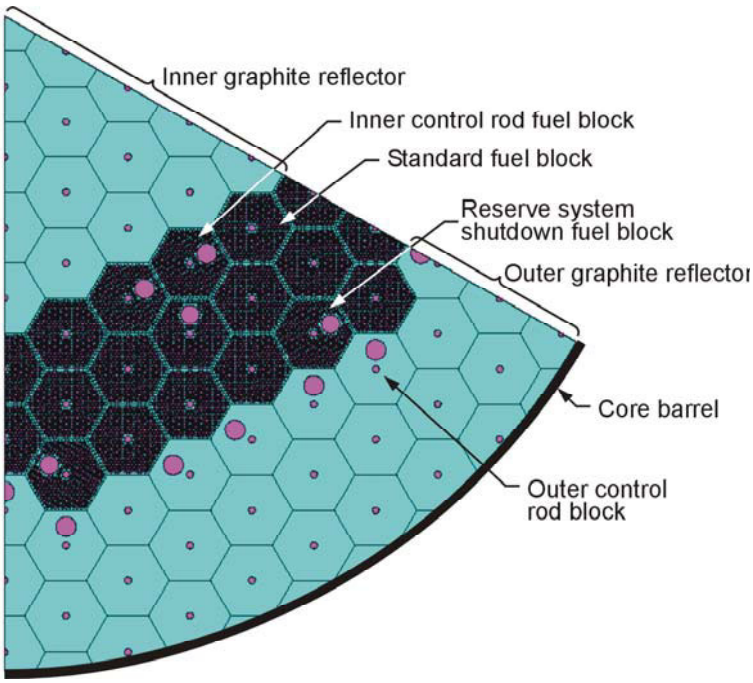

Figure 19. MCNP model of a 1/6-core GT-MHR.

Our three-dimensional block and core models include some very specific features including the fuel-handling hole, tooling hole, dowels, fuel rod gas gaps, and the fuel rod axial end caps. The models do not, however, include the beveled edges on the block, nor the gas gaps between the blocks. These features can readily be incorporated in future models.

Relative to the problem of core heterogeneity, it should be pointed out that our block and core models utilize a homogenized fuel rod composition to describe the fuel particles and graphite binder matrix mixture. This corresponds to single heterogeneity modeling. No attempt has been made yet to develop double heterogeneity models with the TRISO particles explicitly modeled. Future work will focus on double heterogeneity model development in order to better understand the effects of particle and fuel rod self-shielding.

The MOCUP depletion models include fuel rod cross-section updates for 77 individual fission products and 37 actinides. The 77 fission product isotopes typically account for greater than 99.9 percent of the total negative reactivity from the fission product inventory. These fission product isotopes are specifically selected by the analyst, assuming the isotope has an associated MCNP generated library available. Most of our fission product MCNP libraries have been generated at room temperature; the rare earth fission product poisons (e.g. Sm, Er, Gd, Eu) however do have temperature dependent cross section libraries. The 37 actinides range from thorium to californium in order to account for the buildup and reactivity effects of virtually all the important heavy metal isotopes.

The fission product and actinide cross sections are updated at desired burnup increments or time steps over the depletion or power cycle. Updated cross sections include (n,γ), (n,2n), (n,α), and (n,p) for the fission products, and (n,γ), (n,2n), (n,3n), and (n,f) for the actinides. These updated cross sections are then loaded into the ORIGEN2 model for the next burnup increment.

The ORIGEN2 models were developed in standard format with input data that includes the block or core power level (MWt), beginning-of-life or updated neutron cross sections, and isotopic concentrations from beginning-of-life or depleted fuel compositions.

3.4. Neutronic Results

The preliminary neutronic results from our evaluation of the GT-MHR design are presented in this section along with preliminary parametric studies that will allow us to extrapolate the GT-MHR design to the NGNP.

3.4.1. Block Loading Studies

A spreadsheet was first developed in order to calculate fuel composition number densities for various parametric studies. The spreadsheet variables included particle parameters (dimensions, material, and densities), particle packing fraction in the compact graphite matrix, uranium enrichment, and fuel rod or compact radius. In order to gain an understanding of how some of these variables affect the fuel block U-235 loading, parametric studies were conducted with variations in packing fraction (PF), enrichment, and particle kernel diameter. Figures 20, 21, and 22 show the standard fuel block U-235 loading change as a function of packing fraction, enrichment, and particle kernel diameter, respectively. Significant increases in U-235 block loading can be obtained by varying these parameters individually or in combination. U-235 loading is important, particularly since we intend to increase the NGNP power cycle, which in turn requires higher U-235 loadings.

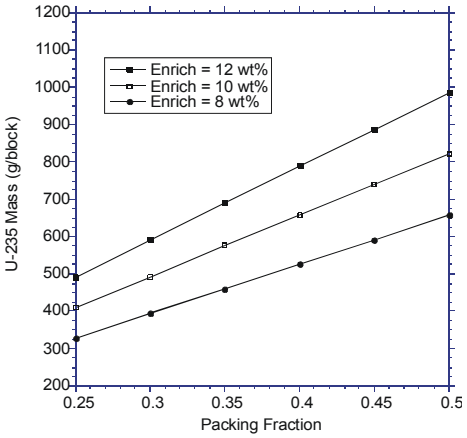

Figure 20. Standard fuel block U-235 mass loading versus fuel particle packing fraction.

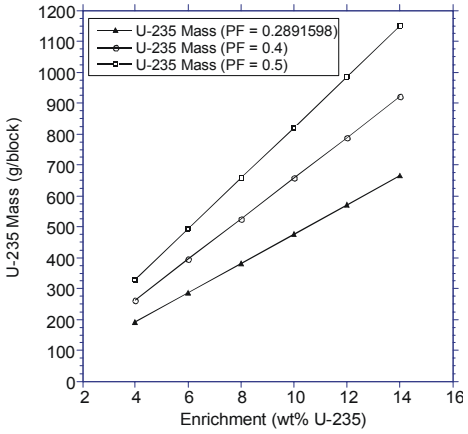

Figure 21. Standard fuel block U-235 mass loading versus fuel enrichment.

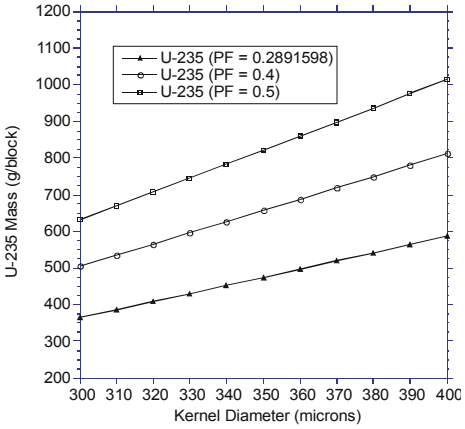

Figure 22. Standard fuel block U-235 mass loading versus fuel particle kernel diameter.

Use of this information will be made as the analysis on increasing the power cycle progresses.

3.4.2. Block K-infinity versus Packing Fraction

K-infinity calculations were performed using the infinite lattice MCNP standard fuel block model. Both the particle packing fraction and uranium enrichment were varied. Figure 23 shows the calculated results. It is apparent that as the enrichment is increased the k-infinity value increases as expected. However, as the packing fraction increases the k-infinity values decrease. This effect can be exploited for the goal of increasing the NGNP power cycle length. The larger packing fractions allow heavier U-235 loading with suppressed reactivity due primarily to thermal neutron self-shielding. Hence, at beginning-of-cycle the reactivity is held down by the self-shielding and released as positive reactivity as the cycle or burnup progresses. See Section 3.4.8 for additional confirmation of this conclusion.

3.4.3. Reactivity Effect of Helium Gas

Helium gas in the core is assumed to be at 7.12 MPa (or approximately 0.003194 g/cc) and reside in the coolant channels. Loss of the helium coolant from the core in an instantaneous loss scenario has been shown through core k-effective calculations to be insignificant. The calculated core k-effectives using the 1/6-core layer model with and without the helium gas are 1.266029 and 1.266255, respectively. Both values have a relative error associated with them of 0.0003 and statistically these two k-effective values are equivalent. It can be concluded that the helium coolant gas has a negligible impact on the core reactivity.

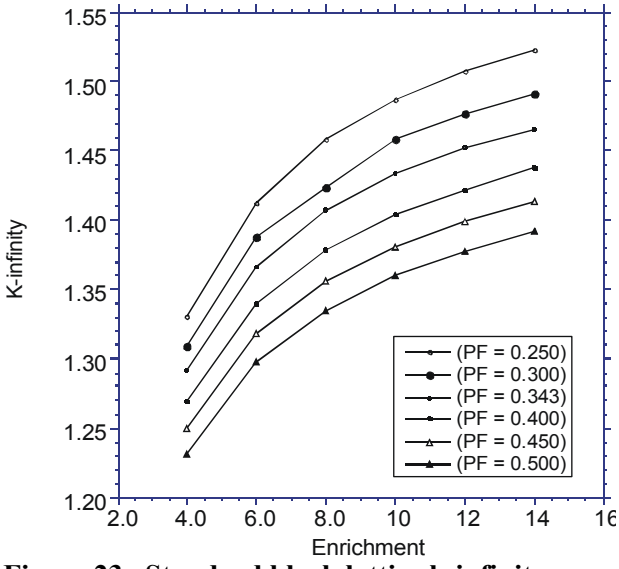

Figure 23. Standard block lattice k-infinity versus fuel enrichment and particle packing fraction (PF).

3.4.4. Model K-effective Value Differences

Beginning-of-life (BOL) block and core k-effective values have been calculated as a function of temperature and level of core geometric model detail. Table 6 compares infinite block lattice k-infinity values (block), 1/6-core single fuel block core height (layer), and 1/6-core full core height (core) model calculated results. The temperature of both the uranium fuel (U-235 and U-238) and the graphite have been varied to determine the temperature defect.

Table 6. Calculated k-infinity values for a standard block lattice model and k-effective values for 1/6-core models as a function of temperature.

Model	Uranium Temperature (°C)	Graphite Temperature (°C)	Core K-effective	Relative error
block	21	27	1.482073	0.0002
block	21	927	1.469797	0.0002
block	1100	927	1.359603	0.0003
layer	21	27	1.340635	0.0003
layer	21	927	1.343303	0.0003
layer	1100	927	1.266029	0.0003
core	21	27	1.328035	0.0003
core	21	927	1.332863	0.0003
core	1100	927	1.251612	0.0003

It is interesting to note the significant differences between the "block" and "layer" models for example. The smaller k-value for the 'layer' model is indicative of the high radial neutron leakage from the annular core configuration. Comparison of the "layer" and "core" models results shows very close agreement and indicates that the axial core neutron leakage is relatively small because of the great length of the core and the reflection afforded by the top and bottom graphite reflectors. Also, the good agreement between the "layer" and "core" models allows us to use the easier to manipulate "layer" models for parametric studies (depletion and power peaking) without significant reactivity loss.

3.4.5. Core K-effective Values Versus Enrichment

In order to see the effect of the fuel enrichment on the core k-effective value, the 1/6-core model was used to calculate the core reactivity (k-effective) as a function of fuel enrichment over a range of enrichments from 10 to 16 wt% U-235 and at a fixed packing fraction of 0.289. Figure 24 shows the calculated results for a 1/6-core model fuel with all standard fuel blocks and for a 1/6-core model fuel with standard,

reserve-shutdown-system, and control rod fuel blocks per Figure 12. The core k-effective increases with increasing enrichment as expected. This is a good mechanism to increase both core reactivity and U-235 block mass loading for power cycle extension. Also, note the relatively close agreement between the two models, despite the slight reduction in core U-235 loading with the use of the reserve-shutdown-system and control rod fuel blocks in the 1/6-core model.

3.4.6. Neutron Flux, Fluence, Displacements-Per-Atom, and Spectra

Neutron flux, fluence, displacements-per-atom (dpa), and spectra results were calculated for the NGNP materials group and are presented in Table 7 and Figures 25 through 27. The calculated flux data (neutrons/cm^2/sec) in Table 7 is given in terms of a three-group energy structure along with the total flux. The annual fluence (n/cm^2/yr) is provided for the thermal and fast groups only. The total dpa rate is given in terms of a daily rate (dpa/day). The neutron spectral plots are provided based on a 95-group energy structure at beginning-of-life core conditions.

The MCNP 1/6-core layer model was used to calculate most of the neutron fluxes, fluences, dpa, and spectra in the NGNP. The uranium temperature in the core was 1100 ˚C and the graphite S(α,β) data was fixed at 927 ˚C throughout the core. The model extends one block high in the axial direction with reflective boundaries applied to the top and bottom axial planes. Therefore, this model and the calculated results represent fairly closely the conditions at the core mid-plane of the NGNP. (The fuel rod neutron flux and spectra was calculated with another model that was normalized to an average block power of 0.588 MWt.)

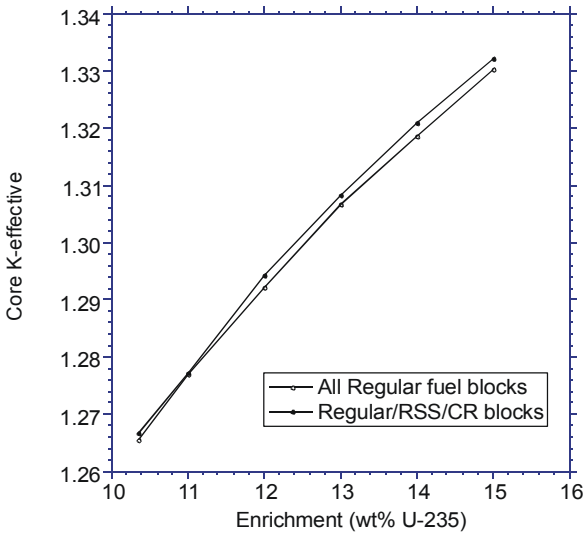

Figure 24. Comparison of k-effective versus enrichment for a 1/6-core model containing all standard fuel blocks versus a 1/6-core model containing regular, reserve-shutdown-system (RSS), and control rod (CR) fuel blocks.

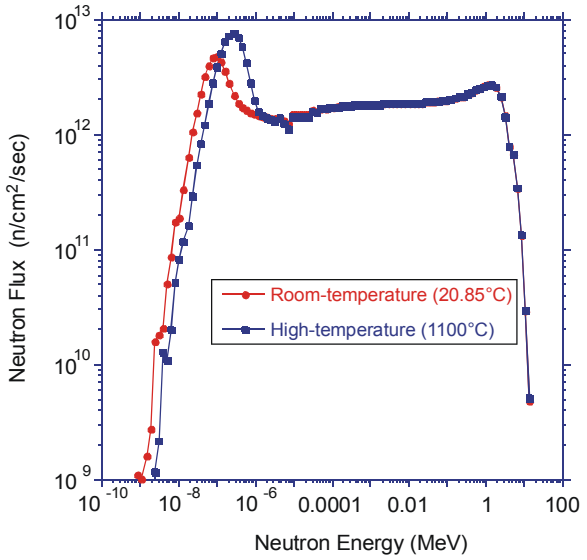

Figure 25. Neutron energy spectra for the fuel rods at two temperatures.

Control rods were not inserted in the reactor core (outer reflector) in the 1/6-core model, and there were no borated shield pins in the permanent side reflector. Hence, the calculated thermal flux at the core barrel location is maximized. Note, however, that the graphite material throughout the core (reflector blocks and fuel block graphite structure) is assumed to contain a 6.9 ppm boron-10 impurity, which has the effect of reducing the thermal flux slightly.

The flux, fluence, and dpa estimates for the reflector blocks are averaged over the entire block volume, and hence no neutron flux gradient information across the block is available currently. The annual fluence estimates are based on a capacity factor of 90% and one year is assumed to be 365.25 days in length. The dpa cross-sections for graphite (carbon), iron, nickel, and chromium are based on Reference 13. For the core barrel materials containing these elemental constituents, the material dpa can be

estimated by simple mass weighting of the individual elemental dpas. All dpa rates are based on the carbon damage cross sections with exception of the core barrel.

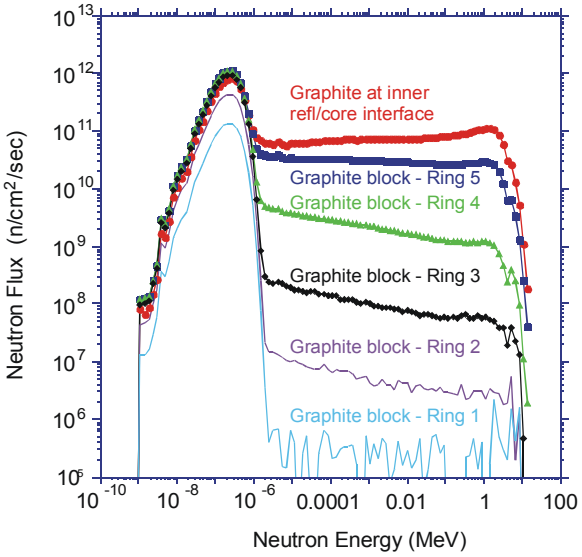

Figure 26. Neutron energy spectra in the inner reflector blocks (927°C) Rings 1-5 and the graphite at the inner reflector- core interface.

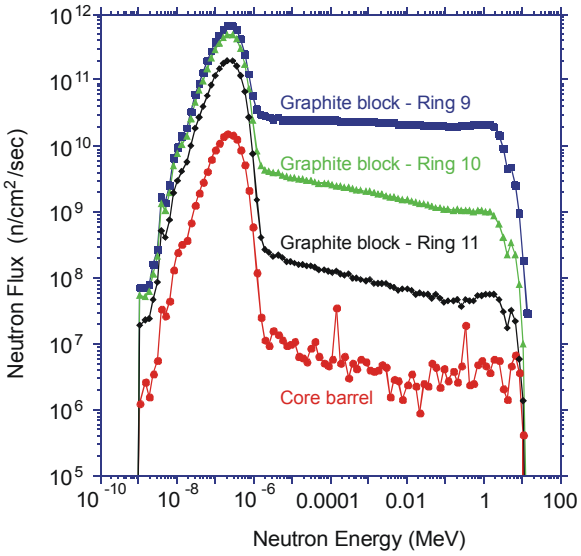

Figure 27. Neutron energy spectra in the outer reflector blocks (927°C) Rings 9-11 and the core barrel.

The neutron spectral information is also broken into three groups:

Group 1 (thermal): 0.0—1.4E-6 MeV
Group 2 (epithermal): 1.4E-6 MeV—0.1 MeV
Group 3 (fast): 0.1—20.0 MeV

The neutron spectra for the fuel rods in a NGNP fuel block are shown in Figure 25. Note the spectra differences between the block lattices at two temperatures, namely, room temperature and high temperature. At the high temperature, the uranium fuel is again at 1100 °C and the graphite at 927 °C. Notice the thermal peak shift upward in energy for the high-temperature case and the slightly higher flux levels relative to the room temperature case. The fuel rod fluxes are averaged over all 210 fuel rods in a standard fuel block. The fluxes in the fuel block graphite (fuel block structural component) are very nearly identical to those calculated fluxes averaged over the fuel rods, and hence are not presented. Also, it is noted here that the exact transport theory methods (MCNP) used to calculate these spectra are in reasonable agreement with previously calculated GT-MHR spectra using diffusion theory methods.

Figures 26 and 27 show the neutron spectra for the reflector blocks in all the core rings. The core center is designated as Ring 1 and contains only the one graphite reflector column. Rings 1, 2, 3, 4, and 5 comprise the core inner reflector with Ring 5 adjacent to the inner active core ring (Ring 6). These spectra were generated with the 1/6-core layer model and normalized to a 1/6-core power of 100 MWt. Each reflector block spectra is averaged over a single block.

In the operating NGNP core, the graphite at the inner reflector/active core interface is expected to face a more intense neutron radiation field than the graphite at the outer reflector/active core interface, because of the flux-depressing control rods in Ring 9 and the greater radial outward neutron leakage in the outer reflector. Hence, the inner reflector/active core graphite flux, fluence, and dpa should bound the outer reflector/active core interface graphite values.

Table 7. Neutron flux, fluence, and dpa as a function of energy group for various locations throughout the prismatic NGNP core.

Location	Neutron Energy Group	Neutron Energy Upper Bound (MeV)	Neutron Flux ($n/cm^2/sec$)	Neutron Fluence ($n/cm^2/yr$)	dpa (dpa/day)
Fuel Compacts	1	1.4E-06	7.808E+13	2.218E+21	
	2	0.1	6.769E+13		
	3	20	3.475E+13	9.870E+20	
		Total	1.805E+14		2.258E-03
Graphite at the inner reflector- core interface	1	1.4E-06	1.025E+14	2.913E+21	
	2	0.1	5.447E+13		
	3	20	2.367E+13	6.724E+20	
		Total	1.807E+14		1.538E-03
Graphite block in the inner reflector- Ring 5	1	1.4E-06	1.298E+14	3.686E+21	
	2	0.1	2.404E+13		
	3	20	6.365E+12	1.808E+20	
		Total	1.602E+14		4.270E-04
Graphite block in the inner reflector- Ring 4	1	1.4E-06	1.127E+14	3.202E+21	
	2	0.1	2.010E+12		
	3	20	2.703E+11	7.676E+18	
		Total	1.150E+14		1.875E-05
Graphite block in the inner reflector-Ring 3	1	1.4E-06	8.517E+13	2.419E+21	
	2	0.1	1.010E+11		
	3	20	1.511E+10	4.292E+17	
		Total	8.528E+13		1.085E-06
Graphite block in the inner reflector-Ring 2	1	1.4E-06	3.596E+13	1.021E+21	
	2	0.1	5.468E+09		
	3	20	1.382E+09	3.925E+16	
		Total	3.597E+13		1.231E-07
Graphite block in the inner reflector-Ring 1	1	1.4E-06	1.102E+13	3.130E+20	
	2	0.1	5.699E+08		
	3	20	3.210E+08	9.118E+15	
		Total	1.102E+13		2.991E-08
Graphite block in the outer reflector-Ring 9	1	1.4E-06	8.451E+13	2.400E+21	
	2	0.1	1.894E+13		
	3	20	5.048E+12	1.434E+20	
		Total	1.085E+14		3.386E-04
Graphite block in the outer reflector-Ring 10	1	1.4E-06	5.879E+13	1.669E+21	
	2	0.1	1.884E+12		
	3	20	2.495E+11	7.088E+18	
		Total	6.092E+13		1.737E-05
Graphite block permanent side reflector-Ring 11	1	1.4E-06	2.211E+13	6.303E+20	
	2	0.1	9.599E+10		
	3	20	1.307E+10	3.713E+17	
		Total	2.230E+13		8.991E-07
Core Barrel	1	1.4E-06	1.708E+12	4.852E+19	
	2	0.1	5.105E+09		
	3	20	1.588E+09	4.511E+16	
		Total	1.715E+12		7.584E-07*
					1.548E-06#
					1.217E-06♣

* Iron, # Nickel, and ♣ Chromium elemental dpa for core barrel constituents.

3.4.7. Water Ingress

A water ingress study was performed with the 1/6-core layer to estimate the core reactivity effect due to the intrusion of water or steam into the core coolant channels. The water density in the coolant channels was varied from 10^{-4} to 1.0 g/cc and applied uniformly throughout the axial coolant channel lengths. Two temperatures were considered: (1) room temperature and (2) high temperature. At the high temperature, the uranium fuel is again assumed to be at 1100 °C and the graphite at 927 °C.

Figure 28 is a plot of the core reactivity (k-effective) versus water density for beginning-of-life conditions and no control rod insertion. For water densities up to approximately 0.001 g/cc, there is only a small positive reactivity increase ($\Delta k < 0.0020$). Above a water density of 0.001 g/cc (18.1 Kg of H_20 in 18 million cc of coolant channels), the reactivity begins to significantly increase and reaches a maximum value at a water density of approximately 0.2 g/cc (optimal moderation) and then drops off rapidly with further increases in water density (water absorption). The calculated core reactivity behavior here agrees well with previously calculated GT-MHR results.

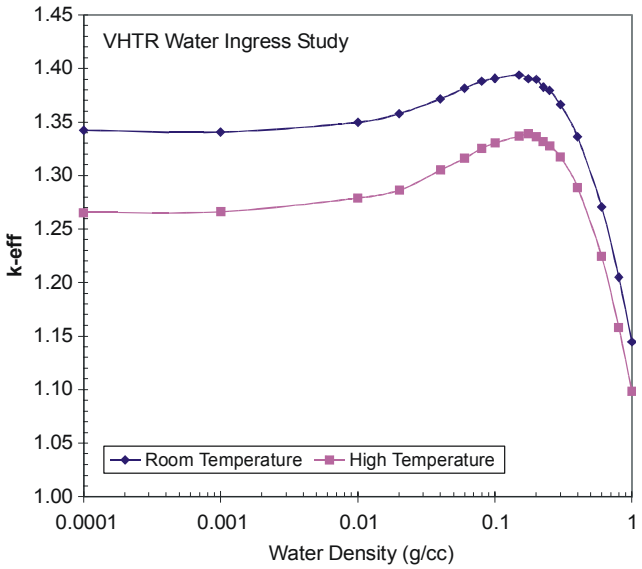

Figure 28. Core k-effective as a function of water density in the coolant channels.

3.4.8. Fuel Block Depletion

Figure 29 shows the burnup or depletion of a single standard fuel block in an infinite lattice of standard fuel blocks. The k-infinity values are plotted as a function of burnup and packing fraction. The packing fraction of 0.289 is the packing fraction of the initial core with an effective single enrichment of 10.36 wt% U-235 (per Reference 3). Two other packing fractions are considered, namely, a packing fraction of 0.4 and a packing fraction of 0.5.

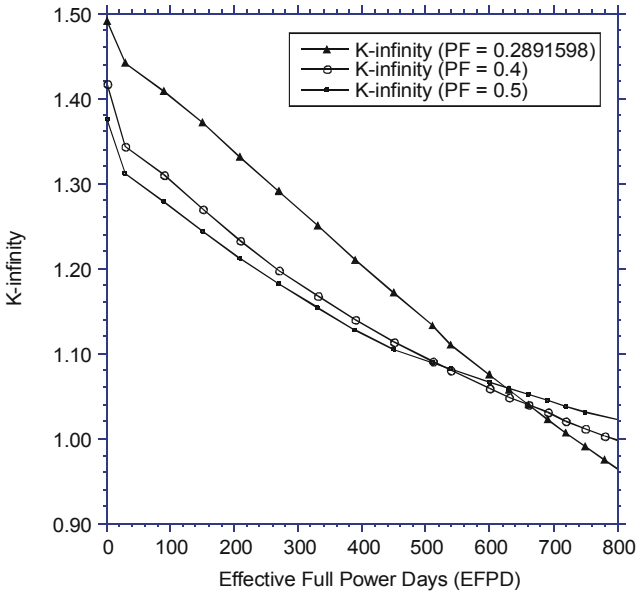

Figure 29. Infinite lattice k-infinity as a function of burnup and packing fraction (PF).

From Figure 29, the fuel block with a packing fraction of 0.289 starts with the highest k-infinity value, but is no longer critical (k-infinity < 1.0) after approximately 720 days. The higher packing fraction cases remain critical for longer times, approximately 800 and 900 days, respectively for a packing fraction of 0.4 and a packing fraction of 0.5, respectively. Hence, it appears that the higher packing fractions may prove useful for extending the NGNP power cycle length.

Figure 30 shows the depletion of the U-235 and the buildup of the Pu-239 as a function of packing fraction and effective full power days. The mass values are again for a single standard fuel block.

The standard block depletion calculations are again based on a single block at a constant average power level of approximately 0.588 MWt.

3.4.9. Core Depletion

Figure 31 shows the calculated core reactivity (k-effective) as a function of burnup in effective full power days. One effective full power day corresponds to a 24-hr period of continuous core power at 600 MWt. The core is loaded with a uniform enrichment (10.36 wt% U-235) and particle packing fraction (0.289) across the three core rings (6, 7, and 8). This effective enrichment corresponds to the General Atomics initial core loading using the specified proportions of the fissile and fertile particle loadings. The k-effective values were calculated using the 1/6-core layer model.

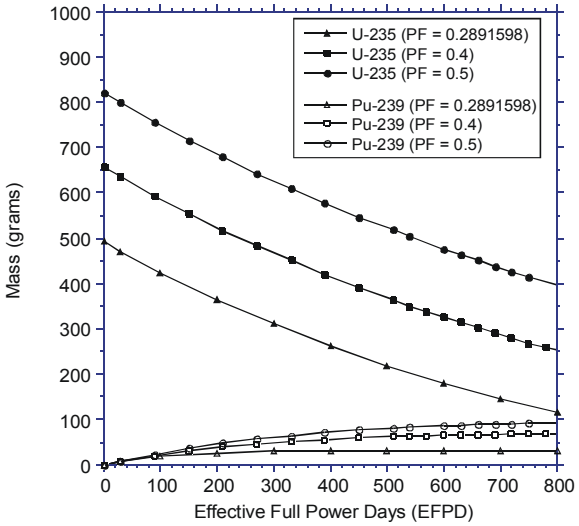

Figure 30. U-235 and Pu-239 mass (grams) in a single standard fuel block as a function of burnup and packing fraction.

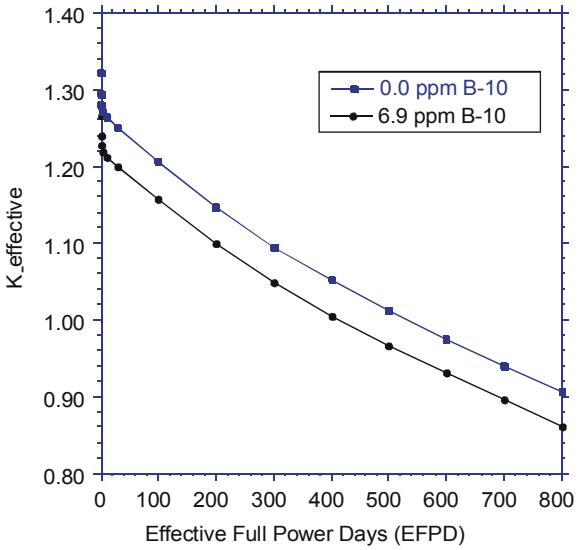

Figure 31. Core reactivity (k-effective) as a function of burnup and two B-10 impurity concentrations.

In all our models (block, layer, and core) we have introduced a 6.9 ppm boron-10 (B-10) impurity in all the graphite structures (inner and outer graphite reflectors, as well as the graphite fuel blocks). Inclusion of this boron impurity is really only appropriate for the beginning-of-life initial core conditions since the B-10 and other impurities will typically burnout during the course of the first power cycle. Introduction of this impurity and maintaining the concentration throughout the power cycle (no depletion of the B-10 impurity) introduces a significant reactivity penalty that will greatly affect the estimated number of effective full power days the core can remain critical. This assumption should however lead to a minimum cycle length estimate.

Since B-10 and other graphite impurities will burn out during the power cycle, a second bounding depletion was performed. This calculation assumed no initial B-10 impurity in the graphite structures and should lead to a maximum number of effective full power days for the initial power cycle. Both depletion curves with and without the B-10 impurity are shown in Figure 31.

In the case of the 6.9 ppm B-10 impurity, the core k-effective at beginning-of-life is slightly greater than 1.26 and drops to 1.21 after only three days because of the negative reactivity fission product buildup. Similarly, for the zero B-10 impurity case, the core k-effective at beginning-of-life is slightly greater than

1.32 and drops to 1.27 after only three days. The core then steadily depletes and losses criticality (crosses the k=1.0 threshold) after approximately 420 EFPD in the case of the 6.9 ppm B-10 and 540 EFPD in the case of zero initial B-10 impurity. This results in a 14-18 month power cycle length and is in good agreement with the General Atomics burnup prediction for the initial core loading of approximately 15.7 months. Extension of the power cycle may require either a higher enrichment or increased packing fraction, or both.

It should be noted that nuclear grade graphite will contain both burnable poisons (e.g. the B-10 considered here) as well as non-burnable poisons. The non-burnable poisons typically do not deplete during irradiation and their impact on core reactivity as a function of burnup will have to be assessed. Identification of both the burnable and non-burnable isotopes in the graphite along with estimates of their concentrations will be required for future neutronic calculations in order to assess their impact on core reactivity. A significant impact may require concentration limits in the material specifications for the structural block graphite, fuel compact binder graphite, and the particle coating materials.

Two re-load options have also been explored using 15.5 wt% U-235 enrichment fissile particles at a packing fraction of 0.279. The first option involved replacing half the core fuel blocks with fresh 15.5 wt% U-235 blocks. In this option, three adjacent blocks (one in Ring 6, 7, and 8) are fresh fuel and the next three adjacent blocks are depleted (420 EFPD from the initial core). This pattern is repeated azimuthally around the annular core. It turns out this is not a particularly good re-load option since the fresh blocks in Ring 6 draw disproportional amounts of total core power and result in very high fuel rod peaking for those fuel rods nearest the inner reflector. The peaking is not as bad for fresh blocks in Ring 8 (plus the control rods will help reduce the thermal flux in this region).

The second re-load option also replaces one half of the core fuel blocks with fresh 15.5 wt% U-235 blocks, but loads the inner active core ring (Ring 6) with depleted blocks (blocks burned for 420 EFPDs from the initial core), the inner active ring (Ring 7) with fresh blocks, and Ring 8 with mostly depleted blocks. This option produces a much more uniform radial core power distribution. The depletion of this re-load option, like the initial core loading, can also achieve a 420 to 540 EFPD burnup, as Reference 3 predicted.

Another fueling zoning option that could be considered is the loading of fresh fuel at the top of the core with fuel block movement axially downward at each cycle. For example, the top-third of the core could be loaded with fresh fuel, once-burned fuel in the middle-third of the core, and twice-burned fuel at the bottom-third. Fuel zone loading, such as this would result in more uniform radial flux distributions and allow for more control over the radial power peaking. However, loading and temperature reactivity effects would need to be further assessed, since the top of the core would now be more reactive relative to the middle and bottom of the core due to the heavier beginning-of-life uranium loading and cooler operating temperatures.

3.4.10. Temperature Coefficients of Reactivity

Three temperature dependent reactivity coefficients were calculated: 1) isothermal, 2) fuel Doppler, and 3) moderator. Uniform fuel and graphite temperature distributions were assumed throughout the core in each of the three coefficient calculations. Although these temperature distributions are somewhat idealized, the predicted trends should be reasonable approximations for the actual reactor temperature response. Also, the initial NGNP core conditions were used in these calculations, namely, an effective 10.36 wt% U-235 enrichment, a particle packing fraction of 0.289, and the 1/6-core layer model.

The calculated k-effective and coefficient magnitudes are presented in the following paragraphs for each of the three temperature coefficient components.

Isothermal. The isothermal temperature coefficient of reactivity was estimated for three burnup conditions: beginning-of-life or 0 EFPD, 200 EFPD, and 400 EFPD over the temperature range of 20-2200 ºC. In this calculation, each calculated core k-effective assumes that the fuel temperature (uranium) and graphite temperature (graphite in the fuel, fuel blocks, and reflector rings) are the same temperature and uniform throughout the reactor.

Figure 32 shows the calculated core k-effective as a function of uniform core temperature. Note the downward trend in k-effective with increasing temperature for all three burnup conditions. This results in a strong negative isothermal temperature coefficient. Note that the curves in Figure 32 are not smooth. This waviness is not due to the inherent statistical uncertainty of the calculated values, but rather the slight mismatch of the uranium and graphite temperature libraries. The graphite S(α,β) data libraries were only available at 27, 327, 527, 927, 1327, and 1727 ºC. The estimated isothermal temperature coefficients (Δk/ΔT) are shown in Figure 33 for the three burnup cases. The coefficients are all negative as expected, and range in magnitude between -1.5E-5 and -1.5E-4 (Δρ / ºC).

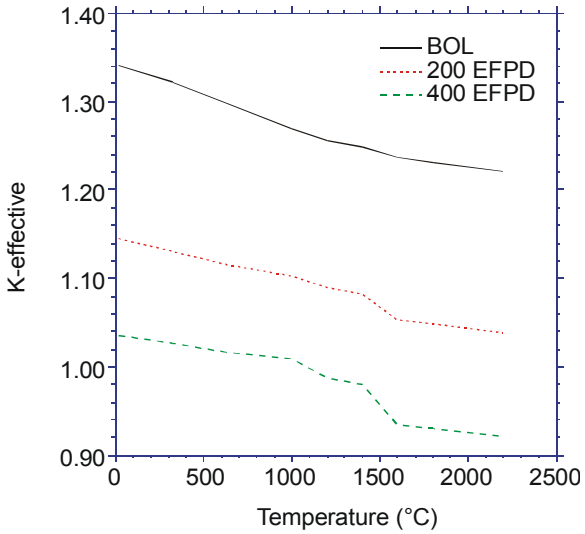

Figure 32. Isothermal core k-effective as a function of core temperature.

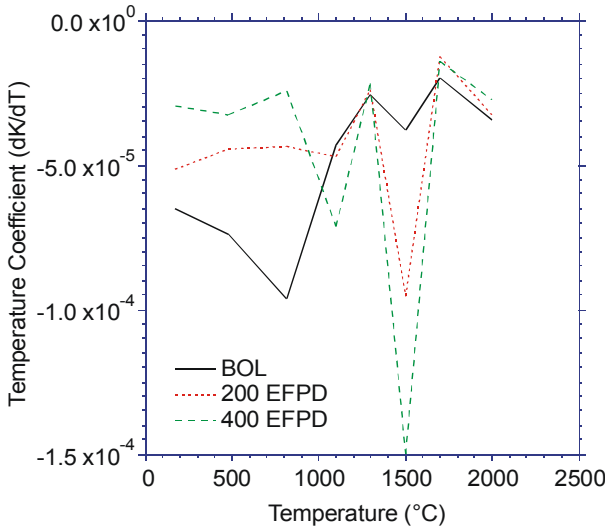

Figure 33. Isothermal core temperature coefficient as a function of core temperature.

Fuel Doppler. The fuel Doppler temperature coefficient of reactivity was estimated for three burnup conditions: 1) beginning-of-life or 0 EFPD, 200 EFPD, and 3) 400 EFPD over the temperature range of 20-2200 ºC. In this calculation, the calculated core k-effective assumes that the graphite moderator temperature (graphite in the fuel, fuel blocks, and reflector rings) is fixed at 927 ºC (1200 ºK) and the fuel (uranium) temperature is varied.

Figure 34 shows the calculated core k-effective as a function of fuel or uranium temperature. Note again the downward trend in k-effective with increasing temperature for all three burnup conditions. This results in a strong negative fuel Doppler temperature coefficient of reactivity.

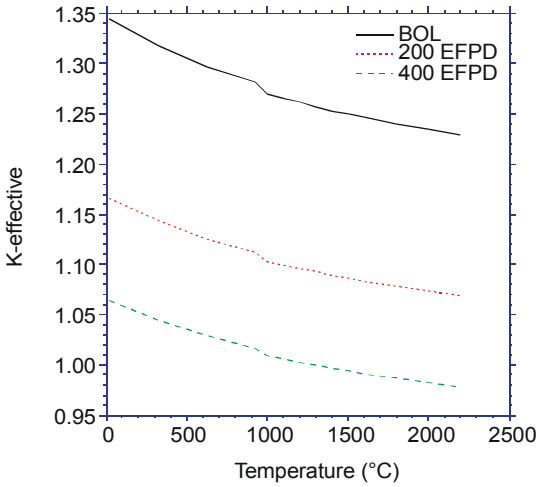

Figure 34. Doppler core k-effective as a function of fuel temperature, graphite moderator temperature fixed at 927 °C.

Also note the discontinuity in the three curves between 927 and 1000 °C. This discontinuity was traced to differences in the MCNP uranium (both U-235 and U-238) cross-section libraries. The cross section libraries at temperatures less than 927 °C were generated using ENDF/B-VI Revision 2 data and our newer cross section libraries at 1000 °C and above were generated with ENDF/B-VI Revision 5 data. Changes in the ENDF/B-VI U-235 data between Revision 2 (1995) and Revision 5 (1998) included modifications to the resonance parameters and fission neutron yields (nubar). The resonance data were re-evaluated over the entire resolved resonance energy range. The capture resonance integral over the energy range 0.5 eV to 20 MeV increased about 6%, while the fission resonance integral decreased about 1%. The changes in nubar were less significant, with the yield increased from 2.4320 to 2.4367 over the energy range of 1.0E-5 eV to 1.0 eV, and increased from 2.4320 to 2.4338 over the energy range 2.0 eV to 10,000 eV. The yield was unchanged above 15,000 eV. The relatively large increase in the capture integral was probably the most significant change, and most likely is the reason for the 1% drop in the eigenvalues shown in Figure 34. The only change made to the U-238 cross section data was a reduction in the capture cross section at 0.0253 eV from 0.3326 to 0.3320 barns, with appropriate adjustments at lower energies to maintain the 1/v behavior.

The estimated fuel Doppler temperature coefficients (Δk/ΔT) are shown in Figure 35 for the three burnup cases. The coefficients are all negative as expected and range in magnitude between -2.0E-5 and -9.0E-5 (Δρ / ºC).

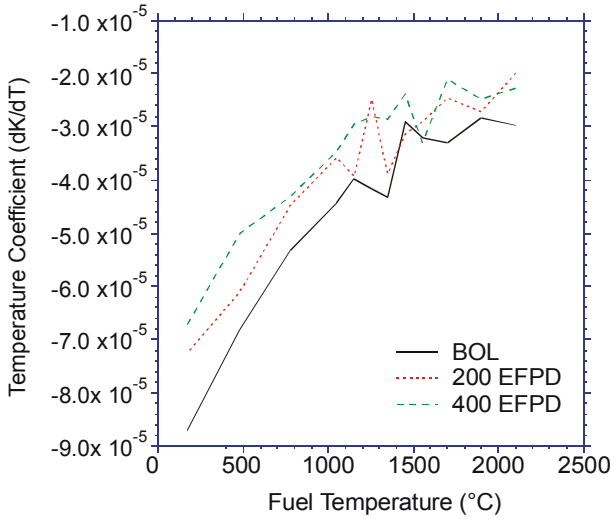

Figure 35. Doppler temperature coefficient of reactivity as a function of fuel temperature with the graphite moderator temperature fixed at 927 °C.

Moderator. The moderator temperature coefficient of reactivity was also estimated for three burnup conditions: beginning-of-life or 0 EFPD, 200 EFPD, and 400 EFPD over the temperature range of 300-2000 ºK (27-1727 ºC). In this calculation, each calculated core k-effective assumes that the fuel temperature (uranium) is held constant at 1100 ºC and graphite temperature (graphite in the fuel, fuel blocks, and reflector rings) is varied.

Figure 36 shows the calculated core k-effective as a function of moderator temperature. Note the upward trend in k-effective at the lower end of the temperature range before the curves bend over and exhibit the desired negative slope for all three burnup conditions. These curves indicate that the moderator temperature coefficient will have a relatively small, but positive value over part of the temperature range.

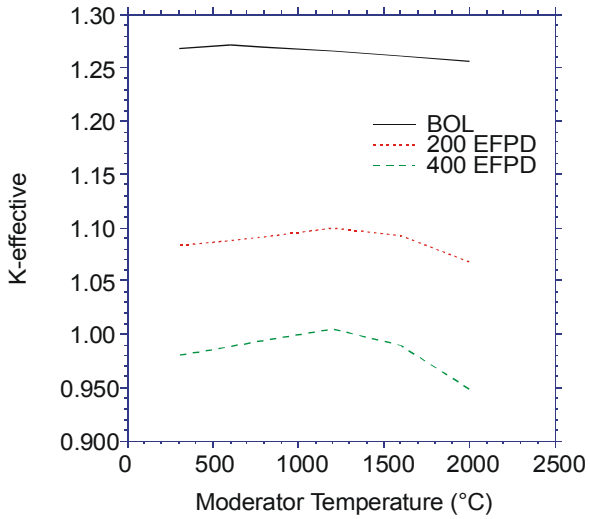

Figure 36. K-effective as a function of moderator temperature with a fixed fuel temperature at 1100 °C.

The estimated moderator temperature coefficients (Δk/ΔT) are shown in Figure 37 for the three

burnup cases. The moderator coefficients shown in Figure 37 are derived from fourth-order polynomial fits to the k-effective curves in Figure 36, hence the relative smoothness of the coefficient functions. Both the positive and negative portions of the moderator coefficient are apparent. The positive portion appears mainly at lower temperatures and is burnup dependent, 20-600 ºC at beginning-of-life and approximately 20-1200 ºC at both 200 and 400 EFPD. The maximum positive magnitude (+4.0E−5 Δρ / ºC) occurs at 700 ºC for the 400 EFPD case. The moderator coefficient is negative at the upper temperature range (1200-2000 ºC) and tends to increase in magnitude with increasing burnup.

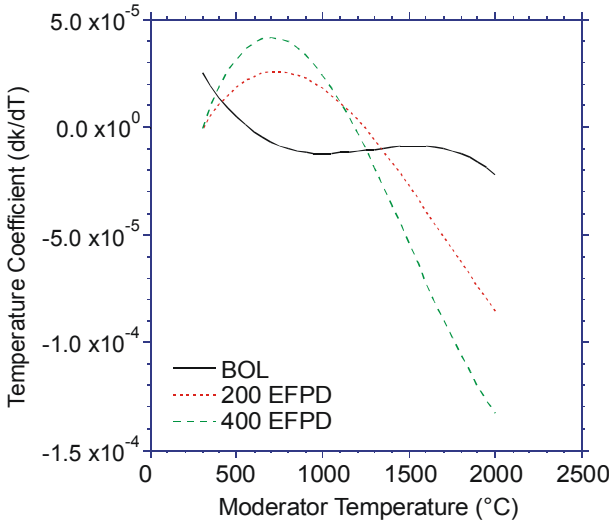

Figure 37. Moderator temperature coefficient as a function of moderator temperature with a fixed fuel temperature of 1100 °C.

3.4.11. Fuel Rod Power Peaking

Parametric studies are currently underway to reduce the power peaking in the fuel rods across the annular core. In particular, we are interested in reducing the power peaking in those fuel rods at the reflector-active core interface. The unshielded fuel rods at the interface experience a relatively large reflected thermal neutron current that results in high relative rod powers. The fuel rods at the outer reflector interface have lower power peaking relative to the fuel rods at the inner interface because of the control rods in the outer reflector (Ring 9) and because of the higher radial neutron leakage. Peaking parametric studies currently under investigation involve the following six options:

1. Loading of discrete burnable poison rods with burnable poisons.
2. Placement of discrete burnable poison rods in fuel rod Rows 1-4 nearest the interface which would involve substitution of burnable poison rods for fuel rods.
3. Variation of the particle packing fraction in the fuel rods in Rows 1-4 nearest the interface.
4. Variation of the uranium enrichment in the fuel rods in Rows 1-4 nearest the interface.
5. Burnable poison loading in the inner graphite reflector blocks (Ring 5 only).
6. Use of different burnable poisons (B-10, Gd, Er, etc).

The fuel rod peak-to-average powers for the initial core loading at beginning-of-life conditions (packing fraction=0.289, 10.36 wt% U-235 enrichment) with no burnable poison loading are presented in Figures 38 and 39 (the figures for this section are all at the end of the section) for three standard and adjacent fuel blocks in Rings 6, 7, and 8 (left to right in the figures). Figure 38 gives the individual rod peak-to-average numerical values and Figure 39 gives a bubble-view of the relative magnitudes of the peak-to-average values. Note the maximum value of 1.58 occurs in the fuel rod row (Row 1, Ring 6) nearest the inner reflector block-active core interface. The MCNP fission power tallies are used here to estimate the fission power of each fuel rod in every fuel block in the 1/6-core model, but only the three standard fuel blocks are presented for brevity.

Option No. 1: Discrete Burnable Poison Rods. Figures 40 and 41 are similar to Figures 38 and 39, except that some of the discrete burnable poison positions at the corners of the blocks are now loaded with boron carbide (B_4C) instead of graphite in an attempt to reduce the power peaking in the fuel rods nearest the interface. Although there are holes for loading the discrete burnable poison in all six corners of each of the hexagonal fuel blocks, only the three positions at the interface are loaded with the B_4C.

The burnable poison rods contain a mixture of B_4C plus graphite shim (61 vol%) and matrix graphite (39 vol%). The B_4C is 5.0% by volume of the B_4C plus graphite shim and matrix mixture and the boron is 90% B-10. The addition of the B_4C reduces the maximum power peak to 1.48 (a 6.7% reduction).

Loading of the other allocated burnable poison positions at the corners of the blocks can significantly impact the core reactivity. However, use of these other positions may be desirable later for core reactivity hold-down, particularly if we need to increase the fuel block uranium loading to achieve the longer power cycle lengths.

Figures 42 and 43 present the rod power peaking factors for the same conditions as Figures 40 and 41, except the B_4C volume percent in the B_4C plus graphite shim and matrix composition is reduced from 5.0% to 1.0%. This effect further reduces the maximum peaking factor to 1.30 (a 17.7% reduction), and, in addition, the core reactivity increases from 1.16 to 1.21. Further improvements should be possible for other, perhaps more optimal, B_4C loadings and with careful placement of the discrete poison rods in the fuel Rows 1-4 nearest the interface.

Option No. 3: Particle Packing Fraction. The effect of particle packing fraction on the fuel rod power peaking was studied by varying the fuel rod particle packing fraction in the fuel blocks (Ring 6) adjacent to the inner reflector, and specifically just those fuel rods in Rows 1-4 closest to the inner reflector interface. (Row 1 was arbitrarily designated as the line of fuel rods closest to the inner reflector interface.) All the fuel rods had a packing fraction of 0.289 and an effective uranium enrichment of approximately 10.36 wt% U-235 in the initial beginning-of-life 1/6-core layer model. The packing fractions considered included: 0.25, 0.289, 0.35, 0.40, 0.45, and 0.50. For each packing fraction, four cases were evaluated. The first case changed the packing fraction in just the first row (Row 1). Then Rows 1 and 2 were changed together, followed by Rows 1, 2, and 3, and finally Rows 1, 2, 3, and 4 (or until all four rows had the same modified packing fraction). The rest of the fuel rods in the core were always maintained at a packing fraction of 0.289. The uranium enrichment was held constant throughout the packing fraction study.

The results of the particle packing fraction studies showed that a reduction in the packing fraction can reduce the power peaking in those fuel rods in the vicinity to the inner graphite reflector interface. Changing the packing fraction from 0.289 to 0.25 in Row 1 reduced the maximum power peaking factor from 1.58 to 1.50 (a 5% reduction). A packing fraction of 0.25 in Rows 1 and 2 reduces the maximum peaking factor from 1.58 to 1.40 (an 11% reduction), see Figures 44 and 45. Further row conversions to a packing fraction of 0.25 did not produce a discernable further decrease in the fuel rod power peaking factors.

Increasing the packing fraction above 0.289 in Rows 1-4 only served to increase the maximum power peaking factor. For example, with a packing fraction of 0.35 in Rows 1 and 2, the maximum power peaking factor increases from 1.58 to 1.87 (an 18% increase); with a packing fraction of 0.40 in Rows 1 and 2, the maximum power peaking factor increases from 1.58 to 2.08 (a 32% increase).

It is concluded that reducing the packing fraction below 0.289 in rows 1-4 can reduce the maximum fuel power peaking factor and should be considered a viable method to achieve needed reductions. This study only considered the packing fraction of 0.25, and it is recommended that future studies consider additional packing fractions below 0.289, and even below 0.25 to locate the optimal packing fraction. Grading the packing fraction across the four rows may also provide some benefit.

Option No. 4: Enrichment. The effect of fissile particle enrichment on the fuel rod power peaking was also studied by varying the fuel rod enrichment in the fuel blocks (Ring 6) adjacent to the inner reflector, and again specifically just those fuel rods in Rows 1-4 closest to the inner reflector interface. As

mentioned above, all the fuel rods had a packing fraction of 0.289 and an effective uranium enrichment of approximately 10.36 wt% U-235 in the initial beginning-of-life 1/6-core layer model. The additional fuel rod effective enrichments considered here included: 4, 6, 8, and 10.36 wt% U-235. Enrichments above 10.36 wt% were not considered, since higher power peaking was expected. As in the packing fraction study, four cases were evaluated for each enrichment. The first case involved changing the enrichment in just the first row (Row 1). Then Rows 1 and 2 were changed together, followed by Rows 1, 2, and 3, and finally Rows 1, 2, 3, and 4 (or until all four rows had the same modified enrichment). The rest of the fuel rods in the core were always maintained at the reference enrichment of 10.36 wt% U-235. The particle packing fraction was held constant throughout the enrichment study.

The results of the particle enrichment studies showed that a reduction in the enrichment reduces the power peaking. For example, reducing the 10.36 wt% enrichment to an 8.0 wt% enrichment in Row 1, Rows 1-2, Rows 1-2-3, and Rows 1-2-3-4 reduces the maximum power peaking factor by 4.6, 10.8, 11.6, and 15.5%, respectively. Figures 46 and 47 present the results for the case with 8.0 wt% enrichment in all four fuel rod rows. The peaking factor results for the 6.0 wt% case were not quite as good as for the 8.0 wt% case. And, peaking factor results for the 4.0 wt% case were not as good as for the 6.0 wt% case.

The power peaking was not mitigated when there were relatively large step-changes in the row enrichment. For example, a step change of 4.0 wt% (Row 1) to 10.36 wt% (Row 2), simply pushed the peak power rod into Row 2 with little or no reduction in the overall maximum peaking factor. Reducing the uranium enrichment from 10.36 wt % to 8.0 wt%, rather than 6.0 or 4.0 wt %, gave the best reductions in the fuel rod peaking.

It is concluded that reducing the enrichment below 10.36 wt% in Rows 1-4 can reduce the maximum fuel power peaking factors and should also be considered a viable method to achieve needed reductions. Grading the enrichment across the four rows may provide the best benefit.

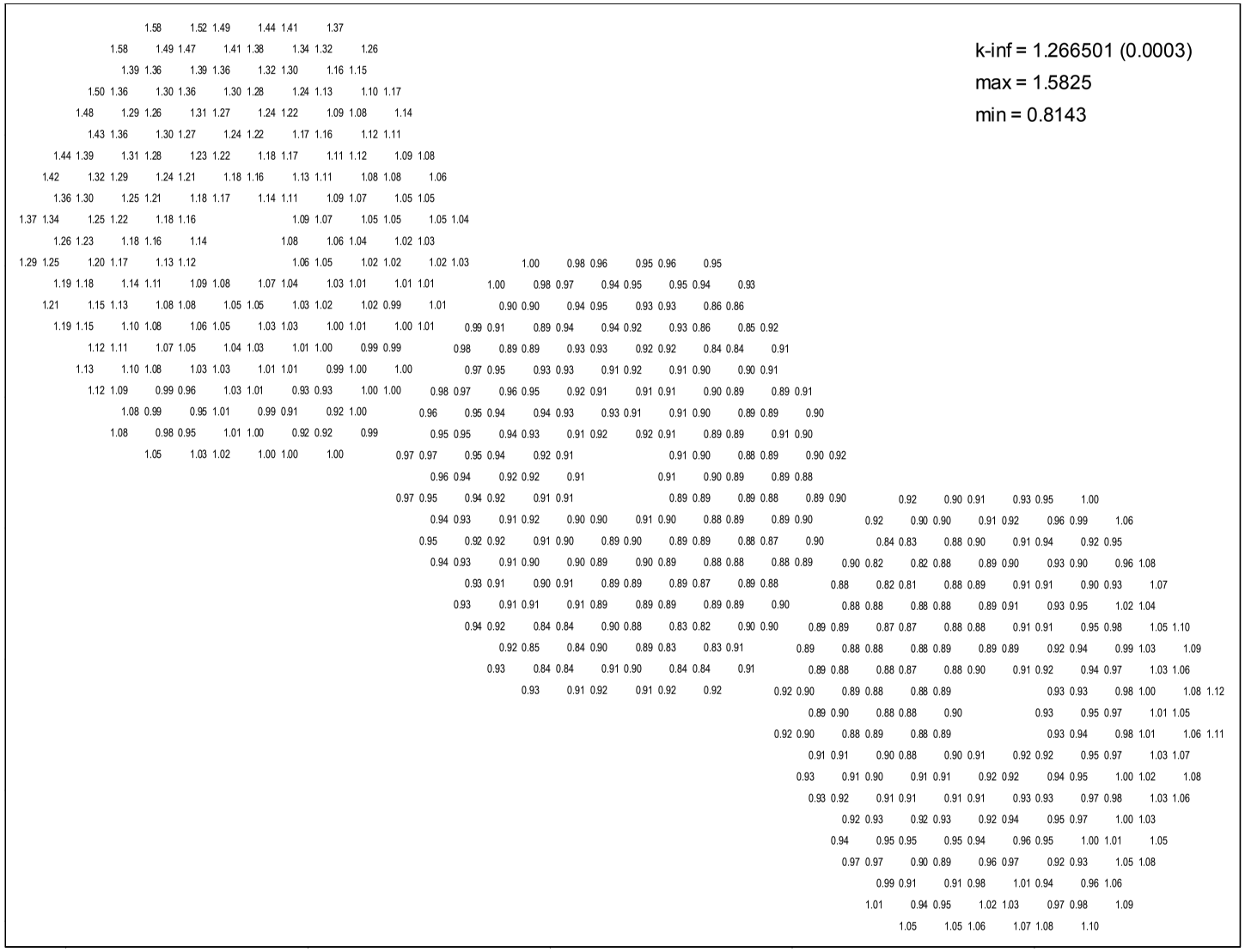

Figure 38. Peak-to-average fuel rod powers for three standard fuel blocks in Ring 6 (upper left), Ring 7, and Ring 8 (lower right) with no burnable poison loading.

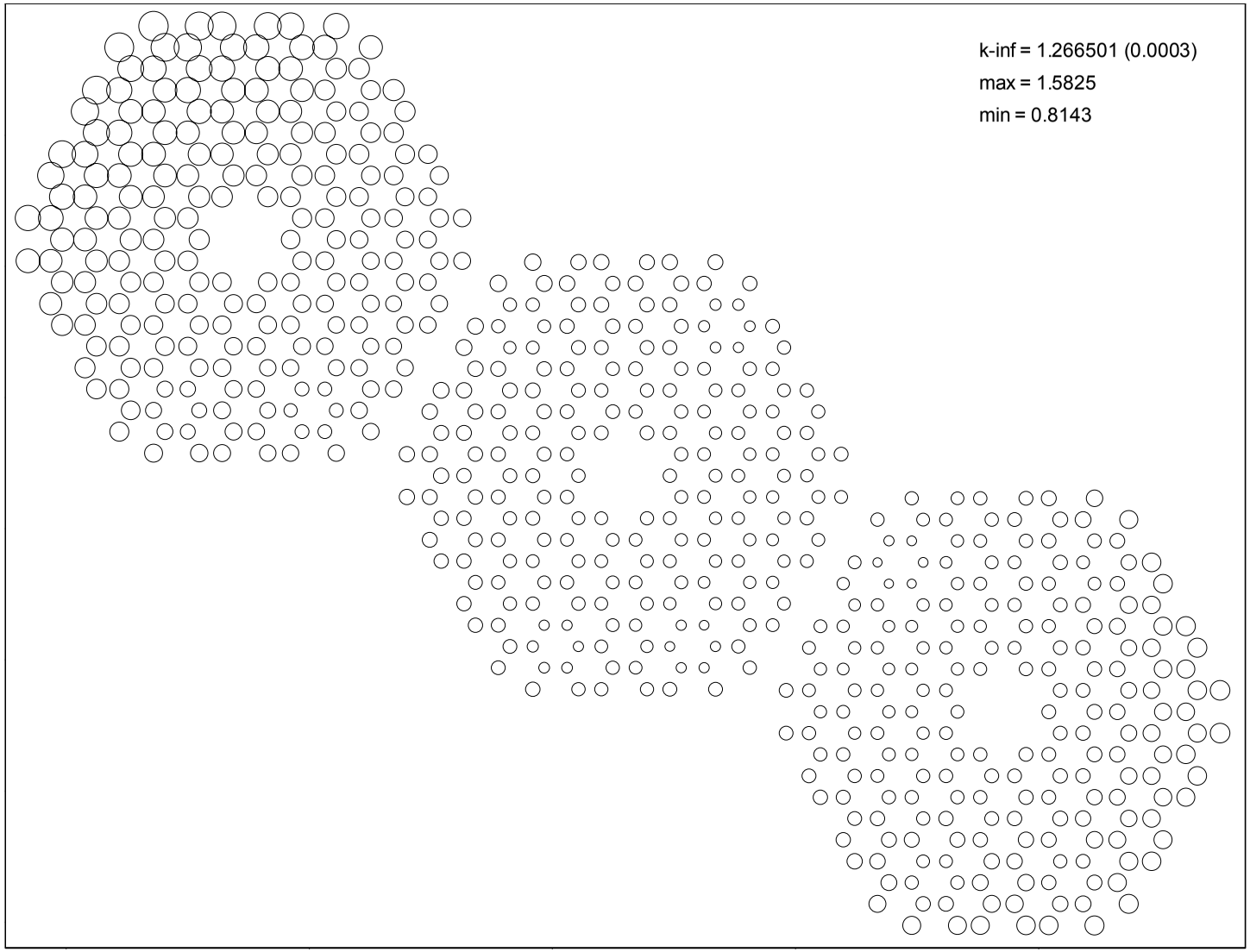

Figure 39. Peak-to-average fuel rod powers for three standard fuel blocks in Ring 6 (upper left), Ring 7, and Ring 8 (lower right) with no burnable poison loading. (The circle diameter is indicative of the relative rod powers).

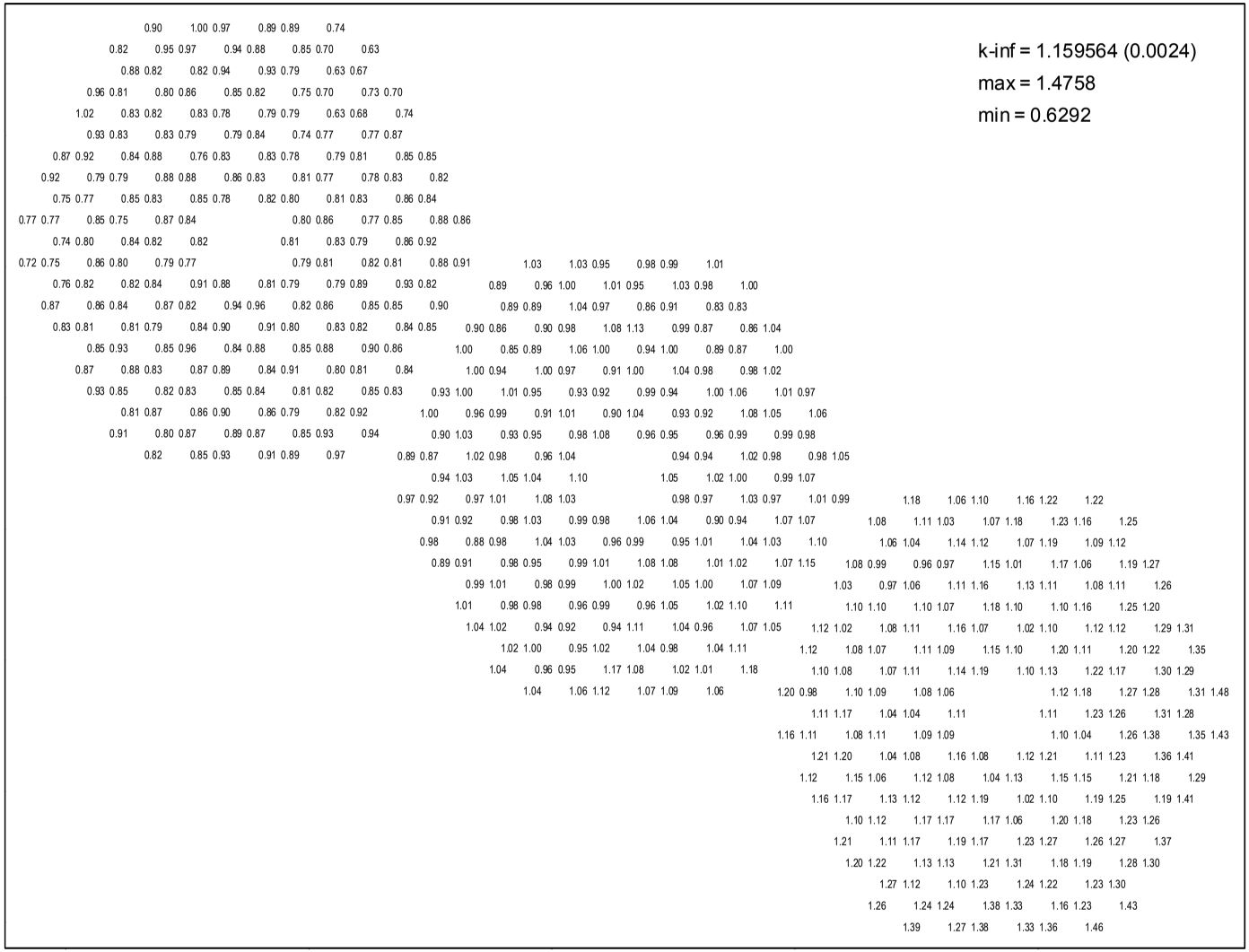

Figure 40. Peak-to-average fuel rod powers for three standard fuel blocks with three discrete burnable poison (B_4C) rods in each fuel block at the inner reflector interface only. The boron is 90% B-10 and the B_4C is 5.0% of the B_4C plus graphite shim and matrix mixture.

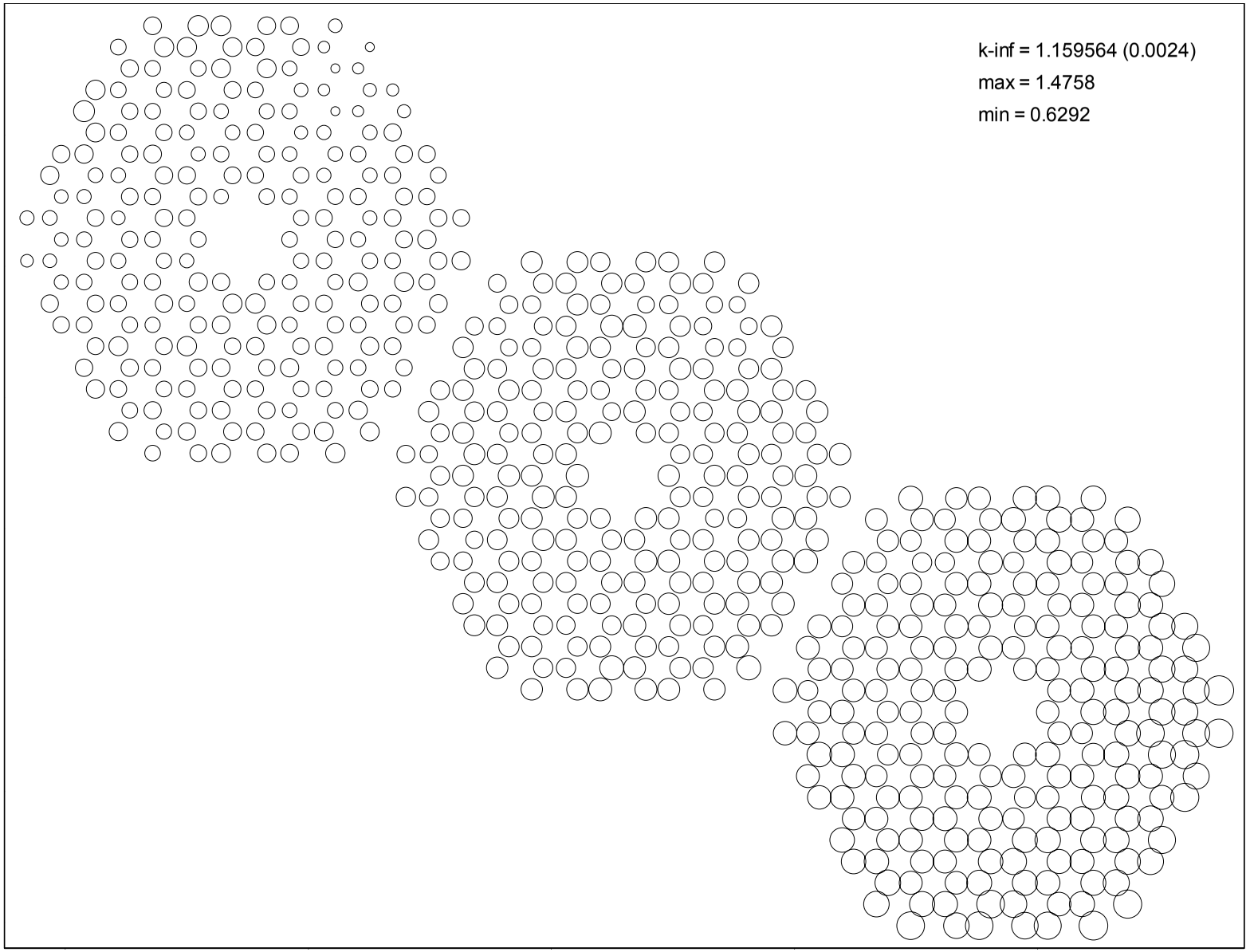

Figure 41. Peak-to-average fuel rod powers represented with circles proportional to the ratio values in Figure 40.

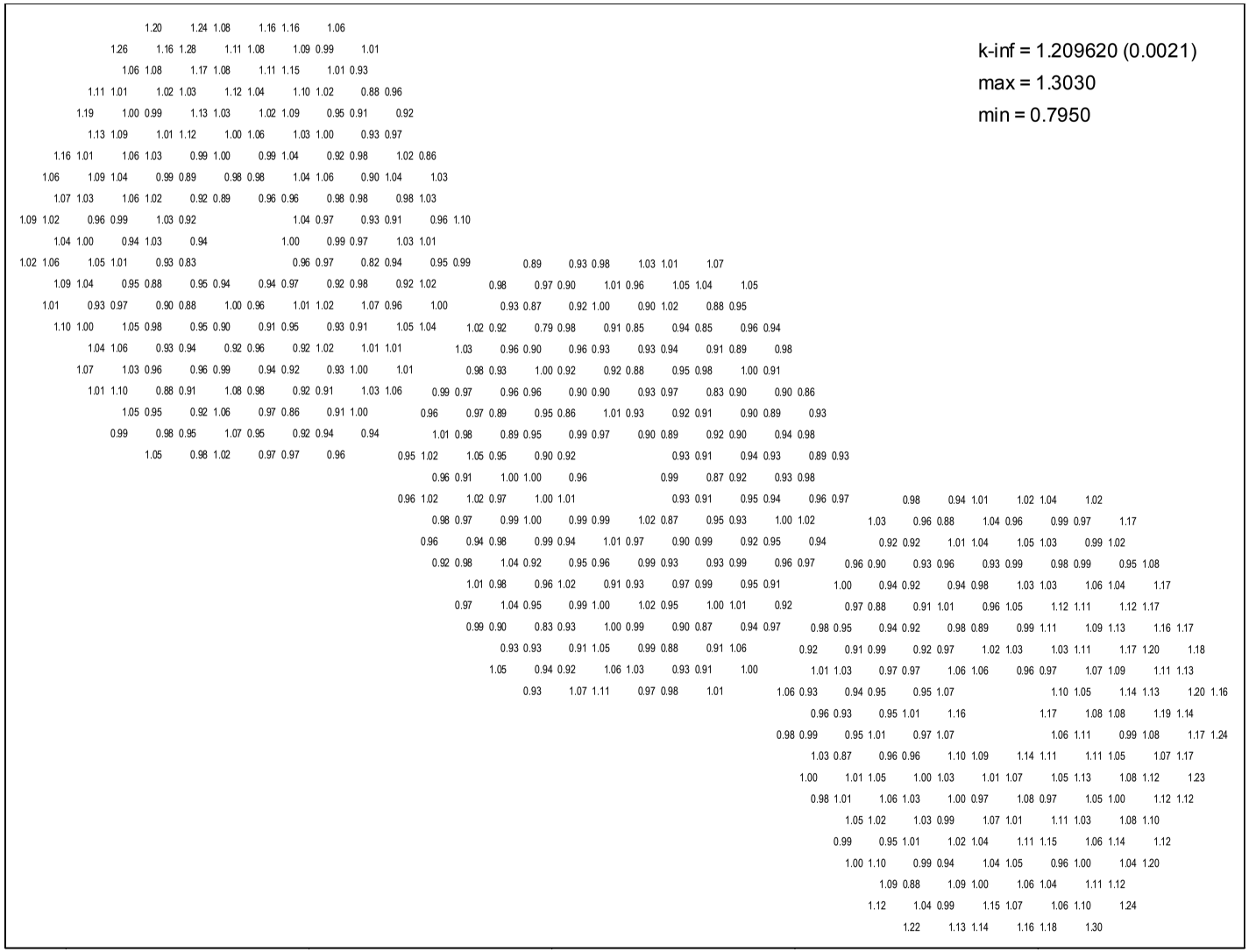

Figure 42. Peak-to-average fuel rod powers for three standard fuel blocks with three discrete burnable poison (B_4C) rods in each fuel block at the inner reflector interface only. The boron is 90% B-10 and the B_4C is 1.0% of the B_4C plus graphite shim and matrix mixture.

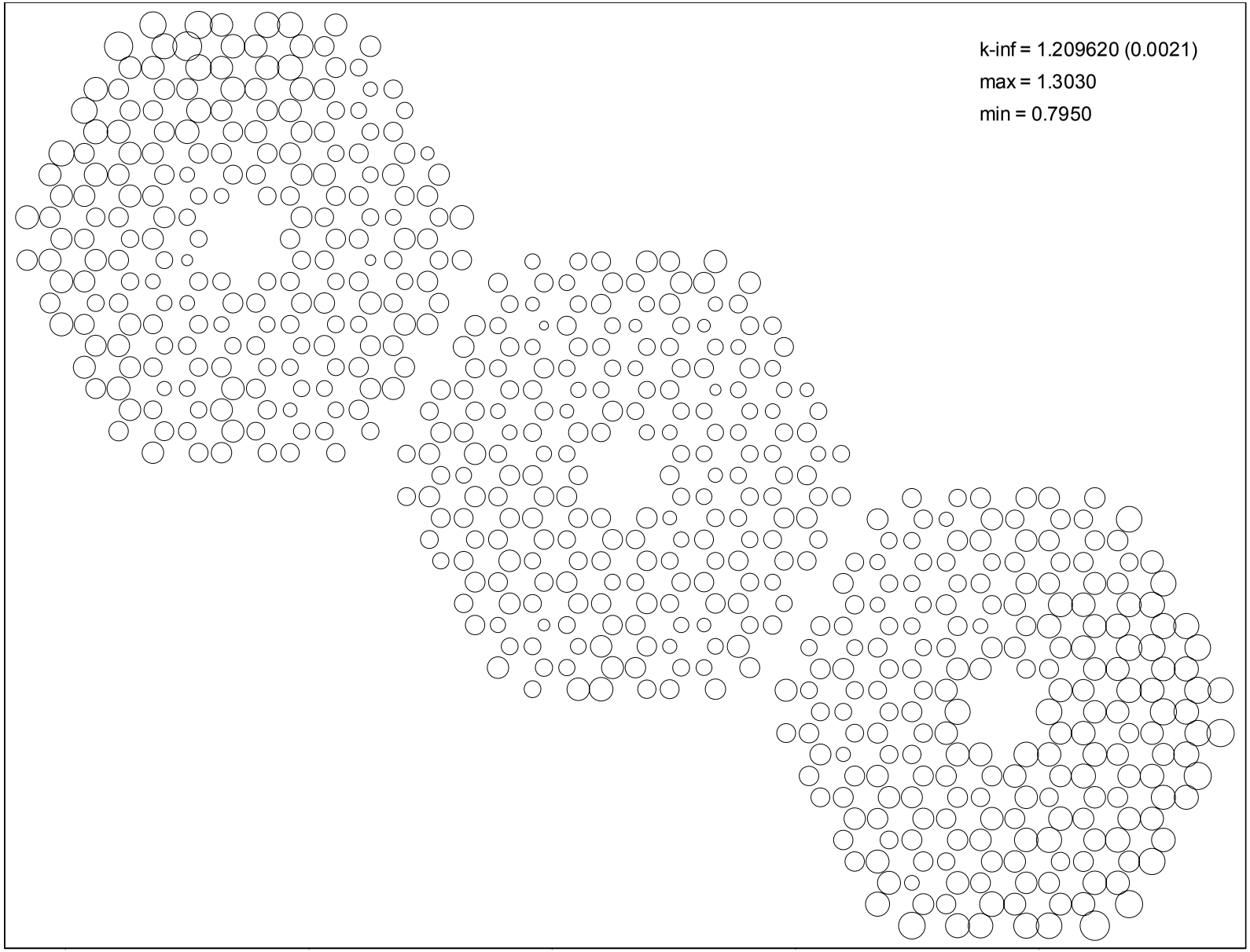

Figure 43. Peak-to-average fuel rod powers represented with circles proportional to the ratio values in Figure 42.

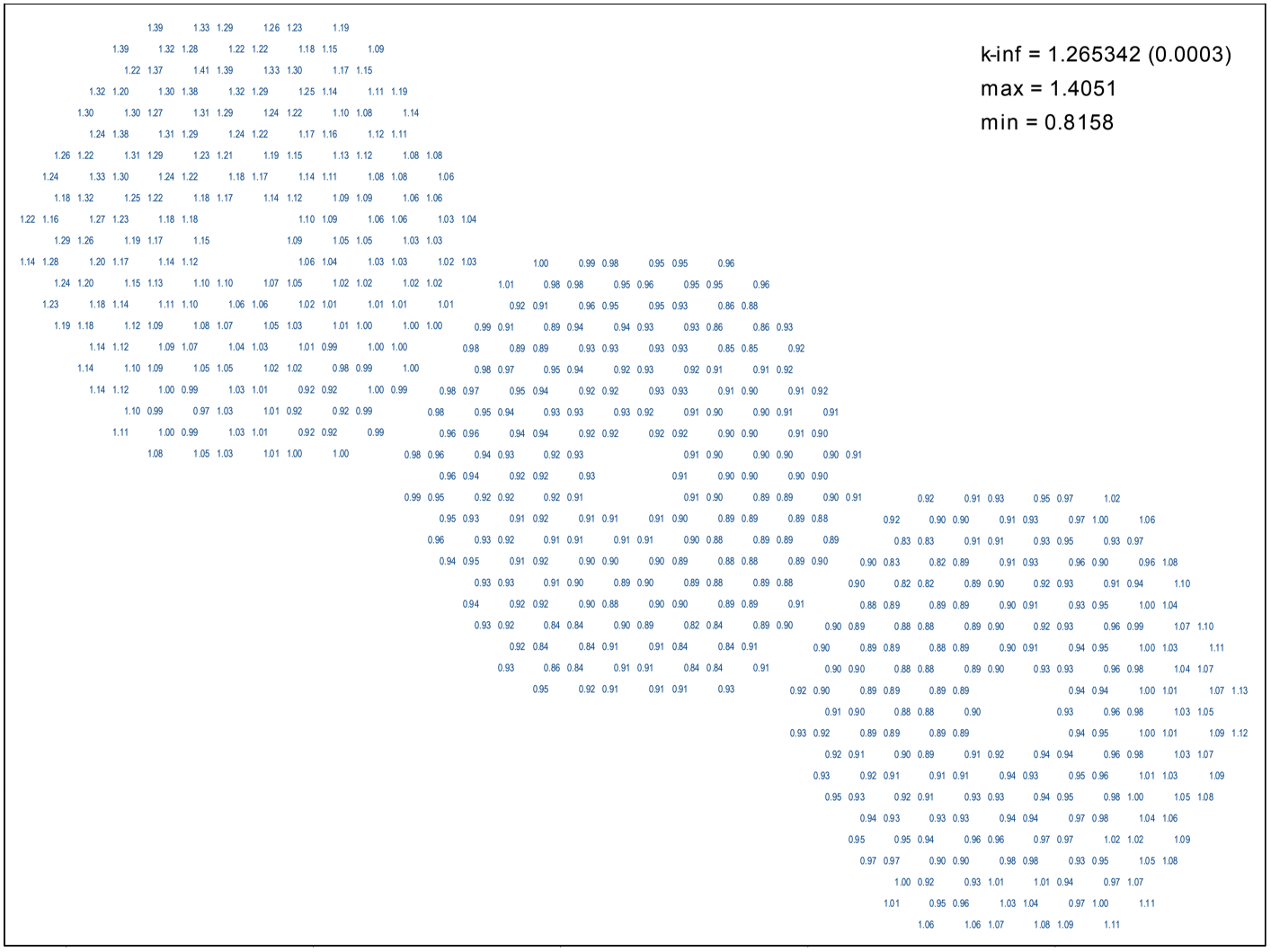

Figure 44. Peak-to-average fuel rod powers for three standard fuel blocks with a particle packing fraction of 0.25 in Rows 1 and 2 (Ring 6 fuel block in upper left hand corner of figure) and the rest of the fuel rods with a packing fraction of 0.289.

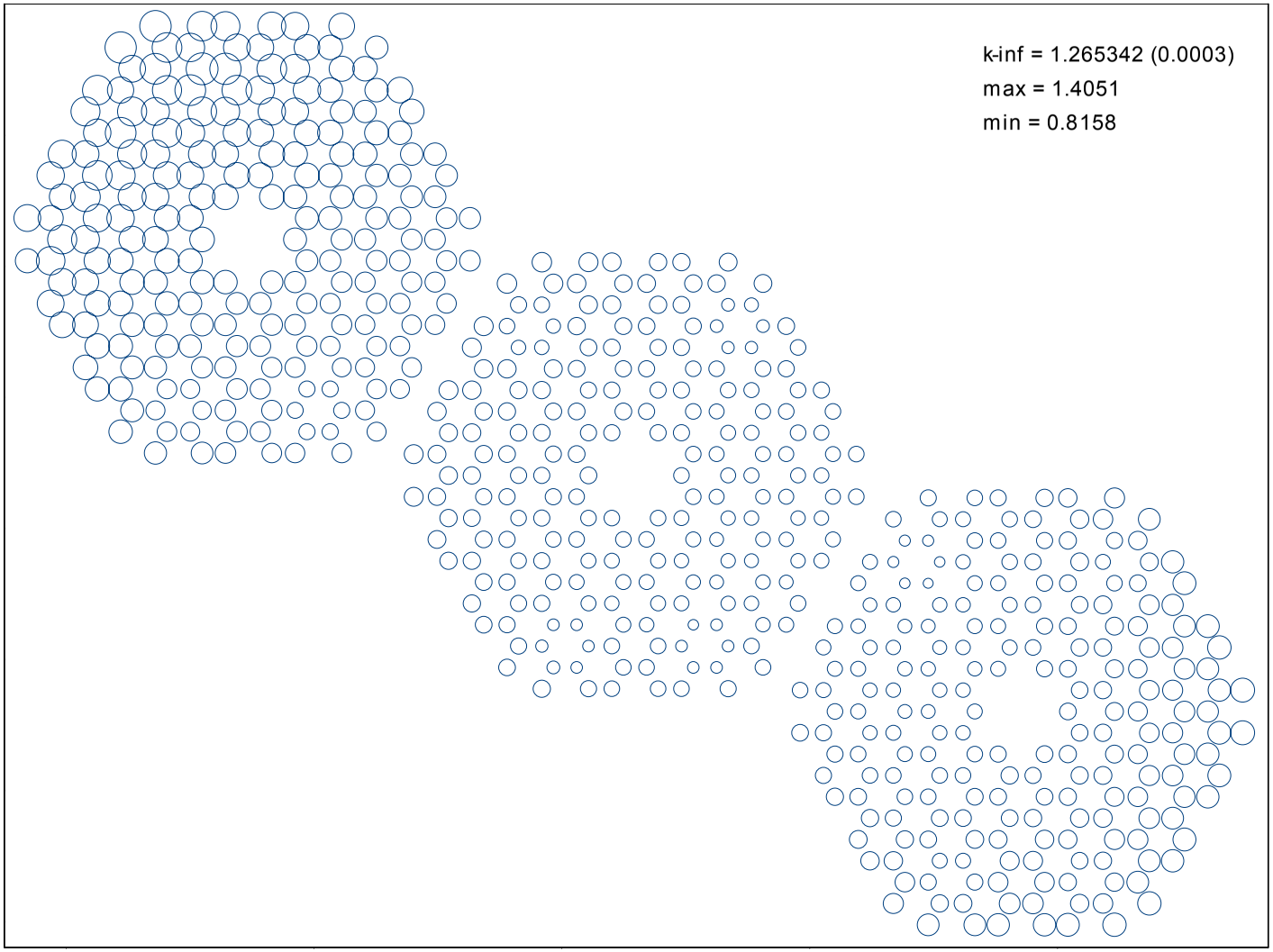

Figure 45. Peak-to-average fuel rod powers represented with circles proportional to the ratio values in Figure 44.

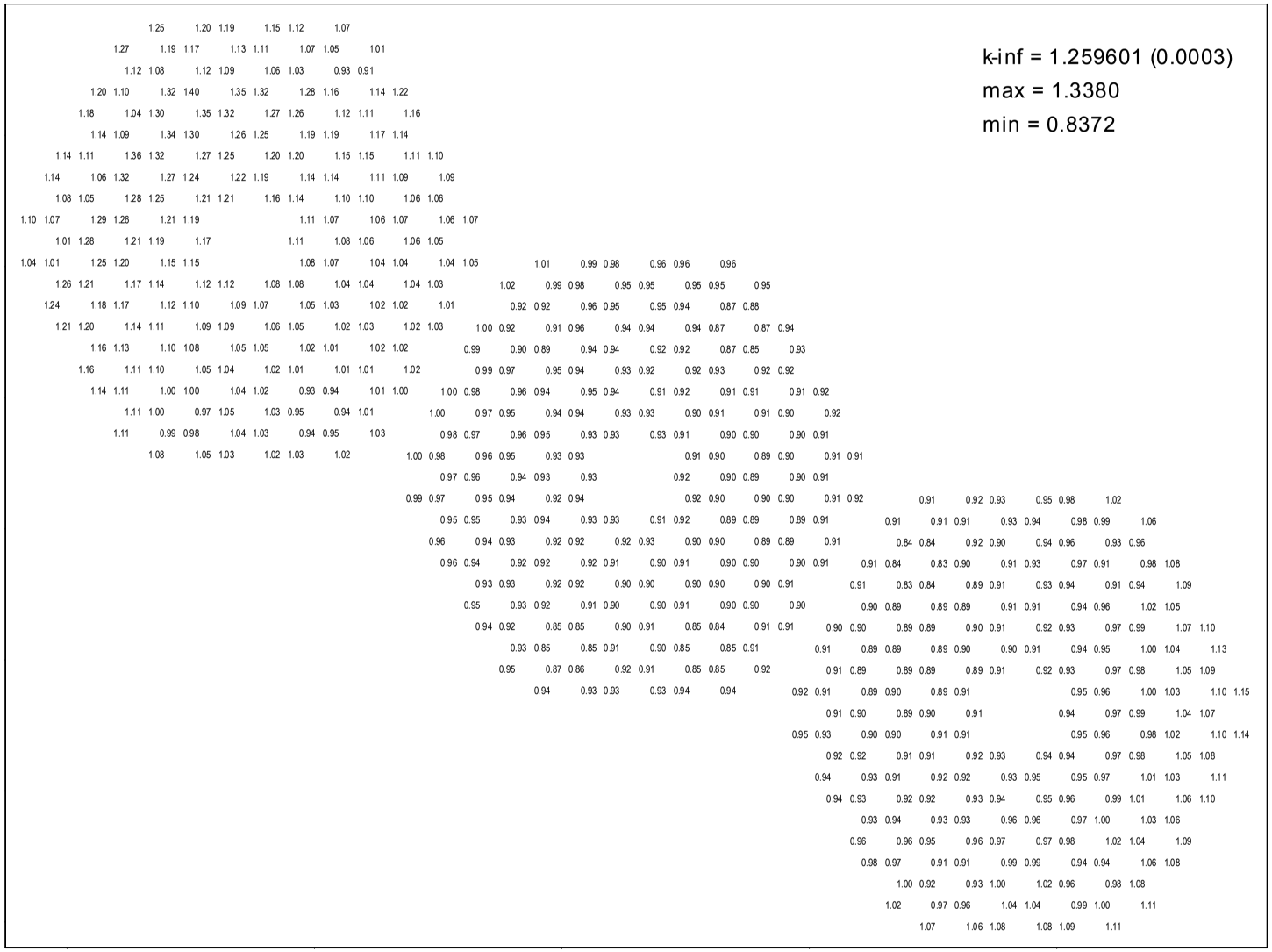

Figure 46. Peak-to-average fuel rod powers for three standard fuel blocks with a reduced enrichment (8.0 wt% U-235) in Rows 1, 2, 3, and 4 (Ring 6 fuel block in upper left hand corner of figure) and the rest of the core fuel rods with an enrichment of 10.36 wt%.

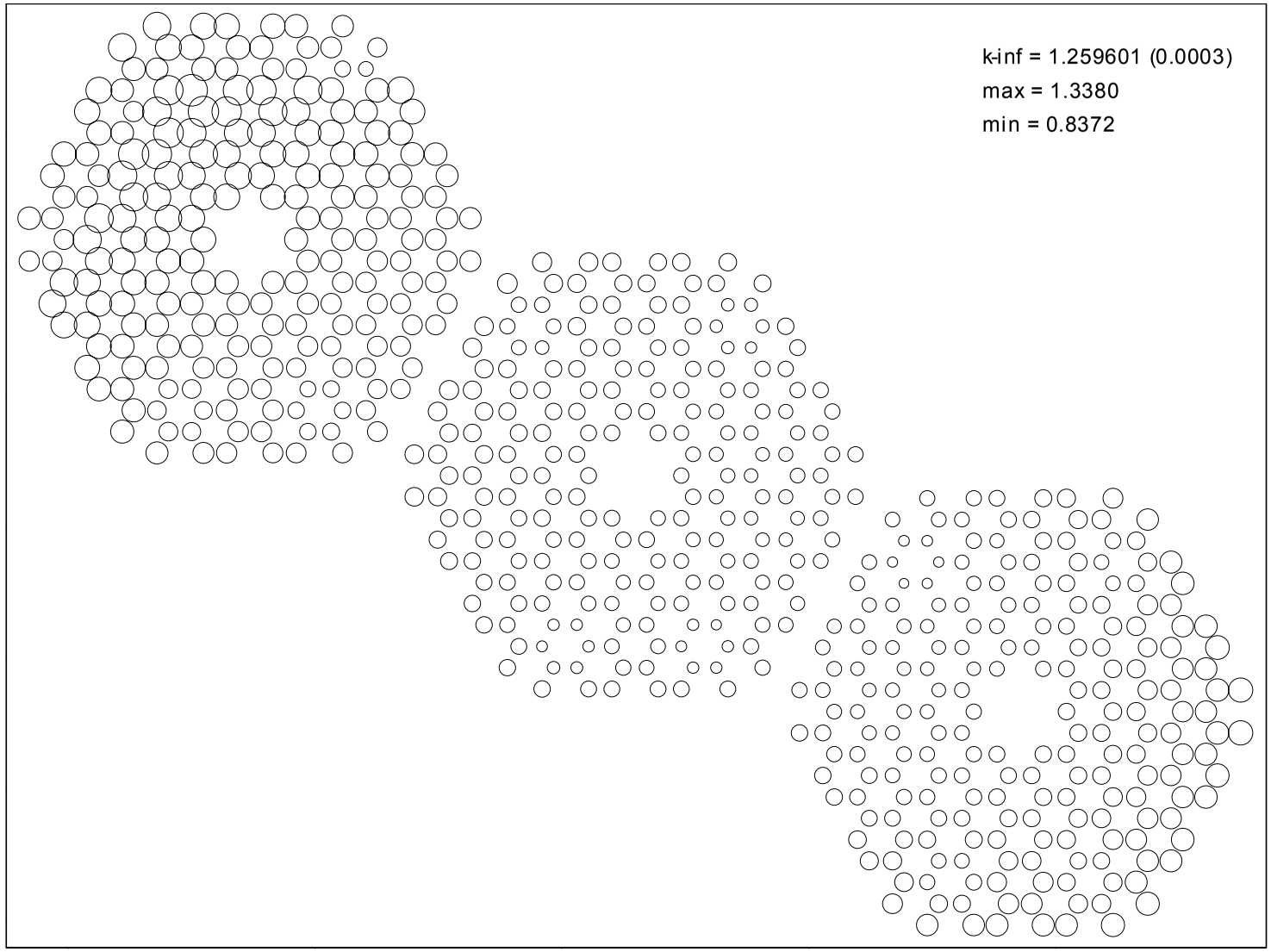

Figure 47. Peak-to-average fuel rod powers represented with circles proportional to the ratio values in Figure 46.

3.4.12. Decay Heat

An equilibrium decay heat curve was generated for a single standard fuel block after 417 EFPD at an average fuel block steady-state power level of 0.588 MWt. The fuel block was assumed to have an approximate 10.36 wt% U-235 enrichment, a particle packing fraction of 0.289, a fuel rod radius of 0.6225 cm, and a single fissile particle with a kernel diameter of 350 microns. The total beginning-of-life uranium block loading was then 492.15 g U-235 and 4,257.97 g U-238. Following the 417 EFPD burnup, the fuel block decay heat was calculated with the ORIGEN-2.1 code from zero to 7.5 days. This relatively short decay time period was sufficient to envelope the transient response times needed for the thermo-hydraulic analyses presented in Section 4 of this report. The primary purpose in generating this decay curve was to compare it to other reference decay heat curves in order to ensure that the decay power used in the thermal-hydraulic analyses were indeed reasonable. Figure 48 shows the ORIGEN-2.1 calculated decay heat curve as a function of decay time.

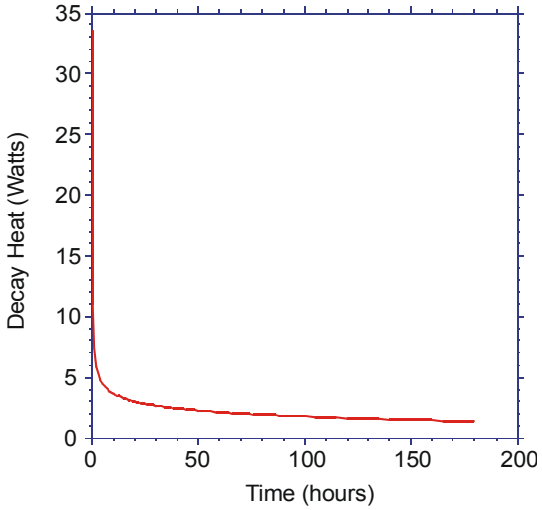

Figure 48. Decay heat curve for a single NGNP standard fuel block.

3.5. Neutronic Stability of the NGNP as a Function of Axial Height (General Atomics)

Xenon 135 is produced directly from fission, and from the decay of iodine135, as follows:

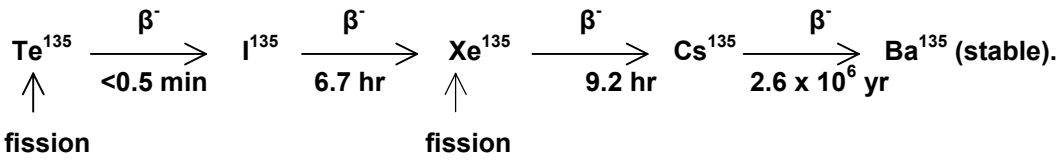

Xenon 135 is lost by decay, and by neutron absorption. As a result of the I-135 and Xe-135 decay times being similar, spatial power oscillations can be induced in the core by out-of-phase fluctuations in the I-135 and Xe-135 atom densities. In general, these spatial power oscillations may, or may not, be damped in magnitude. Whether or not the oscillations are damped does not depend on the magnitude of the initial forcing function, such as control rod motion, but depends only on the characteristics of the reactor, such as the core composition, dimensions, and power density.

The neutron mean free path in graphite-moderated reactors (HTGR) is much larger than that in a LWR of the same power level. Thus, from a neutronic standpoint the HTGR is much smaller than the equivalent LWR. Since the tendency for xenon oscillations in a reactor is proportional to core neutronic size, HTGR cores are more stable than equivalent LWR cores. Large power LWR cores can have divergent xenon induced power oscillations, and control rod programs have been developed to stop these oscillations and ensure stable operation. Such control rod programs could

be used in HTGR cores if needed. Early studies on large HTGR cores, up to 3500 MWt, showed overall stability to xenon oscillations at 2500 MWt, but instability at 3500 MWt. These analyses also demonstrated that control rod power management schemes could keep these oscillations within acceptable limits.[14] During the initial power operation testing of Fort St. Vrain, the USNRC requested that the reactor stability be demonstrated. The power distribution in the core was tilted by the control rods for several hours, after which the reactor was balanced again. The subsequent reactor power distribution turned out to be a highly damped oscillation and did not demonstrate any instability.

3.5.1. Axial Power Stability in 450 MWt and 600 MWt GT-MHR Cores

The stability of the GT-MHR axial power to xenon oscillations has been investigated with a series of computer studies for both the 450 MWt and 600 MWt designs using low enriched uranium fuel of two fuel particle types, one containing 19.9% enriched uranium and the other containing natural uranium. Both of these reactor designs have the same basic core layout, i.e., they consist of 3 rings of hexagonal graphite-block fuel elements arranged around an inner annulus of rings of graphite reflector blocks, and both cores are ten fuel block layers high (Refs 15, 3). The major difference in the two designs is that the 600 MWt core had an additional ring of graphite reflector blocks in the inner annulus (4 rings plus the central column), and thus has 102 fuel columns versus 84 columns for the 450 MWt design.

Stability against xenon induced oscillations, in the case of the 450 MWt core design, was evaluated including the effects of temperature feedback, using the FEVER-POKE-MICROX code package.[16] Since the magnitude of the initiating perturbation does not determine whether the power fluctuations are damped, it was convenient to use an instantaneous startup as the initiating event. This was performed at the time point of interest in the cycle by decreasing the reactor power to zero for a period of fourteen days (the normal refueling time) to allow all of the I-135 and Xe-135 to decay. The reactor power was then increased from 0% to 100% power, and the I-135 and Xe-135 atom densities increased as fissions take place. But as the Xe-135 atom density increases, it effects the axial power distribution, and can result in a spatial power oscillation, depending on the characteristics of the core.

Axial fuel zoning was used in the 450 MWt core design to achieve a relatively stable cosine power shape, which minimizes axial power peaking factors. Three axial fuel zones were used, a top layer of three fuel blocks, a middle layer of 4 blocks, and a bottom layer of 3 blocks. The 19% enriched / natural uranium ratio was varied in each zone. Figure 49 shows the resulting axial power shape and its behavior with burnup. The axial power factors are listed in Table 8.

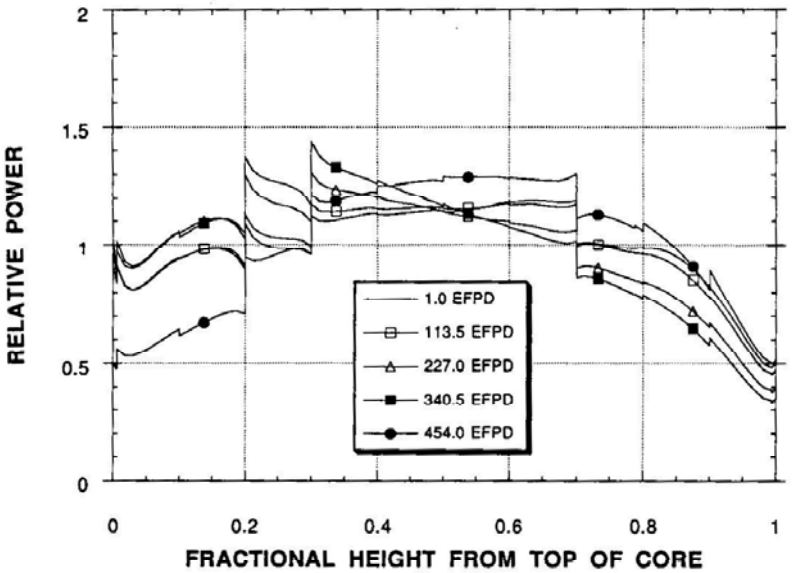

Figure 49. Axial power distribution in the 450MWt core as a function of burnup during the initial cycle.

Table 8. Axial power factors in the initial cycle.

Axial Layer	1.0 EFPD	113.5 EFPD	227.0 EFPD	340.5 EFPD	454.0 EFPD	Cycle Average
1	0.877	0.871	0.972	0.957	0.569	0.881
2	0.965	0.971	1.089	1.085	0.684	0.992
3	0.999	1.041	1.182	1.269	0.960	1.118
4	1.116	1.150	1.235	1.325	1.202	1.217
5	1.137	1.157	1.172	1.219	1.266	1.187
6	1.156	1.160	1.117	1.122	1.290	1.155
7	1.184	1.167	1.072	1.035	1.282	1.127
8	0.998	0.987	0.885	0.836	1.107	0.940
9	0.936	0.896	0.768	0.698	0.973	0.829
10	0.633	0.600	0.508	0.455	0.667	0.553
Average - -	1.000	1.000	1.000	1.000	1.000	1.000

Figure 50 shows the nature of the power fluctuations, due to this xenon perturbation, at the beginning, middle, and end of the initial cycle. In this figure, the axial power factor at the mid-height of the second layer from the top of the core is plotted as a function of time. The axial power fluctuations in the initial core are very damped at the beginning and end of the cycle, and are significantly damped at the middle of the cycle. This result was confirmed by 1-D axial studies for the 600 MWt GT-MHR core using a low enriched uranium fuel cycle. The response to a large power perturbation in this core is shown in Figure 51 at two axial layers, at the end of a typical equilibrium cycle. In this case temperature feedback was included in the model, and it can be seen that the power oscillation due to xenon effects is highly damped without any control rod motion. It can be concluded from these analyses that the ten element high GT-MHR is stable against xenon induced power oscillations, and also the axial zoning factors produce a stable power distribution in the axial direction.

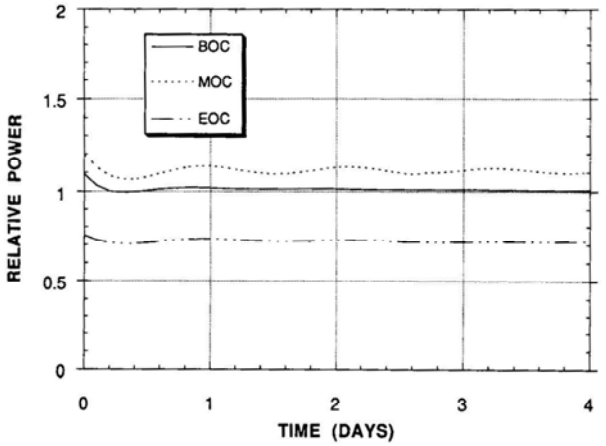

Figure 50. Xenon induced power transient in the initial cycle of the 450MWt core.

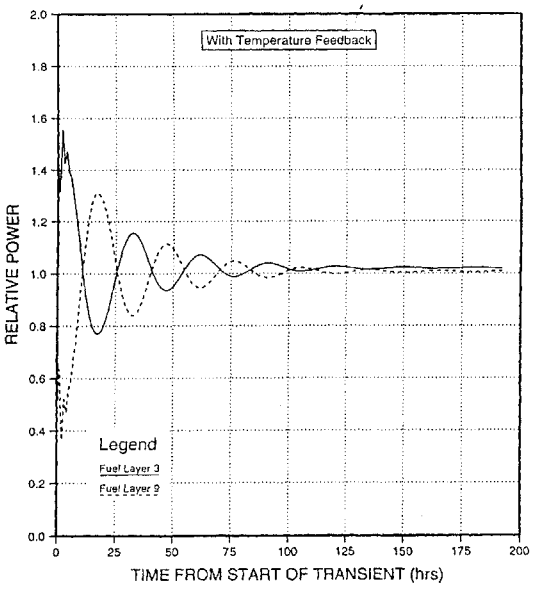

Figure 51. Response to a large axial power perturbation in the 600MWt GT-MHR core.

Three dimensional burnup calculations have also been performed for the GT-MHR production reactor (GT-NPR) over six cycles using the DIF3D code.[17] This core design used highly enriched uranium fuel and lithium targets. These calculations accounted for the axially dependent radial

leakage from the core, since the 3-dimensional model explicitly included all the radial and axial reflectors. However, the damping effect of temperature-induced negative reactivity feedback was not included, unlike the FEVER-POKE-MICROX study. The calculated radial leakages from the core were smallest at the core mid-plane, and slightly larger toward the top and bottom of the core. As expected, this did not have a large effect on the axial power distributions, but it did significantly damp any potential xenon induced axial power oscillations. The reason for this is that, if an axial oscillation starts to move the peak of the axial power distribution away from the core mid-plane toward the top or bottom of the core, then the radial leakage from the core is increased, k_{eff} is then decreased, and the axial oscillation is strongly damped. This same mechanism will also damp axial oscillations in the low enriched uranium fueled GT-MHR core, and 3-dimensional calculations for this core should show a significantly more damped axial power response than shown in Figure 50. This would allow the axial zoning to be less peaked toward the core mid-plane than shown in Figure 51, so that lower axial power factors than listed in Table 8 can be obtained.

3.5.2. Radial and Azimuthal Xenon Stability in the 600 MWt GT-MHR Core

An analysis of the radial stability to xenon-induced transients was also performed for the 102-column GT-MHR core operating at 600 MW(t). Since this is a larger core, operating at ~ 10% higher power density, it should be less stable in the radial direction than the 84-column core at 450 MW(t). As with the axial stability calculation, damping of the power fluctuation with time was used to prove the radial power stability of the core. A two-dimensional GAUGE diffusion theory calculation was performed using 2.4 hour time steps, without control rod motion or temperature feedback included. The end of an equilibrium cycle time point was used, since this time should have the least radial stability due to the lowest fissile and B-10 loadings, and the largest fractional absorption in Xe-135. To start the oscillation, the Xe-135 atom density in a 120° sector of the core was doubled. The Xe-135 in the remainder of the core was left unchanged. Figure 52 shows the time dependence of the radial power factor for the columns with the highest radial power factor (labeled Column 116 in Figure 52) and the lowest radial power factor (Column 65) at the start of the transient. Since these two columns are on opposite sides of the core, the power fluctuations plotted in Figure 52 are out of phase with each other. The strongly damped radial power factor transient proves that a 102-column core at 6.6 W/cc is very stable to radial power changes. Calculations for higher modes of instability, such as azimuthal power transients, were found to be much more rapidly damped.

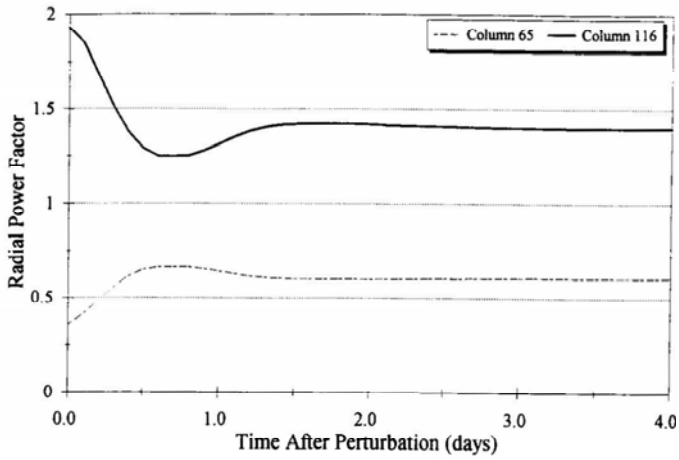

Figure 52. Response to Radial Xenon Power Oscillation.

3.5.3. Effect of Core Height Increase

The effects of increasing the core height by adding fuel blocks was studied as part of an evaluation of a larger GT-MHR type core, in this case one that was a 12-block high, 174 fuel column core operating at 1250 MWt.[18] One-dimensional axial FEVER calculations were performed for this core and showed that a sustained, but non-diverging xenon-induced power oscillation could occur. Axial power stability for this core could not be proven by this conservative 1-dimensional analysis,

in particular since the stabilizing effect of the axial variation in axial leakage was not included. Engineering judgment, based on the ratio of the core height to the neutron migration length indicates that the axial power should be stable. Two-dimensional GAUGE calculations, similar to those discussed above for the 600 MWt radial xenon stability study, were carried out for this large core, and demonstrated that it was highly stable against both radial and azimuthal xenon-induced power oscillations.

3.6. Conclusions

The initial INEEL neutronic evaluations corroborate the General Atomics annular GT-MHR design. The initial core loading (first non-equilibrium cycle) achieves the 420 to 540 EFPD design burnup for the GT-MHR with an initial effective enrichment of 10.36 wt% U-235 uniformly distributed across the 3-ring annular core. The core also exhibits strongly negative isothermal and Doppler temperature coefficients of reactivity over the burnup cycle. In the event of rapid loss of the helium gas (7.12 MPa), there is negligible core reactivity change. The effect of water or steam ingress into the core coolant channels produces a small reactivity effect up to a water density of approximately 0.001 g/cc. The additional neutronic results discussed above further corroborate and benchmark our models relative to the GT-MHR design.

We are currently engaged in additional activities to address more specific NGNP design issues involving the extension of the power cycle length from 420 EFPD (14 months) up to 540 EFPD (18 months) and 720 EFPD (24 months). Depletion calculations will be performed using estimated fuel U-235 enrichments and loadings to achieve these longer cycle lengths.

Also, we are continuing to look at the important issue of reducing the power peaking in the fuel rods nearest the reflector-active core interfaces, primarily the inner reflector-core interface. Parametric studies are being conducted to look at six potential options to reduce the fuel rod power peaking: (1) B_4C burnable poison rods, (2) replacement of specific fuel rods with burnable poisons (B_4C, Gd, Er, etc), (3) graded particle packing fractions in the fuel rod Rows 1, 2, 3, and 4 nearest the interface, (4) graded fuel enrichments, and (5) B_4C loaded in the graphite reflector blocks in Rings 5 and 9 near the reflector/core interfaces, and (6) use of different burnable poisons (B-10, Gd, Er, etc.). The preliminary evaluations of Options 1, 3, and 4 indicate that the power peaking in the NGNP core near the core/inner reflector interface can be significantly reduced.

We also intend to design a preliminary carbon-carbon advanced composite control rod and determine control worths for various B_4C loadings relative to the core U-235 loading and power cycle length. Neutronic model development will also continue with more advanced special core models to meet these and other design evaluation needs.

Finally, it should be noted that there is great flexibility in the design of the prismatic NGNP as evidenced by the multitude of design variables (enrichment, packing fraction, fuel radius, kernel size, burnable poison, etc) that can and will be explored as we develop a viable design and design options for the prismatic NGNP.

4. NGNP Prismatic Core Thermal-Hydraulic Design

Scoping analyses of the steady state and transient response of the prismatic core design version of the NGNP have been performed at both INEEL and General Atomics. Section 4.1 presents the initial core design analyses performed at General Atomics to determine the core inlet and outlet temperatures. Section 4.2 presents the results of the analyses performed at the INEEL to determine the peak reactor vessel and fuel temperatures during high and low pressure conduction cool-down accidents and thereby identify the allowable core power. Section 4.3 presents similar transient analyses performed at General Atomics to determine the peak reactor vessel and fuel temperatures during high and low pressure conduction cool-down accidents. Section 4.4 presents the preliminary results of some computational fluid dynamics (CFD) studies that are ongoing at both General Atomics and the INEEL.

4.1. Core Point Design Parametric Studies at General Atomics

The primary purpose of this study was to investigate design options for the prismatic NGNP that would allow an increase in the average coolant outlet temperature from 850 °C to 1000 °C while maintaining fuel temperatures at acceptable levels and keeping the inlet temperature as low as possible. In addition, the possibility of increasing the reactor power level above 600 MWt was investigated. In general, the feasibility of operating at higher coolant outlet temperatures and/or higher power levels is determined by performing detailed core physics and thermal hydraulic calculations, followed by detailed calculations of fuel performance and fission-product release. The scoping, parametric studies described here should be viewed as the first step in the design process, in that the results should be used primarily to define which design options merit further consideration and more detailed analysis. For high-temperature gas-cooled reactors, a general "rule of thumb" is that fuel performance and fission-product release will be acceptable if the peak fuel temperature remains below about 1250 °C. For the work described here, this criterion was not adopted as a strict requirement, but it is viewed as a goal for the NGNP core design. The impact on vessel temperature (which depends strongly on coolant inlet temperature), core pressure drop, and coolant hot streaks was also assessed for each design option.

4.1.1. Summary of Methodology and Design Criteria

The parametric studies were performed using the POKE computer code.[19] POKE performs a simplified thermal hydraulic analysis for a reactor configuration consisting of a number of regions, each containing parallel coolant channels that are connected to common inlet and outlet plenums. For the present analysis, individual columns were modeled as regions. Because of symmetry, one-third of the core (34 columns) was modeled. Each column consists of an upper reflector, a fueled section, and a lower reflector. The code user specifies the number of axial nodes in the active core. For each region, POKE models an average coolant channel that is coupled to an adiabatic unit cell. Using the coolant-channel temperature as a boundary condition for convective heat transfer, two-dimensional heat-transfer calculations are performed at each axial location in each region to determine the moderator (graphite) and fuel temperatures. For the prismatic fuel block, the unit cell is a right-triangular element containing one-third of the area of a fuel compact and one-sixth the area of a coolant hole (see Figure 53). As indicated in Figure 53, a small gap is modeled between the fuel compact and graphite moderator. Both conduction and radiation are assumed to occur across the gap. Radiation induced shrinkages of the compacts and graphite blocks are considered in the POKE calculations of the various gap conductances.

As discussed in Reference 19, POKE can be run in several modes, depending on which boundary conditions are specified. For the studies described here, the total coolant flow rate and the inlet pressure and temperature were specified and POKE was used to calculate the flow distribution among the 34 columns, and the temperatures of the coolant, graphite, and fuel at each axial location for each column. The coolant inlet temperature is assumed to persist over the length of the upper reflector and the column outlet temperature is assumed to persist over the length of the lower reflector. POKE also calculates the axial pressure distribution in each column and the overall pressure drop across the core. Loss coefficients can be specified for each region, and POKE can also calculate loss coefficients in order to distribute the flow such that the peak fuel temperature or the differences in coolant temperatures exiting each region (i.e., hot/cold streaks) are minimized. In general, peak fuel temperatures occur near the bottom of the core (where coolant temperatures are highest), so optimizing loss coefficients to minimize peak fuel temperatures or coolant hot/cold streaks accomplishes nearly the same result.

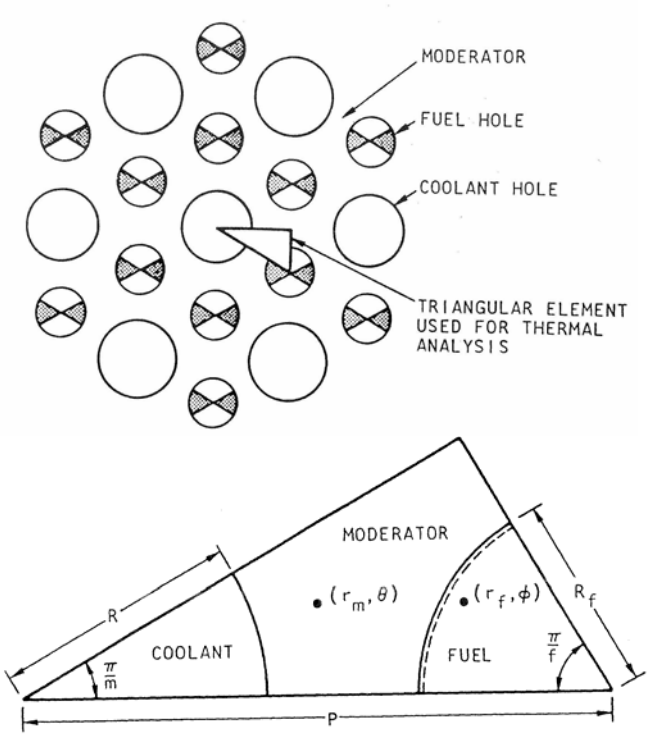

Figure 53. Unit cell used for thermal analysis. R = coolant hole radius, R_f = fuel compact radius, P = pitch of unit cell, m = 6, f = 3.

For the reference GT-MHR core design, a portion of the coolant (20% or more) bypasses the coolant holes and flows into gaps between the blocks and into control-rod channels. The control-rod channels have orifices to minimize bypass flow while also maintaining adequate cooling for the control rods. Approximately 3% of the coolant flows into control-rod channels. Gaps between the fuel columns and between the core barrel and side reflector account for the bulk of the bypass flow. During normal operation, these gaps widen because of thermal expansion of the metallic core support plate and irradiation-induced shrinkage of the graphite. Because of transverse pressure gradients between columns, it is possible for a portion of the flow (referred to as cross flow) to leak from one column to another, along the small gaps between the stacked blocks. For the present analysis, the effect of cross flow was neglected and bypass flow was treated as a parameter ranging from 20% down to 10% of the total flow. In all cases, the ratio of the fraction of the power removed by the bypass flow to the bypass flow fraction was assumed to be 30%, i.e., the temperature-rise of the bypass flow (from the top to the bottom of the core) was assumed to be 30% of the overall coolant temperature rise (this value is based on previous Fort St. Vrain analysis and mesurement). For a bypass flow fraction of 0.2, the fraction of total power removed by the bypass flow would be (0.2)(0.3) = 0.06, which is consistent with previous, more detailed thermal hydraulic analyses of high-temperature gas-cooled reactor cores.

A key input for POKE is the core power distribution. For the present analysis, the power distribution is based on three-dimensional core-physics calculations performed for the reference GT-MHR, which is fueled with low-enriched uranium and operates at a power level of 600-

MWt.[3,20] The active core contains 102 fuel columns with 10 graphite fuel blocks per column. For this design, one-half of the core is refueled every 425 EFPDs, for a total fuel residence time of 850 EFPDs. At discharge, the segment-average fuel burnup is 112,740 MWt-days per metric ton of uranium. The fuel consists of TRISO-coated fissile and fertile particles. The fissile fuel is enriched to 19.8 weight percent U-235 and the fertile particle contains natural uranium. To control excess reactivity, each standard fuel element contains boron in the form of six fixed burnable poison rods.

Figure 54 shows the layout of the core. The core is designed with 120-degree symmetry and the control rods are also operated symmetrically. The outer reflector contains 36 control rods, arranged as 12 groups with 3 rods per group. There are 4 control-rod groups in the active core, again with 3 rods per group. The core also contains 18 channels for insertion of reserve shutdown material (in the form of boronated pellets), in the event the control rods become inoperable. During operation, control rods in the active core are completely withdrawn, and only the control rods in the outer reflector are used for control. For the analyses presented in Reference 20, each graphite block was assumed to have the same fuel loading, and only the fixed burnable poison was zoned axially.

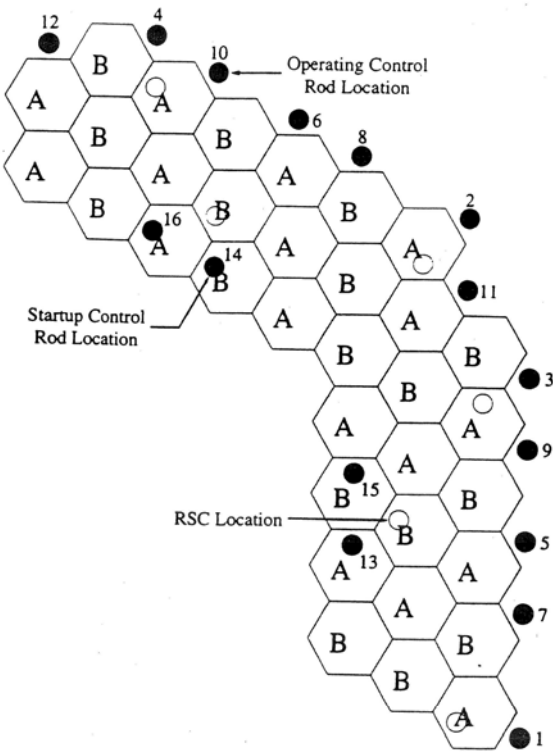

Figure 54. GT-MHR core layout. The letters A and B identify the two fuel segments. The numbered, filled circles identify locations of the control-rod groups. The open circles identify the locations of reserve-shutdown channels.

The core-physics calculations described in Reference 20 were performed for five 425-EFPD cycles, which closely approximated equilibrium conditions. The POKE analyses described here were performed at a fixed point in time, corresponding to the middle of an equilibrium cycle. The local power density is determined within POKE by multiplying the average power density by the product of a column-averaged power factor and axial power factor (local, point-wise power factors can also be input, but these values were not available from Reference 20). The axial power factor is a strong function of control rod position, especially if the fixed burnable poison is depleted and the rod groups are partially inserted.

The baseline refueling scheme for the GT-MHR is to replace entire columns, such that at the beginning of an equilibrium cycle one-half of the core consists of fuel columns that contain fresh ("new") fuel and the other half of the core consists of columns that contain "old" fuel that has been irradiated for one 425-EFPD cycle. Previous studies have shown that power distributions can be flattened if a concept referred to as fuel placement is used. With this concept, each column contains both new and old fuel at the beginning of an equilibrium cycle. In effect, fuel placement reduces the "age" component of power peaking. Although fuel placement was not assessed in the Reference 20 analyses, its effect can be approximated by normalizing the column-averaged power factors with the segment-averaged power factors. Figure 55 shows the column-averaged power factors assumed for this study for refueling by both the conventional column-by-column scheme

and the (simulated) fuel-placement scheme. The axial power factors assumed for this study are shown on Figure 56. This power distribution is representative of a time point between the middle and end of cycle when the control rods are inserted to the axial midpoint of the active core. This type of power distribution generally results in higher fuel temperatures, since more power is shifted toward the bottom of the core where coolant temperatures are also the highest. Also shown on Figure 56 are the axial power factors used to analyze cores consisting of 12 and 14 blocks per column (in order to achieve higher power levels). As indicated on Figure 56, the axial power shapes for the taller cores were assumed to be nearly the same as that of the 10-block high core.

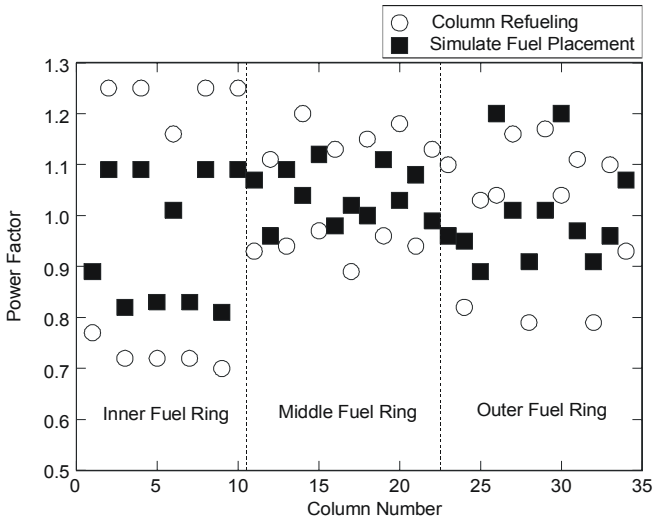

Figure 55. Column-averaged power factors used for POKE analyses

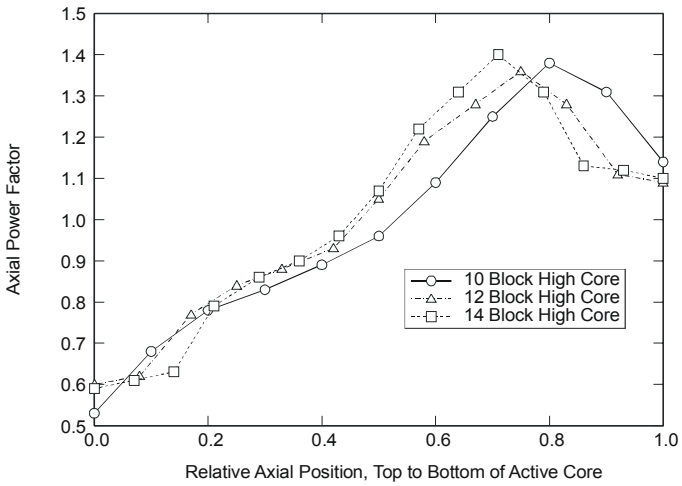

Figure 56. Axial power factors used for POKE analyses

4.1.2. Scoping Studies of Design Alternatives

The design alternatives were investigated in a systematic manner, beginning with analysis of the current 600 MWt GT-MHR design operating with a coolant inlet temperature of 491 °C, an average coolant outlet temperature of 850 °C, a coolant flow rate of 320 kg/s, a bypass flow fraction of 0.2, and conventional column-by-column refueling. For these conditions, POKE calculated a peak fuel temperature of 1267 °C. When the power factors corresponding to fuel placement were used (see Figure 55), the peak fuel temperature dropped to 1218 °C. These power factors were used for the remaining calculations.

For operation at a core-average outlet temperature of 1000 °C, the first alternative investigated was simply to increase the coolant inlet temperature by 150 °C (to 641 °C) and maintain the same ratio of reactor power to coolant flow as the reference GT-MHR design. The bypass flow fraction was assumed to be 0.2. Under these conditions, the calculated peak fuel temperature was 1361 °C. In addition to high fuel temperatures, another obvious drawback to this design approach is that the much higher inlet coolant temperature will impact design and performance of the reactor vessel, including the selection and qualification of the vessel material.

Effect of Reducing Bypass Flow. Several design modifications offer the potential for reducing bypass flow. If materials with higher temperature capability are used to manufacture the control rods (e.g., carbon-carbon composites), less cooling of the control rods is required and the orifices in the control rod channels can be made smaller to reduce flow in these channels. Bypass flow through the gaps between columns can be reduced by using a lateral restraint mechanism to reduce

the gap size. In addition, it should be possible to reduce bypass flow in the gap between the side reflector and core barrel through use of a sealing mechanism or creating increased flow resistance with more tortuous flow paths. In order to assess the potential benefits of reducing bypass flow, calculations were performed using bypass flow fractions of 0.15 and 0.1, and these results were compared with the previous results obtained with a bypass flow fraction of 0.2. Table 9 provides a comparison of key parameters calculated by POKE. Reducing the bypass flow fraction from 0.2 to 0.1 reduces peak fuel temperatures by about 50 °C and reduces coolant hot streaks by about 75 °C. However, with the lower bypass flow fraction, more flow goes through the coolant holes, which increases the core pressure-drop by about 2 psid. However, even with a reduced bypass flow, the peak fuel temperature remains above 1300 °C, and it is doubtful that the bypass flow fraction could be reduced much further. For the remaining calculations, the bypass flow fraction was assumed to be 0.1.

Table 9. Effects of reducing bypass flow.

	Bypass Flow Fraction		
	0.2	**0.15**	**0.1**
Maximum Fuel Temperature (°C)	1361	1334	1309
Maximum Coolant Outlet Temperature (°C)	1169	1145	1124
Core Pressure Drop (psid)	8.1	9.0	10.0

Effect of Controlling Flow Distribution. Previous large HTGR designs used flow-control valves to distribute the flow to regions, which consisted of seven columns for these larger cores. The valves were located above the core and operated on a feedback mechanism based on the temperature of the coolant exiting the region, in order to minimize coolant hot streaks. This flow-control strategy also had the effect of reducing peak fuel temperatures. It is undesirable to use active flow control devices for the NGNP, but it is possible to incorporate orifices in the upper reflector, lower reflector, or both locations. These flow-control elements would remain fixed during a fuel cycle, but could be moved as needed during refueling. To assess the effects of using orifices to control the flow distribution, POKE was run in a mode where it calculates orifice coefficients and distributes the flow to virtually eliminate coolant hot/cold streaks. Two cases using optimized flow distributions were run: (1) the inlet coolant temperature was set at 641 °C and the coolant flow rate was maintained at 320 kg/s and (2) the inlet coolant temperature was lowered to the GT-MHR reference value of 491 °C and the coolant flow rate was lowered to 226 kg/s so that the average coolant exit temperature would be maintained at 1000 °C. Using the conditions for the latter case, a third case was run with a set of discrete, specified loss coefficients for the orifices, since it is recognized that an optimized flow distribution cannot be achieved with fixed orifices. The specified loss coefficients were based on the values that POKE calculated for the cases with optimized flow distributions.

Results for these cases are summarized in Table 10. As seen from these results, controlling the flow distribution has a dramatic effect on reducing the maximum fuel temperature and coolant hot streaks. If the coolant inlet temperature is maintained at 641 °C (corresponding to a flow rate of 320 kg/s), optimizing the flow distribution reduces the peak fuel temperature by approximately 100 °C, but the addition of the orifices increases the core pressure drop by about 4.5 psid. If the coolant inlet temperature is dropped to 491 °C (corresponding to a flow rate of 226 kg/s), there is only a modest increase in maximum fuel temperature (from 1204 °C to 1239 °C), and, because of the lower flow rate, the core pressure drop is lowered by more than a factor of two to 6.9 psid. For the

case with specified orifice coefficients, the maximum fuel temperature was only somewhat higher than the optimized flow case (1276 °C vs. 1239 °C).

Table 10. Effects of controlling flow distribution.

	Flow Control Scheme			
	None	Optimized by POKE	Optimized by POKE	Specified Orifice Coefficients[a]
Inlet Coolant Temperature (°C)	641	641	491	491
Coolant Flow Rate (kg/s)	320	320	226	226
Average Outlet Coolant Temperature (°C)	1000	1000	1000	1000
Maximum Fuel Temperature (°C)	1309	1204	1239	1276
Maximum Outlet Coolant Temperature (°C)	1124	1030	1042	1086
Core Pressure Drop (psid)	10.0	14.5	6.9	6.7

a. Specified values of 0, 10, 20, 30, 40, 50, 60, 70, and 80 were used and distributed among the columns, based on the distribution calculated by POKE to optimize flow distribution.

Table 11 provides a more detailed comparison of core design parameters for the fixed orifice case with those for the reference GT-MHR. These results show that using fixed orifices to control the flow distribution is a promising design solution for increasing the coolant outlet temperature without significantly increasing fuel temperatures. Controlling the flow distribution also allows for reducing the coolant inlet temperature and coolant flow rate, such that the operating temperature for the reactor vessel and the core pressure drop for the NGNP would be about the same as that for the reference GT-MHR. These proposed design changes will also be beneficial for maintaining acceptable temperatures during accident conditions, since the initial NGNP core temperatures prior to the accident are not significantly higher than those for the reference GT-MHR.

Figure 57 shows a comparison of fuel temperature as a function of volume fraction for the reference GT-MHR operating at a coolant outlet temperature of 850 °C and the NGNP operating with fixed orifices and a coolant outlet temperature of 1000 °C. Although the peak fuel temperature for the NGNP is only slightly higher than the goal of 1250 °C, a larger fraction of the NGNP core operates at higher temperatures than the reference GT-MHR core, which may ultimately have some effect on the selection of NGNP point design conditions because of the impacts of higher temperatures on fuel performance and fission-product release.

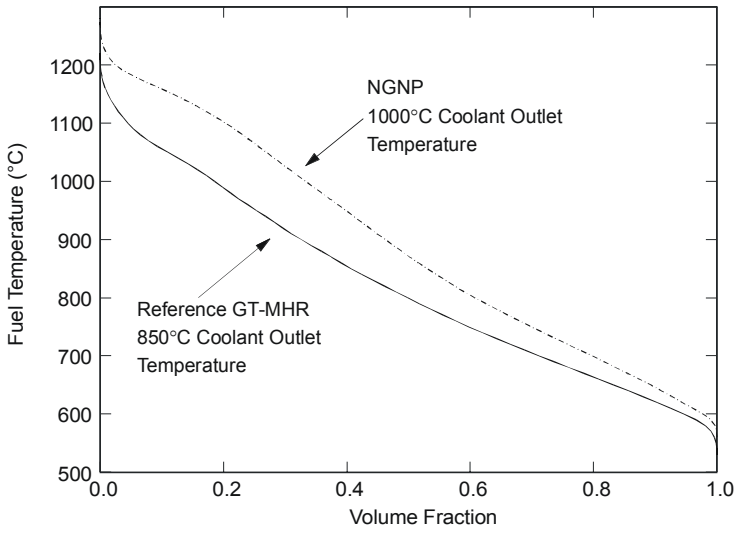

Figure 57. Fuel temperature distributions as a function of fuel volume fraction.

Figure 58 shows the axial temperatures in the NGNP hot coolant channel, where the peak fuel temperature of 1276 °C occurred at the bottom of the active core. At the bottom of the core, the total temperature drop from the fuel centerline to the bulk coolant is approximately 200 °C, with approximately one-half of this temperature drop occurring across the coolant boundary layer.

Table 11. Comparison of GT-MHR and NGNP core design parameters.

	GT-MHR	NGNP (Proposed)
Reactor Power Level (MW_t)	600	600
Fuel Columns	102	102
Fuel Blocks Per Column	10	10
Refueling Scheme	Fuel Placement	Fuel Placement
Flow Control Scheme	None	Fixed Orifices
Coolant Inlet Temperature (°C)	491	491
Average Coolant Outlet Temperature (°C)	850	1000
Coolant Flow Rate (kg/s)	320	226
Bypass Flow Fraction	0.2	0.1
Maximum Fuel Temperature (°C)	1218	1276
Average Fuel Temperature (°C)	821	891
Maximum Graphite Temperature (°C)	1142	1208
Average Graphite Temperature (°C)	770	841
Core Inlet Pressure (psia)	1025	1025
Core Pressure Drop (psid)	6.9	6.7
Maximum Coolant Outlet Temperature (°C)	1021	1086
Ratio of Maximum Coolant Channel Flow to Average Coolant Channel Flow	1.07	1.22
Ratio of Minimum Coolant Channel Flow to Average Coolant Channel Flow	0.89	0.64

Increasing Total Reactor Power. Taller reactor cores were evaluated as a potential approach for increasing total reactor power. The power density was kept the same as that for the 10-block-high, 600-MWt core, since this parameter has a strong effect on core temperature response during accident conditions. Both 12-block-high (720 MWt) and 14-block-high (840 MWt) cores were evaluated. The column-averaged power factors were also assumed to be the same as those for 10-block-high core. As shown on Figure 56, the axial power distributions for the taller cores were assumed to be nearly the same as those for the 10-block-high core.

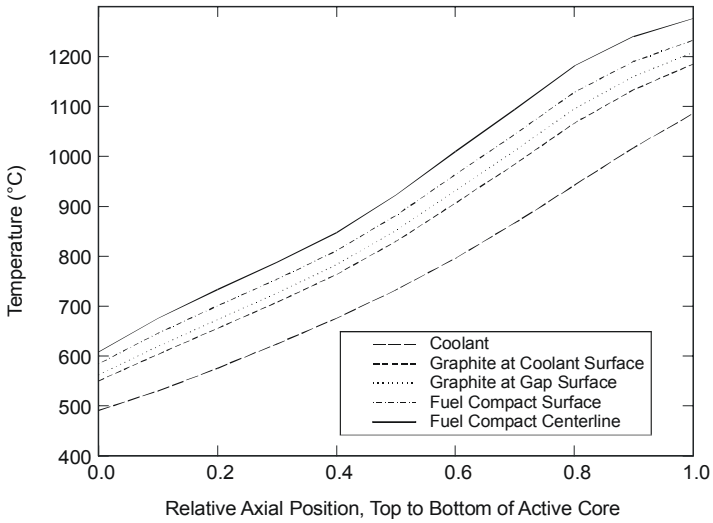

Figure 58. Axial temperature distribution in the prismatic NGNP hot coolant channel.

The calculations were performed assuming a 491 °C coolant inlet temperature, 1000 °C average coolant outlet temperature, and optimization of the flow distribution. For the higher-powered cores, the coolant flow rate was increased in proportion to the power level, in order to maintain the same coolant temperature rise as the 600 MWt core. Table 12 provides a comparison of results for

the higher-powered cores with those for the 600 MWt core. If stable core-physics designs can be developed for the taller, higher-powered cores, these cores should operate at about the same fuel and graphite temperatures as the 600 MWt core. The maximum fuel temperatures for the higher-powered cores are actually predicted to be somewhat lower than those for the 600 MWt core, probably because the higher flow rates enhance convective heat removal to some extent. Because of the higher coolant flow rates, the pressure drops for the higher-powered cores are considerably higher than those for the 600 MWt core.

Table 12. Assessment of higher-powered cores.

	Power Level (MW_t)		
	600	**720**	**840**
Fuel Columns	102	102	102
Fuel Blocks Per Column	10	12	14
Refueling Scheme	Fuel Placement	Fuel Placement	Fuel Placement
Flow Control Scheme	Optimized (by POKE)	Optimized (by POKE)	Optimized (by POKE)
Coolant Inlet Temperature (°C)	491	491	491
Average Coolant Outlet Temperature (°C)	1000	1000	1000
Coolant Flow Rate (kg/s)	226	271	448
Bypass Flow Fraction	0.1	0.1	0.1
Maximum Fuel Temperature (°C)	1239	1228	1221
Average Fuel Temperature (°C)	890	877	867
Maximum Graphite Temperature (°C)	1163	1152	1143
Average Graphite Temperature (°C)	841	827	817
Core Inlet Pressure (psia)	1025	1025	1025
Core Pressure Drop (psid)	6.9	11.1	16.5
Maximum Coolant Outlet Temperature (°C)	1042	1042	1042
Ratio of Maximum Coolant Channel Flow to Average Coolant Channel Flow	1.23	1.23	1.23
Ratio of Minimum Coolant Channel Flow to Average Coolant Channel Flow	0.64	0.64	0.64

4.1.3. General Atomics Design Recommendations for Prismatic NGNP

Based on the scoping studies described here, the following recommendations are made for additional design studies:

1. Work should continue on the nuclear design of the core, with the objectives of reducing power peaking factors and developing control schemes that minimize the durations of partial control-rod insertion and peaking of power generation in the bottom portions of the core where coolant temperatures are higher. Future thermal hydraulic calculations should be performed with a finer spatial resolution using local power densities, in order to better capture three-dimensional effects.

2. More detailed assessments of controlling the flow distribution should be performed. More detailed flow-network models should be developed, including explicit modeling of bypass flow and cross flow. Evaluations should be performed at multiple time points in the fuel cycle, to determine the best column-by-column placement of fixed orifices in order to minimize peak fuel temperatures and the fraction of fuel that operates at high temperatures for extended periods. Studies should also be performed to determine the best axial locations for orifices (top reflector, bottom reflector, or both), in order to minimize transverse pressure gradients and the resulting impacts on block movement and cross flow.

3. Efforts should be initiated to advance the mechanical design of the core and reactor internals, in order to minimize the fraction of flow that bypasses the coolant channels.

4. Although not explicitly addressed as part of this study, some additional benefits could be derived from improving the thermal design of the prismatic fuel element, and it is recommended that design work be performed in this area. Potential improvements include using compacts with an annular-fueled region (to reduce thermal resistance of the compact), reducing the gap width between the fuel compacts and graphite (to reduce thermal resistance of the gap), and using a larger number of smaller-diameter fuel holes per element (to reduce local heat-generation rates). Heat transfer in the coolant holes could be enhanced (to reduce the thermal resistance of the boundary layer) by drilling the holes in a manner that leaves the surfaces relatively rough. However, the surface roughness would also increase the friction factor and core pressure drop. The effects of using surface roughness can be evaluated parametrically, including using roughened elements only near the bottom of the core.

4.2. INEEL High And Low Pressure Conduction Cool-Down Accident Analyses

This section presents the results of the analyses performed at the INEEL to determine the peak reactor vessel and fuel temperatures during high and low pressure conduction cool-down (HPCC and LPCC) accidents and thereby identify the allowable core power. The calculations were done with the RELAP5-3D/ATHENA computer code.[21]

4.2.1. Computer Code Description

The RELAP5-3D/ATHENA computer code uses a one-dimensional, six-equation model to simulate a variety of thermal-hydraulic systems. A three-dimensional hydrodynamic component is also available, as is a three-dimensional nodal kinetics model. RELAP5 was originally developed, and has been extensively used, to simulate the behavior of light water reactors, but contains generalized models that allow application of the code to a wide variety of nuclear and non-nuclear systems. The ATHENA configuration of the code allows for working fluids other than water to be used; for these analyses, helium is the working fluid in the primary system. The containment and reactor cavity cooling system (RCCS) are modeled as containing dry air. The heat structure model allows the user to describe the physical structures of the plant, with user-defined material properties; one-dimensional (radial) heat conduction is calculated in the structures. Convective heat transfer is modeled from the structures to the adjacent coolant, and a radiation and conduction enclosure model allows for direct thermal communication between heat structures.

4.2.2. Model Input Description

Basic design information used to develop the input model was obtained from the *Gas Turbine-Modular Helium Reactor (GT-MHR) Conceptual Design Report.*[3] The model used for the calculations that have been performed includes the reactor vessel, the reactor cavity, and the RCCS. The remaining portion of the primary coolant loop is not included in this model.

The initial nodalization of the reactor vessel is presented in Figure 59. The inlet boundary conditions provide 600 °C helium at a flow rate that produces a vessel outlet coolant temperature of 1000 °C. The coolant enters the reactor vessel, then flows up between the reactor vessel and core barrel to the top of the vessel; a dead volume representing the helium in the shutdown cooling system is also modeled. The helium then flows through an upper plenum volume and into the core. The core is modeled with three coolant channels, each representing the flow through one of the fueled rings. There are ten axial nodes over the length of the active core (one for each of the fuel blocks), and one node each for the upper and lower reflectors. The helium then enters an outlet plenum, from which it flows out of the vessel.

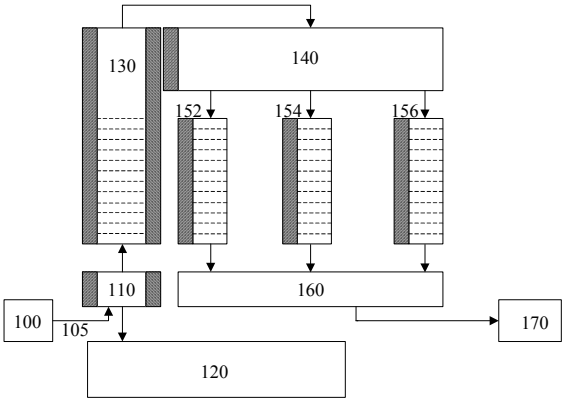

Figure 59. Reactor vessel nodalization for the RELAP5-3D/ATHENA VHTR model.

Heat structures are used to model most of the structural components in the vessel. The reactor vessel cylinder and upper head are modeled, as is a portion of the lower head. The inner, outer, upper, and lower reflectors are included, as is the upper plenum shield. The fuel blocks include both the fuel matrix and the graphite. The core barrel is modeled as an integral portion of the outer reflector. Figure 60 illustrates the convective, conductive, and radiative heat transfer modeled between the various structures and the coolant.

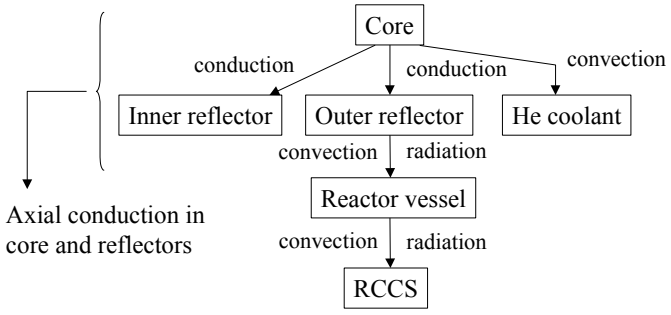

Figure 60. Heat transfer interactions in the RELAP5-3D/ATHENA VHTR model.

The fuel is modeled as being in 102 blocks on each level, with 10, 12 or 14 levels in the active core (the 10-block high core is the base case). The block height is 0.793 m, yielding an active core height of 7.93, 9.52, or 11.10 m. The core outer diameter is 4.8393 m. The inner ring contains 30 assemblies with a peak-to-average power factor of 1.1. The middle ring contains 36 assemblies with a power factor of 0.92, and the outer ring contains 36 assemblies (the six corner assemblies are not fueled) with a power factor of 1.0. A symmetric chopped cosine axial power profile is used, with a peak-to-average ratio of 1.2.

The upper reflector is 1.189 m high, and the lower reflector is 1.585 m high. The center reflector diameter has an equivalent diameter of 2.952 m. The side reflector outer diameter is 6.6504 m. The core barrel inner diameter is 6.6504 m, and it is 0.0762 m thick. The reactor vessel inner diameter is 7.2263 m, and its thickness is 0.2159 m. There are 10395 coolant channels, with an

effective coolant channel diameter of 0.01588 m. The core bypass flow is not included in the base model.

A point kinetics model is being used. The decay power is calculated using a decay heat curve provided by General Atomics that was calculated with the GARGOYLE computer code for the end of the sixth fuel cycle in a high-temperature gas-cooled reactor. The scram curve was taken from a model of the Seabrook plant; the details of the negative reactivity insertion during scram are not considered important for the long-term transients currently being modeled.

The RCCS is modeled as an air-cooled system.[22] Air at 43 °C enters the inlet plenum above the downcomer, then flows through the downcomer (which is attached to the containment wall) to the bottom of the reactor compartment, where it is distributed to the riser channels. The hot air leaving the risers is collected in a plenum, then discharged back to the atmosphere. Figure 61 is a nodalization diagram for the RCCS and reactor cavity.

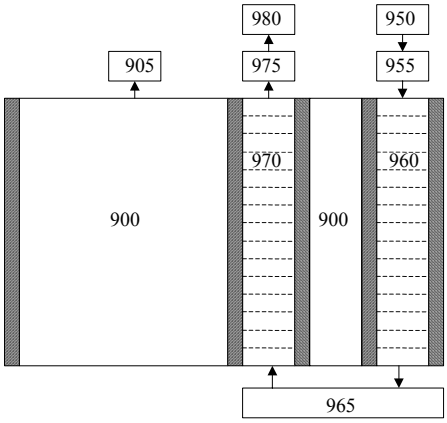

Figure 61. Reactor cavity and RCCS nodalization for the RELAP5-3D/ATHENA VHTR model.

The risers are 292 5 x 25.4 cm (2 x 10 in.) ducts that are physically separated from the downcomer. The short sides face the reactor vessel, and there is a 5-cm (2-in.) gap between the adjacent risers. This configuration is shown in Figure 62, which illustrates the radiation paths between the reactor vessel, riser, downcomer, and containment wall. The riser itself is modeled with three separate heat structures, representing the front wall (facing the reactor vessel), the back wall (facing the downcomer), and the sides. Conduction between these three structures is modeled. The downcomer wall facing the risers is modeled as a highly reflective surface, with 7.6 cm (3 in.) of microtherm insulation.

The containment concrete wall is modeled integrally with the RCCS downcomer outer wall. It includes steel from the downcomer, a 1-m thick concrete wall, and 5 m of surrounding soil. A constant temperature boundary condition (27 °C) is applied to the outer surface of the soil. The reactor cavity air volume is modeled as a large single volume that is vented to the atmosphere (the pressure remains constant). It communicates thermally with the reactor vessel, RCCS riser, and RCCS downcomer.

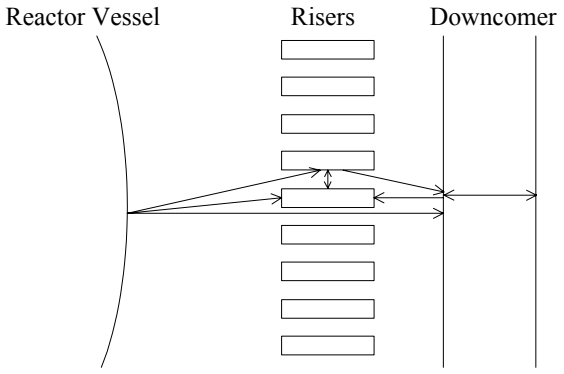

Figure 62. Radiation paths between the reactor vessel and RCCS. [22]

Emissivity values of 0.8 were used for the core barrel, reactor vessel, and RCCS structures, except for the reflective surface of the RCCS downcomer facing the reactor vessel, for which an emissivity of 0.1 was used. These values were recommended by Oak Ridge National Laboratory based on their experience modeling gas-cooled reactors, and are consistent with those used in the General Atomics analyses.

Some changes to the input model have been made as a result of the benchmarking and transient analysis efforts. These changes are described in the following sections.

4.2.3. Model Benchmarking

The basis for the model benchmarking to date has been the information provided in the GT-MHR conceptual design description report.[3] This report includes information on the steady-state performance of the RCCS, as well as transient fuel and reactor vessel peak temperatures during high and low pressure conduction cooldown events. For the benchmarking effort, the NGNP model boundary conditions were changed to match the GT-MHR steady state values, namely inlet and outlet temperatures of 491 and 850 °C, respectively.

The steady state benchmarking effort focused on the performance of the RCCS. The flow loss coefficients at the junctions in the inlet plenum, outlet plenum, and lower distribution header were adjusted to provide the desired flow rate through the RCCS ducts. The desired (GT-MHR reported values) and the RELAP5 calculated conditions are summarized in Table 13. The calculated reactor vessel temperature is a little lower than desired. The peak RCCS structure temperature is high, although it is not clear what the peak temperature in the GT-MHR report refers to; in the RELAP5-3D calculation, it is on the side of the riser facing the reactor vessel, and the average riser temperature at this elevation (including the sides and back) is 303 °C.

Table 13. GT-MHR steady state conditions (600 MWt, 43 °C RCCS inlet air temperature).

Parameter	Desired Value (GT-MHR Reported Value)	RELAP5 Calculated Value
RCCS power (MW)	3.30	3.31
RCCS flow rate (kg/s)	14.3	14.2
RCCS air outlet temperature (°C)	274	272
Reactor vessel outside temperature (°C)	446	425
Peak RCCS structure temperature (°C)	323	348
Peak containment concrete temperature (°C)	49	48

The results of the initial transient benchmarking calculations suggested that the base model was over-predicting the fuel and reactor vessel temperatures. A detailed review of the initial INEEL and General Atomics models of the GT-MHR identified the decay power as the major reason for the differences in the transient calculations. General Atomics used a GARGOYLE-calculated value for the end of the sixth fuel cycle, while the initial INEEL calculations used American National Standard 5.1 (ANS-5.1), assuming all fission was in U-235. The General Atomics decay heat curve was about 30% lower than the ANS-5.1 value. For comparison, the decay heat from an average fuel block with a burnup of 417 EFPD was calculated at the INEEL using the ORIGEN2.1 code. This calculation resulted in decay powers a little lower than the General Atomics calculation, which may be the result of modeling just an average block rather than the whole core. The three decay heat curves are compared in Figure 63, where it can be clearly seen that ANS-5.1 is not appropriate for this reactor.

The modeling of the core bypass paths was another area of difference in the models.

The decay heat curve provided by General Atomics was subsequently used in the RELAP5-3D simulations of the high and low-pressure conduction cooldown transients in the GT-MHR design. Axial and radial power profiles used in the General Atomics analysis were also input to the RELAP5-3D model for consistency. The first calculations resulted in peak fuel temperatures that were very close to those in the GT-MHR report for the low-pressure case, and about 50 °C higher for the high-pressure case. The transient pressure for the high-pressure case was also an issue, however. In the base calculation, it was held at the steady state operating pressure. In the General Atomics analysis, the pressure was calculated to decrease to about 5.0 MPa. A second RELAP5-3D calculation was performed, in which the pressure was reduced to 5.0 MPa during the first four hours of the transient. The reduced thermal performance of the coolant at the lower pressure resulted in an 84 °C increase in the peak fuel temperature.

Two core bypass flow paths were then added to the RELAP5-3D model, one in the inner reflector and one in the outer reflector, and convection from the reflector blocks to these coolant channels was modeled. Figure 64 shows the corresponding nodalization of the reactor vessel. The flow areas of the two bypass paths were based on the number of blocks in each region, assuming that the area corresponds directly to the total cross sectional area. Loss coefficients in the bypass channels were adjusted to provide the desired total bypass flow of 17.2%.

Including the core bypass paths had the desired effect of reducing the HPCC peak fuel temperature to 15 °C below the General Atomics value, as the natural convection helped move heat away from the fuel blocks. The time that the peak occurred was nearly the same as in the General Atomics analysis as well. Figure 65 presents the peak fuel temperatures from the high-pressure conduction cooldown calculations. However, the bypass also lowered the temperatures in the LPCC transient, so that the peak fuel temperature was 74 °C below that in the General Atomics calculation. Table 14 summarizes the results from these benchmarking calculations.

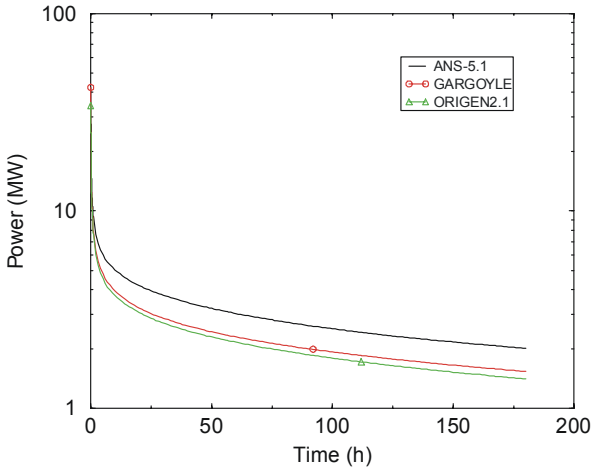

Figure 63. Comparison of decay heat calculations.

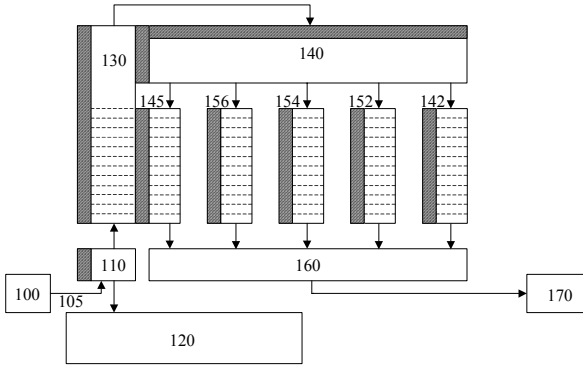

Figure 64. Reactor vessel nodalization with two core bypass channels.

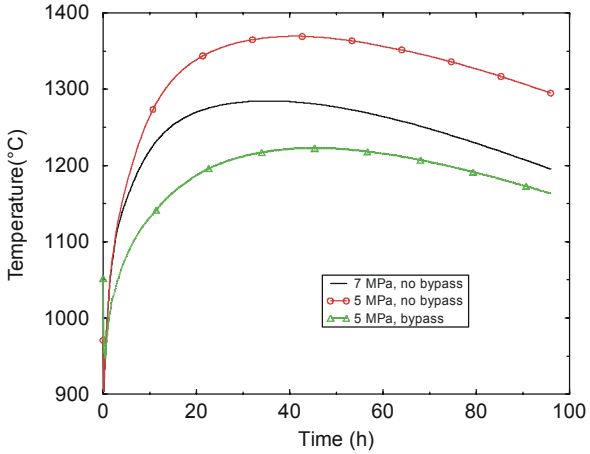

Figure 65. Peak fuel temperatures for the GT-MHR HPCC transient.

Table 14. Results from the GT-MHR benchmarking calculations.

Features	Peak Fuel Temperature (°C) (time [h])			Peak Vessel Temperature (°C) (time [h])		
	Steady	HPCC	LPCC	Steady	HPCC	LPCC
GT-MHR report		1238 (46)	1521 (72)	480	497 (57)	490
Base model, no bypass	971	1285 (35)	1514 (53)	455	471 (62)	520 (72)
Base model, 5.03 MPa transient pressure		1369 (41)			490 (66)	
2 core bypass channels, 5.03 MPa transient pressure	1052	1223 (45)	1447 (63)	454	457 (70)	502 (81)

Figure 66 shows the peak vessel temperatures from the three high-pressure calculations. Consistent with the fuel temperatures, the vessel temperature increased when the system pressure decreased, and decreased when the core bypass flows were modeled. The bypass flows yielded lower peak temperatures for two principal reasons. First, the outer reflector initial temperature was lower, so that there was less stored energy to be removed early in the transient. Second, the bypass flows reduced the axial temperature difference during the transient, making the vessel temperatures more uniform and thus reducing the peak value.

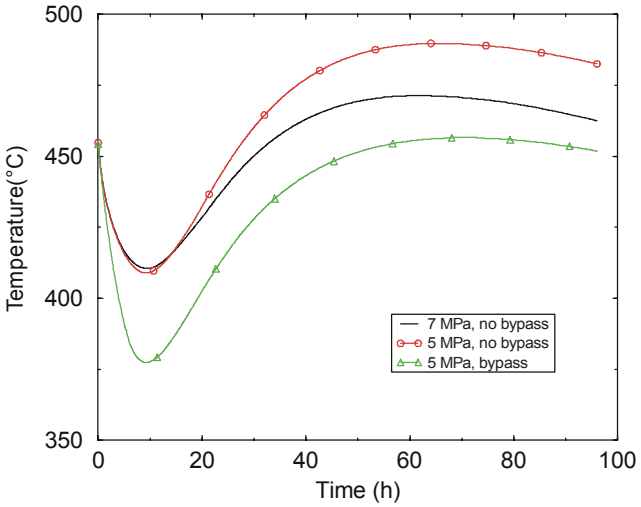

Figure 66. Peak reactor vessel temperatures for the GT-MHR HPCC transient.

4.2.4. NGNP Transient Analyses Results

Three series of plant transient calculations have been performed. Scoping calculations were performed to investigate how various reconfigurations of the core affected the transient thermal response, and how different input modeling choices affected the plant response. The final series investigated what peak core power could be achieved for different core heights.

Two accident scenarios were simulated, high and low pressure loss of flow (conduction cooldown) transients. For the HPCC transient, the pressure was maintained at the steady state value, and the flow coasted down linearly over 60 s. For the LPCC transient, the pressure was reduced from the steady state value to atmospheric pressure in 10 s, and air ingress was not modeled. In both cases, reactor scram was initiated at the beginning of the event. The calculations simulated four days of plant response. Reactor vessel temperatures presented are the volume-average temperature through the wall.

4.2.4.1. Core Configuration Investigations

A series of calculations was performed to address how changing the core geometry would impact the transient temperature response of the reactor. The fueled annulus was kept three blocks wide, but the rings occupied by the fuel were varied, as was the total height of the core. The thicknesses

of the upper, lower, and outer reflectors were left unchanged from that of the GT-MHR; in the core, only the inner reflector thickness changed as the fuel rings were moved. Outside the core, the core barrel and reactor vessel diameters also changed as the active core diameter varied. The results of these calculations are summarized in Table 15. These scoping calculations used the initial RELAP5-3D input model, in which the decay power was overstated (the ANS 5.1 decay heat curve was used). Therefore, care needs to be taken in interpreting the calculated temperatures. Since the peak temperatures are over-predicted, it is the differences in the peak temperatures between the various cases that are informative.

Table 15. Results of the core configuration sensitivity calculations.

Fuel Rings	Core Height (blocks)	Reactor Core ΔP (kPa)	Peak Fuel Temperature (°C)			Peak Vessel Temperature (°C)		
			Steady	HPCC	LPCC	Steady	HPCC	LPCC
6-8	10	55	1119	1596	1807	551	597	643
6-8	11	59	1112	1535	1728	552	583	627
6-8	12	62	1107	1481	1659	552	572	611
5-7	11	75	1064	1707	1937	551	597	644
7-9	10	40	1113	1457	1622	552	595	634
7-9	12	45	1102	1360	1502	553	571	606

Figures 67 and 68 show the peak fuel temperatures for the HPCC and LPCC transients, respectively; peak reactor vessel temperatures for these transients are shown in Figures 69 and 70. In these calculations, the peak fuel and vessel temperatures both occur in the low-pressure transient. The basic characteristics of the temperature responses were similar in all of the calculations. The fuel temperatures experienced a brief cooling at the beginning of the transient as the reactor scrammed, then increased gradually to a maximum value before slowly decreasing. The reactor vessel temperatures had a more pronounced and longer period of cooling early in the transient, then began a gradual increase to a peak before slowly decreasing again.

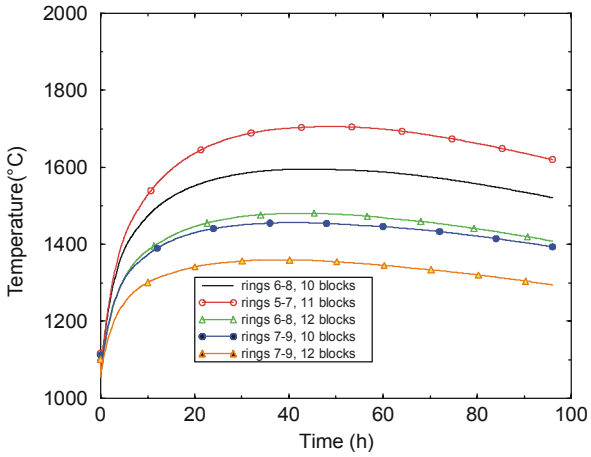

Figure 67. Peak fuel temperatures during a HPCC transient for the core configuration sensitivity calculations.

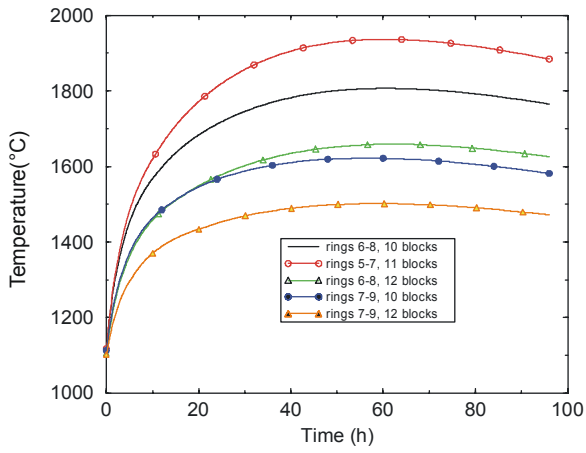

Figure 68. Peak fuel temperatures during an LPCC transient for the core configuration sensitivity calculations.

Moving the fueled region in one ring (from Rings 6-8 to Rings 5-7) and extending the core height one block, which provides about the same power density as in the base model, yields similar reactor vessel temperatures to the base case, but increased fuel temperatures. The steady state pressure drop across the core was also higher, because of the increased core length and reduced number of coolant channels (there was an overall flow area reduction).

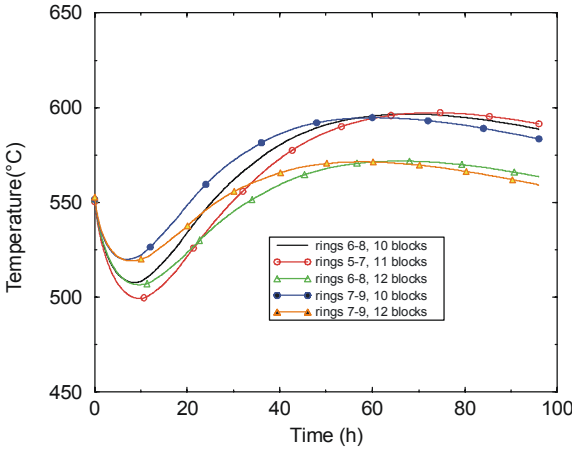

Figure 69. Peak reactor vessel temperatures during a HPCC transient.

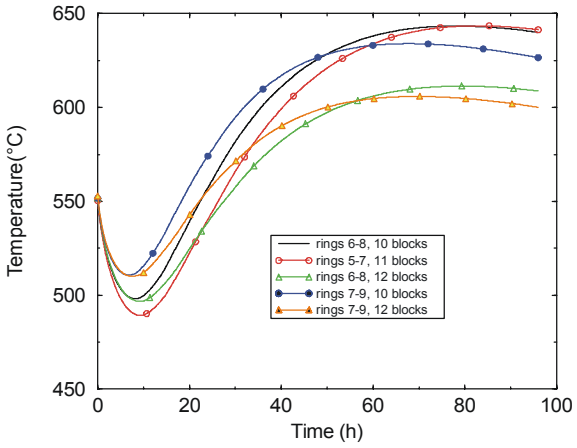

Figure 70. Peak reactor vessel temperatures during an LPCC transient. (These temperatures are within the ASME Code allowables for 9Cr-1Mo steel.)

Increasing the height of the core reduces the peak temperatures. The reactor vessel temperature decreased about 16 °C each time a block was added to the core height. The peak fuel temperature during the LPCC was reduced 79 °C with an 11-block high core, and it was reduced an additional 69 °C by adding another block.

Moving the fueled annulus out one ring, to Rings 7-9, had a much larger impact on the transient temperatures. The number of fuel assemblies on each level increased from 102 to 120, resulting in a nearly 20% decrease in power density. The peak transient fuel temperatures for this configuration were slightly lower than for the 12-block high core, while the reactor vessel temperatures were close to the base case. Moving the fueled annulus out one ring and increasing the core height to 12-blocks yielded a peak fuel temperature 300 °C lower than the base case for the LPCC, and peak vessel temperatures 26 °C and 37 °C lower than the base case for the high and low pressure transients, respectively.

Based on earlier neutronic core design work at General Atomics on the GT-MHR, it should be feasible to increase the core height of the 600MWt NGNP from 10 to 12 blocks without developing a xenon oscillation problem and maybe to 14 blocks (see the discussion of this subject in Section 3.5). However, moving the core out one ring may present significant problems. For example:

- There will be an increase (15% to 20%) in the radial core leakage due to the increased radial surface area. This will increase the fuel loading requirements and significantly reduce the effectiveness of the reflector control rods.
- The current reactor vessel diameter is about at the limit that can be made in a single forging. If the vessel diameter is not changed, then the outer reflector thickness is reduced, increasing neutron leakage and the dose to the vessel.
- A greater reach would be required for the fuel-handling machine, and could be a design issue.

These issues need further evaluation if there is a desire or need to move the fuel annulus out one ring.

The results of the core configuration studies presented above show that moving the fuel out one ring could significantly reduce the peak fuel temperatures during conduction cooldown transients. However, there are neutronic and manufacturing issues associated with the larger core diameter that need further evaluation if this approach is to be pursued. While the potential reductions are not as large, a more expedient means to reduce the peak transient temperatures is to increase the core height.

Sensitivity calculations were also performed to investigate how a few other changes to the core affected the plant transient response. The studies included reducing the coolant channel diameter, changing the power profile, and increasing the heat capacity of the inner reflector. The results from these calculations are summarized in Table 16. The shape of the temperature response during these simulations was similar to that shown in Figures 67-70. As with the core configuration sensitivity calculations, these simulations used the initial RELAP5-3D input model with an overstated decay power, and thus it is the differences in the peak temperatures, not the absolute values, that are of interest.

Table 16. Results of the modeling sensitivity calculations.

Features	Reactor Core ΔP (kPa)	Peak Fuel Temperature (°C)			Peak Vessel Temperature (°C)		
		Steady	HPCC	LPCC	Steady	HPCC	LPCC
Base case	55	1119	1596	1807	551	597	643
Coolant channel diameter reduced 10%	62	1125	1628	1805	551	603	643
Flat axial and radial power profiles	55	1094	1530	1684	551	585	618
Inner reflector heat capacity increased 100%	55	1119	1522	1694	551	583	622

Sensitivity calculations were performed with the coolant channel diameter reduced 10%, to see how increasing the amount of graphite in the fuel blocks would affect the transient temperatures. The peak fuel and reactor vessel temperatures calculated for the LPCC, which was the bounding transient, were essentially unchanged from the base case calculation.

Calculations were performed with flat axial and radial power profiles to investigate how much benefit might be gained from adjusting the neutronics design to reduce the power peaking. The resulting peak fuel and vessel temperatures were 123 °C and 25 °C lower than in the base case, respectively.

One of the functions of the inner reflector is to provide heat capacity to reduce the fuel temperatures during loss of flow events. A pair of sensitivity calculations was performed to investigate how the peak temperatures would change if the heat capacity were doubled. The peak fuel and vessel temperatures during the LPCC were reduced 113 °C and 21 °C, respectively, from the base case.

These calculations indicate that reducing the peaking factors and increasing the heat capacity in the center reflector are design modifications that may be helpful in reducing the peak transient temperatures, although not as much as moving the fuel out one ring. Reducing the coolant channel area to increase the amount of graphite in the fuel blocks provides no benefit.

4.2.4.2. Extended Power Scoping Calculations

A series of best-estimate calculations was then undertaken to investigate how much the core power could be increased for taller cores while still maintaining the peak transient fuel temperature under 1600 °C. The fuel remained in Rings 6-8, and core heights of 10, 12, and 14 blocks were considered. Decay heat during the transient was modeled using the General Atomics-provided values. Only the low-pressure loss of forced flow transient was simulated, since this results in higher fuel temperatures than the high pressure transient. These calculations were scoping thermal analyses only, and did not consider other implications of extending the core height, such as the effects on the neutronics or the mechanical stability of the blocks.

The analyses discussed in Section 4.1 above indicated that a core inlet temperature of 490 °C can be supported, and that a total bypass flow of about 10% is probably needed to reduce the fuel temperatures during steady state operation. Two sets of calculations were performed using these boundary conditions.

In the first set of calculations, the RELAP5-3D input model with two core bypass channels was used, since this more accurately represents the physical configuration. Operating powers of 600, 700, and 800 MWt were modeled in cores that were 10, 12, and 14 blocks high; there was also a 14-block high case at a power of 900 MWt. Table 17 summarizes the results of these calculations, and Figures 71 and 72 provide graphs of the results.

Table 17. LPCC transient results, inlet coolant temperature of 490°C, 10% core bypass.

Block Height	Power (MWt)	Core ΔP (kPa)	Peak Fuel Temperature (°C)		Peak Vessel Temperature (°C)	
			Steady	LPCC	Steady	LPCC
10	600	28	1211	1471	450	509
10	700	38	1218	1620	452	547
10	800	48	1225	1769	453	584
12	600	32	1196	1354	452	486
12	700	38	1218	1486	452	521
12	800	55	1208	1618	454	555
14	600	35	1185	1261	453	467
14	700	47	1190	1379	454	500
14	800	61	1196	1497	455	532
14	900	77	1201	1613	456	563

For a given core height, the maximum temperature varied linearly with the power. For a given power level, the peak temperature varied nonlinearly with the core height. Based on these calculations, the estimated power levels that would result in peak transient temperatures below 1600 °C are 686 MWt for a 10-block core, 786 MWt for a 12-block core, and 889 MWt for a 14-block core. The peak reactor vessel temperature at a given power decreased as the core height increased, as expected, because the power density decreased and more surface area was available to transfer the heat from the reactor vessel to the RCCS. The peak reactor pressure vessel temperature during the low-pressure conduction cooldown event for the three different cases remains below 560 °C as indicated in Figure 72.

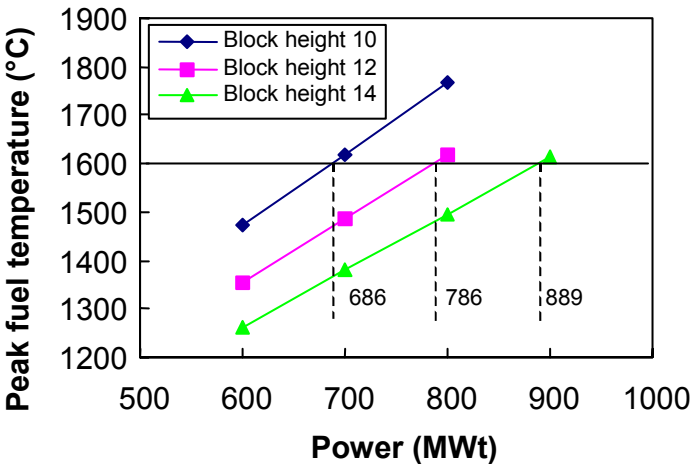

Figure 71. Maximum fuel temperatures for the LPCC transient with 10% core bypass.

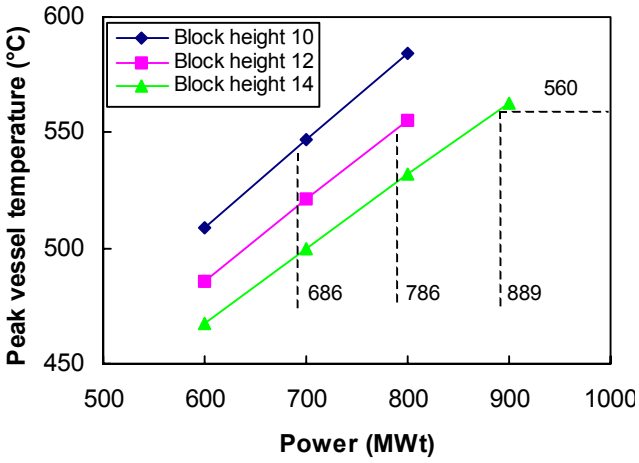

Figure 72. Maximum reactor vessel temperatures for the LPCC transient with 10% core bypass.

Figures 73 and 74 show the peak fuel and reactor vessel temperatures from most of these calculations. The timing of the peak temperatures appears to be affected more by the total power than by the core height, with higher powers yielding later peak temperatures, for both the fuel and the reactor vessel. For a given power level, the peak temperature occurs later for taller cores.

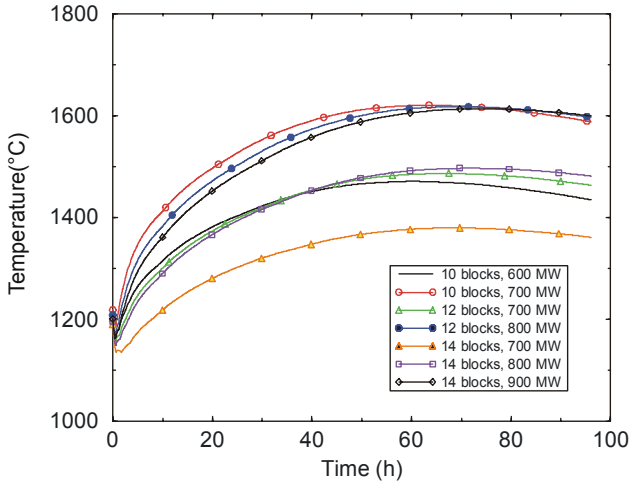

Figure 73. Peak fuel temperatures the LPCC transient with 10% core bypass.

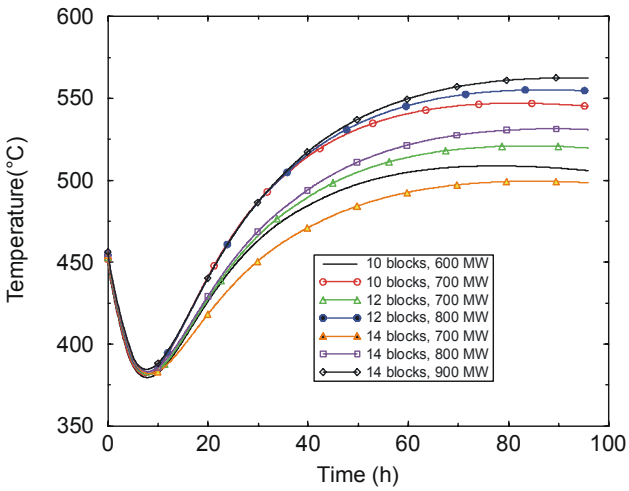

Figure 74. Peak reactor vessel temperatures the LPCC transient with 10% core bypass.

Since the benchmarking calculations indicated that the peak temperature in the LPCC transient may be under-predicted by the input model with two bypass channels, most of the cases were run again without the bypass channels; only the 800 MWt case for the 10-block core was not. The results from these calculations are presented in Table 18. Based on these calculations, the estimated power levels that would result in peak transient temperatures below 1600 °C are 624 MWt for a 10-block core, 723 MWt for a 12-block core, and 833 MWt for a 14-block core. These results are also shown in Figures 75 and 76 for the fuel and vessel temperatures, respectively.

Table 18. LPCC transient results, inlet coolant temperature of 490°C, no core bypass.

Block Height	Power (MWt)	Core ΔP (kPa)	Peak Fuel Temperature (°C)		Peak Vessel Temperature (°C)	
			Steady	LPCC	Steady	LPCC
10	600	33	1156	1565	451	534
10	700	45	1162	1709	453	571
12	600	38	1144	1447	452	511
12	700	50	1148	1571	454	545
12	800	65	1153	1699	455	578
14	600	42	1135	1355	454	493
14	700	56	1139	1465	455	524
14	800	72	1143	1562	456	551
14	900	91	1146	1678	457	582

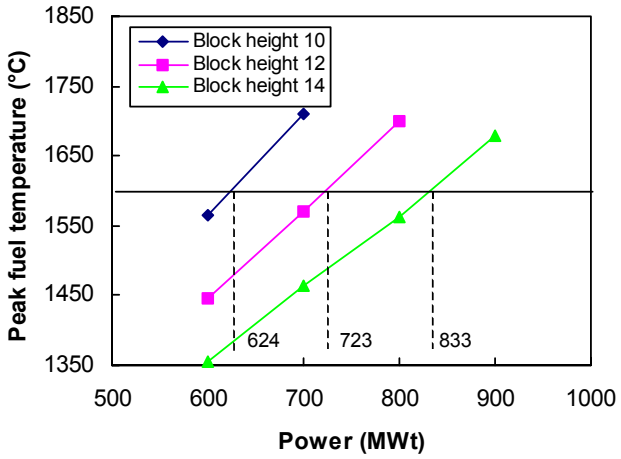

Figure 75. Maximum fuel temperatures for the LPCC transient with no core bypass.

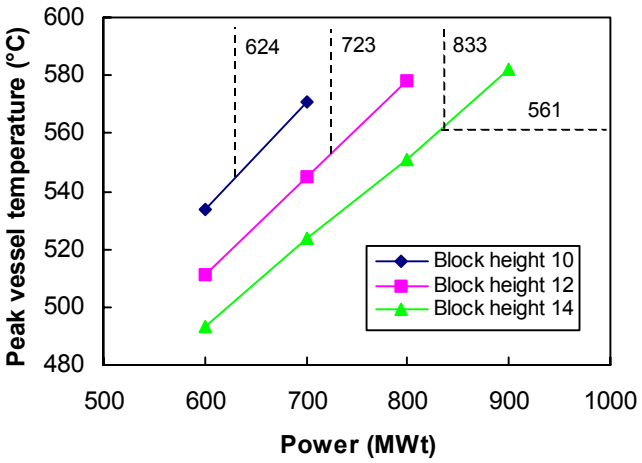

Figure 76. Maximum reactor vessel temperatures for the LPCC transient with no core bypass.

4.2.5. Summary

A RELAP5-3D/ATHENA model for the prismatic core design NGNP has been developed and used to perform scoping transient calculations. Benchmarking calculations compared to the GT-MHR results reported by General Atomics showed good agreement with the steady state and high pressure conduction cooldown transient conditions, and suggested that the current model may be under predicting the peak transient fuel and reactor vessel temperatures for a low pressure conduction cooldown.

A series of calculations investigating the basic core geometry was performed in which the three fueled rings were changed, as was the core height. Moving the fueled region of the core in one ring while extending the height one block resulted in higher peak temperatures than the base configuration. The relative changes in the peak temperature associated with increasing the core height by one or two blocks, and for moving the fuel out one ring were determined. As expected, moving the fuel out can result in greatly reduced peak fuel temperatures, although there are neutronic considerations that must be accounted for if this modification is pursued any further.

Sensitivity calculations were also performed to determine the power that could be obtained for different core heights without exceeding a peak transient fuel temperature of 1600 °C. With a coolant inlet temperature of 490 °C and 10% nominal core bypass flow, it is estimated that the peak power for a 10-block high core is 686 MWt, for a 12-block high core is 786 MWt, and for a 14-block core is about 889 MWt. Cases were also run with no core bypass modeled, as this configuration yielded better agreement with the GT-MHR benchmark case for the low-pressure conduction cooldown transient. In these calculations, the estimated peak operating powers were 624 MWt for a 10-block core, 723 MWt for a 12-block core, and 833 MWt for a 14-block core. These analyses looked only at the thermal response during a low-pressure conduction cooldown, and did not consider any neutronic or mechanical implications of taller cores. These issues will begin to be addressed in the FY-04 work.

4.3. Prismatic Core Conduction Cooldown Parametric Analyses at General Atomics

Parametric analyses were performed at General Atomics for the limiting temperature transient, the low-pressure (depressurized) conduction cooldown (LPCC) design basis event. As discussed in the previous section, this accident is both a loss of coolant and loss of forced convection cooling event that results in peak core temperatures that could potentially exceed the peak design basis accident fuel temperature limit of 1600 ºC. The parametric analyses at General Atomics examined combinations of core configurations and power level selections designed to provide a nominal full power mixed mean core outlet temperature of 1000 ºC that would allow the prismatic NGNP to meet the accident condition fuel limit of 1600 ºC. The TAC2D computer code and model originally developed for the 850 ºC core outlet temperature GT-MHR was used for the parametric analysis.

4.3.1. Computer Code Description

The TAC2D computer code was developed at General Atomics for obtaining temperature solutions in a wide variety of two-dimensional systems.[23] TAC2D uses the finite difference method to calculate steady state and transient temperature distributions. The code is particularly useful to problems in which conduction heat transfer is significant. Convection heat transfer is modeled by defining coolant flow paths in the nodal model. The code has both one-dimensional radiation across gaps and a radiation enclosure model that transfers heat between nodes. The code can model in rectangular, cylindrical, or circular (polar) coordinate systems. A cylindrical coordinate system was used in the GT-MHR and prismatic NGNP analyses. This method was also used to analyze the 350 MWt MHTGR that was documented in the Preliminary Safety Information Document and submitted to the NRC for pre-application review.[24]

4.3.2. Model Description

The model is an r-z cylindrical configuration that extends axially from the top of the concrete floor of the reactor building down to the bottom of the concrete silo and through 2.4 m (8 ft) of earth. The model extends past the concrete silo wall in the radial direction and through 16.5 m (54 ft) of earth. The model consists of 90 radial gridlines and 152 axial gridlines. The fueled region of the core is represented by three rings composed of 30, 36, and 36 fuel columns from the inner to outermost ring. Each fuel ring has three radial nodes.

Coolant flow paths are used to model the downcomer and riser channels of the RCCS. Coolant flow paths are also used to approximate the natural air circulation between the reactor vessel and the RCCS riser panels, and between the RCCS riser panels and the RCCS downcomer. No flow paths are modeled within the core. A detailed radiation heat transfer model is used between the reactor vessel, RCCS riser front-surface, RCCS riser back surface, and RCCS downcomer surface. One-dimensional radiation heat transfer is used in the gaps between the reflector and fuel columns, and in various cavities and plenums both interior and exterior to the reactor vessel.

Detailed models of graphite and fuel thermal conductivity are used that account for the effects of fast neutron fluence, irradiation temperature, fuel particle loadings and orientation. Graphite irradiation damage is determined and its effect on thermal conductivity is accounted for. These models also allow for partial annealing of this irradiation damage at elevated temperatures.

4.3.3. NGNP Transient Simulations

By limiting core power and improving the core design, one can limit the peak core temperature to 1600 ºC, thereby limiting fission product release during the LPCC. One possible means of achieving the 1000 ºC core outlet temperature for the prismatic NGNP is to raise the core inlet temperature in the GT-MHR by 150 ºC. This would raise the core inlet temperature from 490 ºC to 640 ºC and raise the core outlet temperature from 850 ºC to 1000 ºC. To evaluate this case, the initial temperatures in the TAC2D model for the core, reflectors and vessel were all increased by 150 ºC over the values in the original GT-MHR model. The TAC2D analysis predicts that the reactor power would need to be limited to about 588 MWt to limit the peak core temperature to 1600 ºC during the LPCC event.

In order to further examine the effect of core inlet temperature, it was reduced from 640 ºC to 540 ºC while keeping the core outlet temperature at 1000 ºC. The effect is to reduce by 100 ºC the temperature of the vessel and other components closely associated with the coolant entering the core. The core and reflector temperatures are also reduced but by lesser amounts since the core outlet temperature was not reduced. With a core inlet temperature of 540 ºC, the TAC2D analysis predicts that a reactor power capability of 600 MWt for limiting the peak core temperature during the LPCC to 1600 ºC. The relationship between reactor thermal power and core inlet temperature is depicted in Figure 77. Vessel temperatures during the transient never exceed the initial values for steady state operation.

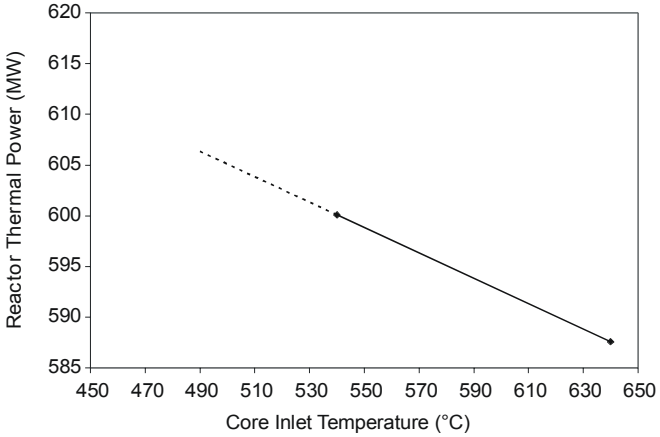

Figure 77. Reactor power and core inlet temperatures that result in a peak core temperature of 1600ºC.

Control of the distribution of the coolant flow in the core is shown in Section 4.1 above to allow the coolant inlet temperature to be dropped to 491 ºC with only a modest increase in maximum fuel temperatures during steady state operation. The power and core temperature profiles from the POKE analysis reported in Section 4.1 were used as input to the TAC2D analysis of the LPCC. For the prismatic NGNP with 10 fuel blocks per column, the TAC2D results predict that a reactor

thermal power of 621 MW will limit the peak core temperature during a LPCC to 1600 ºC. The peak vessel temperature found in this analysis was 529 ºC.

Increasing the number of fuel blocks per column was evaluated as a means of increasing reactor power. Two cases were evaluated, 12 fuel blocks and 14 fuel blocks per column. The POKE power and core temperature profiles for these cases were used as input to the TAC2D analysis. The TAC2D results for the 12- and 14-block high cores show that the reactor thermal power can be increased to 686 MW and 754 MW respectively while limiting the peak core temperature to 1600 ºC. These results are depicted graphically in Figure 78 along with the 10-block high TAC2D analysis. The power density in the 12- and 14-block high cores is lower than the power density used in the POKE analysis, which would result in lower maximum fuel temperatures during steady state operation. The peak vessel temperatures for the 10-, 12-, and 14-block high TAC2D analyses of the LPCC are presented in Figure 79 and show very little variation as one would expect since they all have the same peak core temperature.

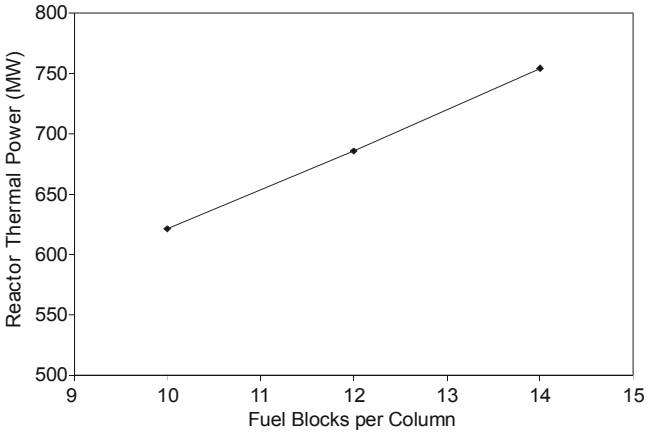

Figure 78. Reactor power and fuel block heights that result in a peak core temperature of 1600 ºC with a 491 ºC core inlet temperature and orificed core.

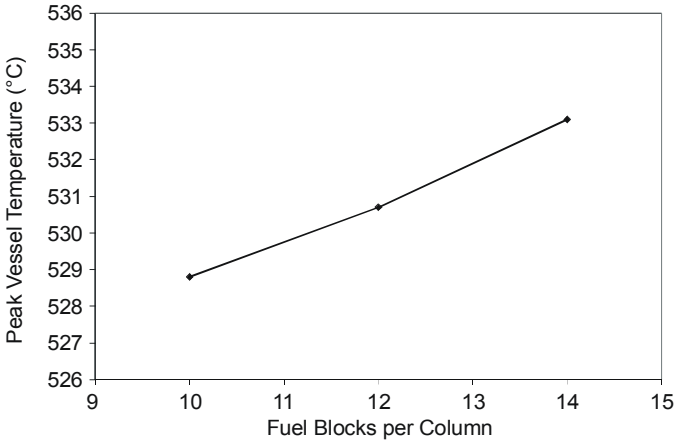

Figure 79. Peak vessel temperatures versus core height with reactor power that result in peak core temperature of 1600ºC.

4.4. Computational Fluid Dynamics (CFD) Studies

Studies are underway to examine the mixing of the high temperature jets that exit into the lower plenum from the reactor core in the NGNP. The issue concerns whether "hot" streaks are present in the lower plenum that move through the lower plenum and hot duct and then are present at the exit to the duct. An excessively non-uniform temperature profile at the hot duct exit will affect the performance of the components linked to the NGNP, whether the component is a power turbine or an intermediate heat exchanger. Whether a design has excessive "hot" streaking characteristics during steady state or transient operation should be examined.

The lower plenum exit temperature profiles are being studied using a commercial CFD code via a collaborative relationship between the INEEL, General Atomics, and the Fluent Corporation. The preliminary model, provided courtesy of Fluent, and our initial steady-state results are shown in Figure 80. The portion of the NGNP that has been modeled, i.e., the lower plenum, is circled in the upper sketch. The center figure shows the computational mesh of the lower plenum and the lower

figure shows a preliminary calculation of the helium fluid temperatures in the lower plenum in a plane at right angles to the reactor vessel vertical axis. Included in the figure is a "cut" through the hot duct to the duct exit. In the preliminary calculation some "hot" streaking was calculated—however, the calculation is only preliminary and additional work is required before observations and conclusions will be drawn.

Whether or not excessive non-uniformities in the hot duct temperature profiles will be present during operational transients will be examined using the Fluent CFD code linked to the RELAP5/ATHENA model shown in Figure 59. The Fluent computational mesh will be substituted for Component 160 in the RELAP5/ATHENA model. The first attempts to perform this coupled calculation have begun.

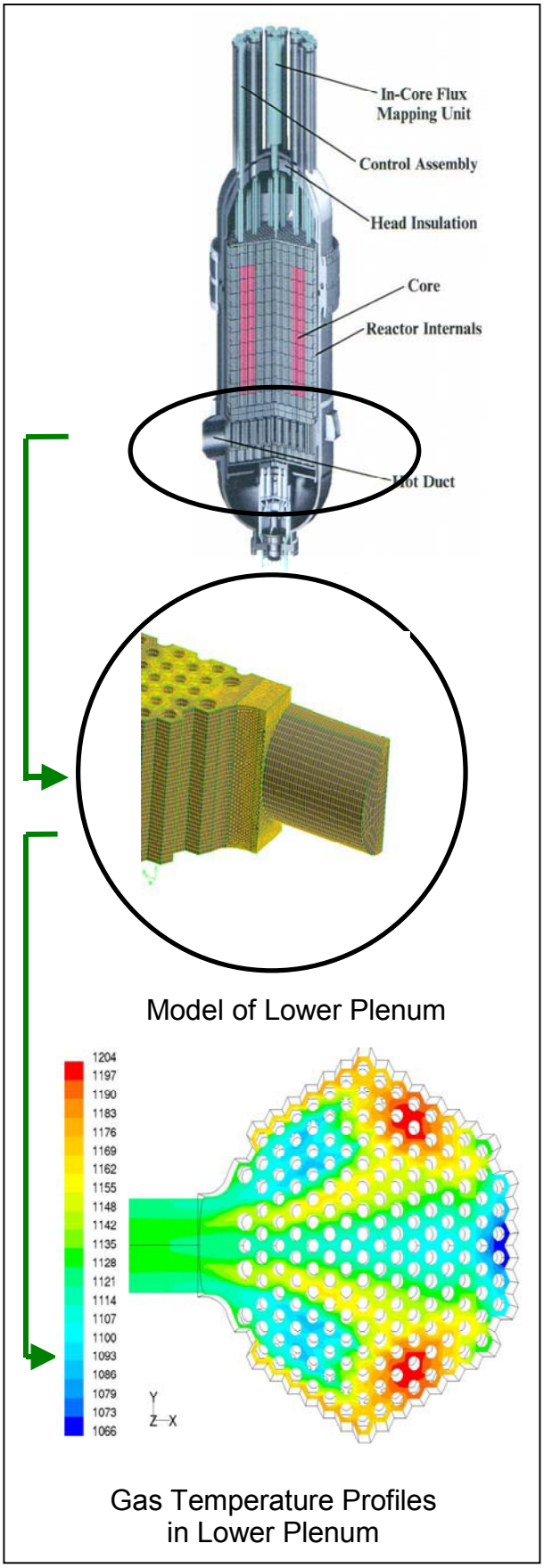

Figure 80. CFD model of the NGNP lower plenum and calculated temperature profiles.

5. NGNP Pebble-Bed Reactor Point Design

5.1. Introduction

This section summarizes the preliminary preconceptual design of a pebble-bed version of the NGNP. Both the prismatic and pebble-bed versions of the NGNP were required to fulfill certain design objectives. It was specified that they would supply helium coolant at a pressure vessel outlet temperature of 1000 °C, in order for the hot helium to be usable in thermal-chemical water splitting processes for the production of hydrogen. A coolant inlet temperature of 600 °C was taken for consistency with the initial prismatic design, so that the balance of plant could be as close to that for the prismatic version as possible. However, the phenomena that constrain the coolant inlet temperature for the prismatic NGNP do not apply to the pebble-bed version, so in a more comprehensive design effort, where the balance of plant would also be addressed, lower coolant inlet temperatures should be investigated. It was also specified that both versions of the NGNP would be passively safe. Also, it was implicitly specified that the NGNP would supply at least 600 MWt of power. The last of these requirements was based on the use of the General Atomics Gas Turbine – Modular Helium Reactor (GT-MHR)[3] as the basis for the prismatic design. The GT-MHR design is rated at 600 MWt to achieve economy of scale; to be directly comparable, both versions of the NGNP should be designed to supply the same amount of power, so that is the design goal for the pebble-bed version of the NGNP.

One of the chief advantages of the small pebble-bed reactor (PBR) is its passive safety, and it was uncertain at the outset of this study whether a PBR rated at 600 MWt would retain that advantage. The largest PBR yet constructed, the THTR,[25] produced 750 MWt and 300 MWe, but it was built before the concept of passive safety had been articulated. The first PBR, the German AVR,[26] produced 46 MWt and 15 MWe, and the new HTR-10 in China[27] is rated at 10 MWt. If a single 600 MWt PBR module could not be shown to be passively safe, then the only acceptable way to supply 600 MWt would be to build two reactors producing a total of 600 MWt. The most obvious way to pursue the latter course would be to build two modules of 300 MWt each, and that is the choice that is analyzed quantitatively in this study. But it is not the only way; if a large module and a small module were combined, the smaller one might be used, for example, as a super-heater for helium already heated by the larger one. A large part of this report is devoted to an assessment of the feasibility of a 600 MWt PBR module. One aspect of the relative costs of a single 600 MWt module versus two 300 MWt modules is also addressed – namely, the costs of the pressure vessels.

In the course of the design project reported here, an idea conceived in another project was applied to achieve better fuel utilization and increased safety: a pebble design was developed with "optimal moderation." The traditional pebble design was selected so that the reactivity insertion caused by a water ingress accident in the German AVR reactor would not exceed the negative reactivity available from safety rod insertion.[28] Later PBR designs duplicated that pebble without regard to the potential for improved performance in a different reactor. In the development of this point design, although a parametric study of all aspects of pebble configuration was beyond the scope of this project, the moderator-to-fuel ratio was optimized by varying the interface diameter between the fueled zone in the pebble and the outer shell of pure graphite, while holding all other parameters constant, including the number of fuel microspheres per unit volume in the fueled zone within each pebble. It was found that either the fuel utilization could be significantly improved, or, without degrading fuel utilization, the reactor could be made immune to reactivity insertions caused by water ingress. This pebble optimization is made possible because the PBR maintains a steady state by continuous online fueling, unlike batch-loaded reactors, in which a large amount of

excess reactivity is gradually burned away and the moderator-to-fuel ratio changes throughout the fuel cycle.

For the candidate 300 MWt modules, thermal-hydraulic studies were performed using the MELCOR computer code[29] to assess their performance in accidents involving loss of forced coolant flow in pressurized and depressurized situations; these accidents are respectively termed HPCC and LPCC events, even though some natural convection will always remain. A passively safe designs was confirmed by MELCOR at this power level. MELCOR analysis of the 600 MWt and 700 MWt designs is planned early in FY-04.

The performance of the pressure vessel and the graphite reflector was also assessed. A design decision was made to require the pressure vessel to meet the same fast-neutron fluence limits stated for the prismatic NGNP in a materials requirements document.[30] This limitation is one of the factors that determine the required thickness of the graphite reflector adjacent to the outer surface of the core. A review of the literature on graphite performance led to the design of inner and outer reflectors with replaceable sections.

The pebble-bed version of the NGNP also makes use of several design innovations developed at the INEEL to achieve passive safety. These innovations, for which patents are being pursued, invoke inexorable laws to ensure the function of safety systems. That is, they are not activated in the sense of the engineered safety systems in light-water reactors; instead, they are prevented from activation by the conditions that exist in a normally operating reactor. When normal operation ceases, the conditions that prevent their activation are lost, and they are actuated inevitably. One of them would apply either of two kinds of automatic scramming control rods, and the other would apply an innovative valve to flood the reactor vault with high-pressure nitrogen in order to prevent an air ingress accident.

At the outset of this point design project, no design existed of a passively safe 600 MWt PBR. Therefore, much of this section is devoted to describing the development of such a reactor (and also a design at 700 MWt).

The remainder of this section is organized as follows:

- Section 5.2 describes the scope of the pebble-bed NGNP study, and describes common features of the pebble-bed and prismatic balance-of-plant components
- Section 5.3 describes the analysis tools used in the pebble-bed NGNP study, with special attention to the INEEL's unique PBR reactor physics and fuel cycle code PEBBED
- Section 5.4 presents the detailed design studies that were performed to define the PBR NGNP designs at 300, 600, and 700 MWt
- Section 5.5 describes the new optimization algorithm in PEBBED
- Section 5.6 defines the MELCOR safety studies and describes passive safety systems unique to the PBR NGNP
- Section 5.7 discusses licensing issues that have been raised for the PBR
- Section 5.8 gives a summary and conclusions.

5.2. Scope

When this point design project was undertaken, work had already been done to define a potential prismatic NGNP design (see Section 3 of this report). This reference prismatic NGNP is based on

the GT-MHR design, which included a detailed balance-of-plant design in addition to the design of the core, reflector, pressure vessel, and pressure vessel internals. However, the balance-of-plant design for the reference prismatic NGNP differs from that for the GT-MHR in a few details, related to the NGNP's dual mission of producing electricity and producing hydrogen, as discussed in Section 1 of this report.

The reference prismatic design specifies a coolant pressure of 7.12 MPa, very close to the pressure selected for the pebble-bed version of the NGNP. Since the two versions of the NGNP are required to supply outlet helium at the same temperature, since the coolant inlet temperature for the pebble-bed version was chosen for expediency to be the same as that for the prismatic version, and since both are being required to produce at least 600 MWt of thermal power, the coolant mass flow rates will be very similar in the two versions. Therefore, the balance-of-plant design selected for the prismatic NGNP can be used by the 600 MWt pebble-bed version of the NGNP with essentially no changes. If the pebble-bed version of the NGNP consists of two modules of 300 MWt each, two ducts will be required to transfer helium between the reactor cores and the power conversion vessel, and the power conversion vessel will have to be modified appropriately; very few other changes will be required. (Although high temperature valves may be needed to protect each reactor in the event of a scram of just one reactor.) Accordingly, this report addresses only a few minor details of the part of the plant outside of the pressure vessel. The scope of this report is largely restricted to the pressure vessel, core, reflector, and other pressure vessel internals.

5.3. Analysis Tools

The principal computational tools used in the pebble-bed reactor physics analyses are PEBBED[31] and MCNP.[8,9] MCNP is discussed in Section 3.3; it is probably the Monte Carlo reactor physics code most widely used in the world today. PEBBED is an INEEL code developed over the past few years under Laboratory-Directed Research and Development (LDRD) support. Although it is still being developed intensively, PEBBED has been applied already to studies of PBR nuclear-weapons-proliferation potential and other practical issues.[32,33,34]

PEBBED simultaneously solves the neutron diffusion equation and the equations for the concentrations of specified nuclides (the burnup equations) in a steady-state reactor with a flowing core. The standard analysis tool for PBRs has been the VSOP code,[35] which not only is based on thirty-year-old computational techniques, but which must follow the evolution of a steady state in time from a specified initial state. In contrast, PEBBED finds the steady state directly in a small number of computational iterations regardless of the quality of the initial guess. Furthermore, PEBBED now contains an automated optimization technique based on a "genetic algorithm," which allows hundreds of cases to be run in a few hours in an intelligent search for configurations that best meet a combination of design goals. Therefore, PEBBED is much better suited than VSOP to performing design studies requiring parameter searches with many repetitive code runs. Furthermore, PEBBED uses an analytical approach to the burnup equations, rather than a finite-difference scheme. Presently, PEBBED uses a finite-difference approach to the neutron diffusion equation, in one-, two-, or three-dimensional Cartesian or cylindrical geometry, but a nodal method in one-, two-, or three-dimensional cylindrical geometry is being implemented. When the nodal package is operational, PEBBED will incorporate the latest state of the art in computational methods. Currently, PEBBED uses cross sections supplied by the INEEL's COMBINE code[36] or MICROX.[37] However, a new cross-section calculation method is being developed for PEBBED under a NERI project with the Georgia Institute of Technology.

The thermal-hydraulics analyses for the PBR NGNP were performed with MELCOR. MELCOR is a severe accident code being developed at Sandia National Laboratory for the U.S. Nuclear Regulatory Commission to model the progression of severe accidents in light-water nuclear power plants. However, because of the general and flexible nature of the code, other concepts such as the pebble-bed reactor can be modeled. For the analysis presented in this report a modified version of MELCOR 1.8.2 was used. The INEEL modifications to MELCOR 1.8.2 were the implementation of multi-fluid capabilities[38] and the ability to model carbon oxidation.[39] The multi-fluid capabilities allow MELCOR to use other fluids such as helium as the primary coolant.

5.4. Neutronics Studies

The 300 MWt pebble-bed version of the NGNP is based on an early South African pebble-bed modular reactor (PBMR) design.[40] The distinguishing feature of this design is the dynamic central reflector, a column of pure graphite pebbles that recirculates along with the fuel pebbles. The key specifications of this PBMR design are presented in Table 19. In the following subsections, studies are discussed that led to the selection of design specifications for the 300 MWt and 600 MWt versions of the pebble-bed NGNP.

Table 19. Specifications of the PBMR.

Power (MW)	**268**
Inlet Temp (^{o}C)	**503**
Outlet Temp (^{o}C)	**908**
Coolant Flow Rate (kg/s)	**125.7**
Active Core Volume (m^3)	**81.8**
Core Radius (cm)	**175**
Inner Reflector Radius (cm)	**App. 87**
Outer Reflector Thickness (cm)	**75**
Active Core Height (m)	**8.4**
Pressure Vessel Outside Diameter (m)	**6**
Mean Pebble Temperature (^{o}C)	**800**
Peak Pebble Temperature (^{o}C)	**1041**
Peak ΔT across Pebble (^{o}C)	**59**
Peak Pebble Power (W)	**1379**
Mean Core Power Density(W/cm^3)	**3.28**

5.4.1. Pressure Vessel

For the 300 MWt pebble-bed NGNP, the PBMR pressure vessel dimensions are preserved. For the 600 MWt pebble-bed NGNP, we imposed the constraint that the maximum fast neutron fluence in the pressure vessel must not exceed the limiting value chosen for the prismatic NGNP pressure vessel, namely, $3x10^{18}$ neutrons/cm^2 over 60 years.

One important factor that must be considered in deciding between a single 600 MWt module and two 300 MWt modules is the total pressure vessel cost. Is it more expensive to build two pressure vessels for 300 MWt reactors or one pressure vessel for a 600 MWt reactor? Time and budget constraints did not permit a detailed cost estimate for the pressure vessels, but the INEEL Fuels and Materials Department did a brief comparative study. Based on costs involved to meet requirements of the ASME Code, considering the fabrication of 4 heads versus 2 heads, additional inspections required, and additional attachments and piping, their rough estimate is that the two smaller vessels would cost from 40 - 50 % more than the one larger vessel. This estimate was based on a vessel internal pressure of 7.1 MPa (1032 psi), a vessel height of 19 m, and vessel internal diameters of 6 m and 8 m for the 300 MWt and 600 MWt versions, respectively. These dimensions do not represent the final configuration of the 600 MWt pebble-bed version of the NGNP vessel, and they are more useful for comparing the relative costs of the pebble-bed version of the NGNP and the prismatic NGNP. The estimates by the Fuels and Materials Department were made early in the design process for the pebble-bed version of the NGNP. As it eventually evolved, the pressure vessel for the 600 MWt pebble-bed NGNP is only a little larger than that for the 300 MWt pebble-bed NGNP, so the

pressure vessels for two 300 MWt pebble-bed NGNPs would actually cost closer to twice as much as the pressure vessel for one 600 MWt pebble-bed NGNP.

However, in the cost comparison, no account was taken of the technical challenges presented by the great size of the pressure vessels for either design. The pressure vessel for the prismatic NGNP would be very much larger than any previous pressure vessel ever constructed for anything. The list of possible suppliers is very small, and none of them is located in the United States. The pressure vessel(s) for either version of the pebble-bed NGNP would be somewhat smaller, although still very large. If there are more potential suppliers for the smaller pebble-bed NGNP vessels than for the prismatic NGNP vessel, then some reduction of cost may be possible for the pebble-bed NGNP pressure vessel.

5.4.2. Fuel Region/Moderator Studies

The pebble design for both the HTR-10 and the PBMR are very similar to the early German reactors because both new designs adopted the same pebble technology – in the case of the HTR-10, the same actual manufacturing equipment – as was certified in Germany for use in pebble-bed power reactors such as the HTR-Modul 200.[5] This "standard" pebble[41] features a TRISO coated particle with a 500 μm kernel of 8% enriched UO_2. Enough particles are embedded in the graphite matrix of the fuel region to yield a heavy metal loading of between 7 and 9 grams (11,000 to 15,000 particles). However, this pebble design is not optimized for the new reactors, and the optimization criterion used for the HTR-Modul 200 is not necessarily appropriate for all PBRs. Therefore, the first task in the pebble-bed version of the NGNP physics design work was to improve the pebble design for these specific reactors. Time and budget did not permit a thorough optimization process, but one easily varied parameter was optimized: fuel-to-moderator ratio, by varying the interface radius between the fueled zone of the pebble and the outer pure graphite shell (keeping constant the pebble outer radius (3cm) and the number of fuel microspheres per unit volume in the fueled zone).

The concept of optimizing the moderation by varying the interface radius originated in another project.[42] The principle is that if the fuel-to-moderator ratio were selected to give a maximum in k-effective, then the fuel would be utilized most efficiently and any change in the moderation would yield a decrease in reactivity. Also, any water ingress would shut the reactor down. Detailed investigation showed that the first benefit of optimal moderation – better fuel utilization – is realized, but that complicating effects, such as neutron absorption and spectral shifts, cause the interface radius for which any water ingress decreases reactivity to differ from the dry optimum value.

The validity of the optimum moderation concept was first verified by an MCNP model in which all the pebbles were identical, with fuel depletion and a lumped-fission-product buildup adjusted to provide criticality in a reflected reactor with a core 10 m high and 3 m in diameter and no central reflector. The model was doubly heterogeneous, representing each pebble and each microsphere explicitly by the repeating structures feature of MCNP, but it arranged the pebbles and microspheres in regular body-centered cubic lattices. This model does not represent a real reactor, but it does validate the optimal moderation concept by showing that there is a peak in k-effective. The peak occurs in this model at an interface radius of about 1.9 cm for a PBR of roughly the PBMR size. Initial calculations suggested that there would be no reactivity insertion from any amount of water in the core, but later, more refined calculations showed a reactivity insertion of up to $0.90. Figures 81 and 82 summarize the MCNP calculations. The figure captions refer to a uniform reactor, but this does not mean that the materials have been homogenized; it means that

although the pebbles and microspheres are individually modeled, as stated above, they are all the same.

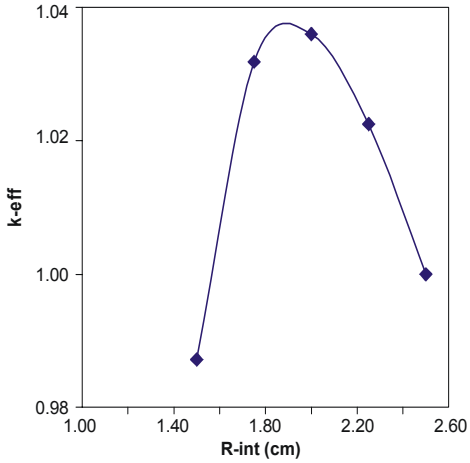

Figure 81. MCNP calculations for optimal moderation in a uniform dry core (MCNP model).

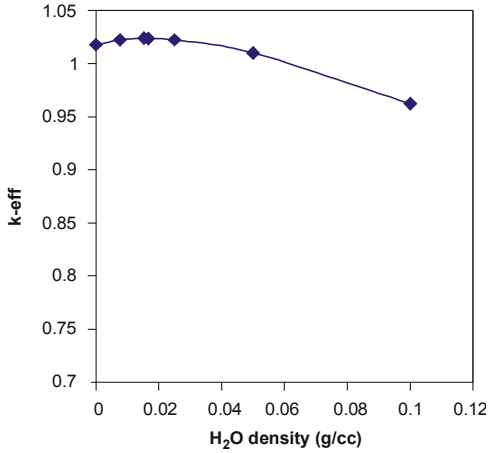

Figure 82. Assessment of reactivity changes caused by water ingress in uniform PBR core with pebbles optimized for a dry core (MCNP model).

By itself, MCNP cannot model a flowing core. To analyze the optimal pebble concept for a real PBR core, the INEEL's PEBBED code, developed specifically for PBRs, was used in conjunction with the cross-section generation codes COMBINE and MICROX-2. Both COMBINE and MICROX perform unit-cell spectrum and cross-section calculations that take into account the double heterogeneity of coated particle fuels. The cross sections are used by PEBBED to perform core simulation. COMBINE is an INEEL code, so it is readily available for this work; however, it is a light-water spectrum code that is not well suited for graphite-moderated fuel. In particular, COMBINE is unable to treat upscattering and resonance absorption simultaneously at epithermal energies. One result is the over-estimation of absorption in nuclides such as Pu-240 that have strong resonances around 1 eV. MICROX does not share this deficiency. MICROX cross-section tables used in this study were prepared by researchers at Penn State University.

5.4.3. Infinite Pebble (k_∞) and Equilibrium Core (k_{eff}) Multiplication Factor vs. Radius of Fuel Region

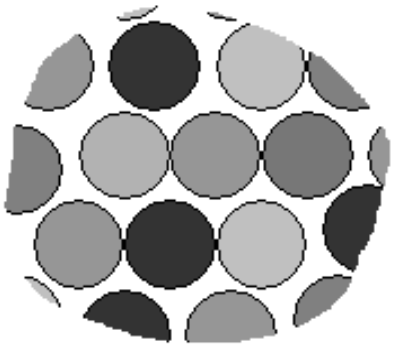

Figure 83. Pebbles at various stages of burnup in a region of a PBR core.

In a recirculating PBR, any region of the core is composed of pebbles at various stages of burnup (see Figure 83). The neutron spectrum to which a given pebble is exposed is a function of this mixture. For this study, cross-sections were generated for the average burnup of all the pebbles in the core. Because the average burnup is itself a function of cross section, an iterative approach is required. First, the infinite core eigenvalue (k_∞) and cross sections for the known fresh pebble composition are generated using COMBINE or MICROX. These are fed to PEBBED, which performs an equilibrium cycle calculation to obtain the core eigenvalue (k_{eff}) and the overall core burnup distribution, from which the average composition can be determined. These average number densities are returned to the cross-

section code to generate new cross sections. This process is repeated until successive values of k_{eff} produced by PEBBED differ by no more than \$0.05.

The core eigenvalue is a function of the discharge burnup target and the pebble flow rate through the core. For this work, pebble flow rates were limited to 4000 pebbles per day for each 300 MWt of reactor power. This is typical of the PBMR and other recirculating designs in which the burnup of each pebble must be measured upon discharge from the core to determine whether it can be reloaded. Final discharge burnup was set at a minimum of 80 MWd per kilogram of fresh heavy metal (MWd/kg_{hm}). This value could be raised as high as 94 MWd/kg_{hm} (10% FIMA) to lower the core eigenvalue in particularly economical designs.

The aforementioned cross-section generation process was repeated for a series of pebble designs that differed in the radius of the fuel region (and thus the number of particles contained in each pebble). Furthermore, the overall leakage characteristics are also a function of core geometry, so that the optimal fuel region size for a pebble in one type of core may be suboptimal for another. Pebble optimization calculations were thus performed for the two designs described later in this chapter.

Figures 84 and 85 indicate the COMBINE and MICROX results for the infinite core multiplication factor as a function of fuel region radius. Both indicate improved moderation as the fuel region is decreased from the standard pebble value of 2.5 cm. COMBINE computes a much larger drop in the multiplication factor than does MICROX.

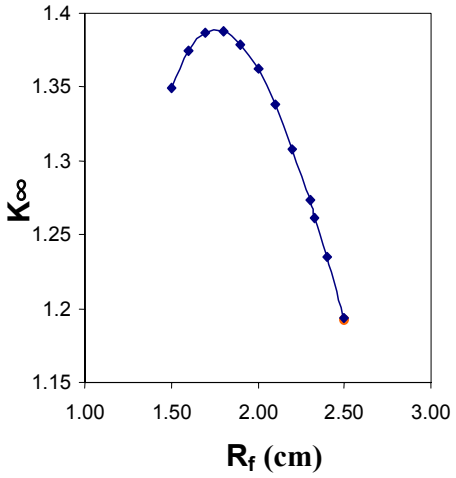

Figure 84. COMBINE infinite pebble multiplication factor vs. fuel region radius - 300MWt core.

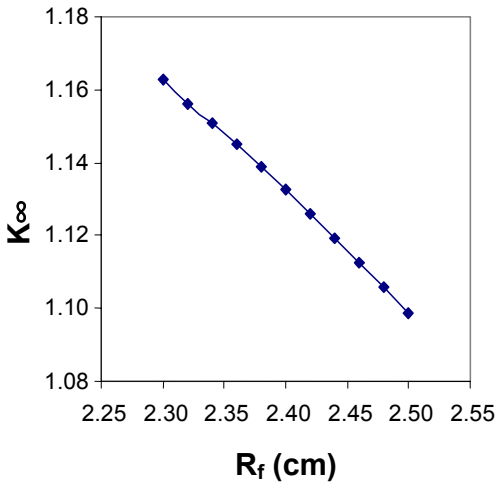

Figure 85. MICROX infinite pebble multiplication factor vs. fuel region radius - 300MWt core.

The PEBBED equilibrium core eigenvalue calculations obtained using the MICROX cross-sections are shown in Figure 86. The 300 MWt core indicates peak moderation at a fuel region radius of 2.4 cm while the 600 MWt core peak is shifted slightly to 2.39 cm. Given the same particle packing fraction, the fuel region radius numbers correspond to a particle loading of about 13,271 particles per pebble for the 300 MWt core and 13,106 particles per pebble for the 600 MWt design. The performance and safety aspects of these designs will be discussed in later sections.

5.4.4. Water Ingress

The GT-MHR employs a shutdown cooling system in which decay heat carried by the helium in the core during periods when the reactor is shut down is passed to a water loop in a heat exchanger near the core. Therefore, the potential exists for water to enter the core. It is likely that a similar system will be required for the pebble-bed NGNP, so an analysis of water ingress into the pebble-bed core is presented below.

Initial studies of the effect of water ingress into the coolant spaces between the pebbles were performed using COMBINE-generated cross-sections. The "Dry" peak corresponding to optimally moderated fuel was found to occur at a fuel region radius of 2.33 cm, substantially different from that computed using MICROX cross-sections. However, the results of the water ingress calculations qualitatively agree with subsequent MICROX runs and the previous MCNP study and thus are discussed here. Figure 82 above indicates the effect of water ingress on core multiplication factor as computed with a full-core MCNP model. Figure 87 illustrates the results generated by COMBINE and PEBBED for various fuel region radii and steam densities. The dark blue curve ("Dry") in Figure 87 represents the core multiplication factor for the helium-cooled core with no water present.

The other curves in Figure 87 show the eigenvalue of the core with various densities of steam mixed in with the helium. Clearly the reactivity effect of steam ingress is positive for interface radii above about 2.15 cm. The magnitude of the insertion decreases with decreasing fuel radius, so that the steam ingress effect for the optimally moderated pebbles is significantly less than for the standard pebble design. Below 2.15 cm, the COMBINE/PEBBED results indicate that steam ingress has a negative reactivity effect. Figure 88 illustrates this more clearly: for a fuel zone radius of 2.1 cm, the reactivity insertion of any amount of steam is negative.

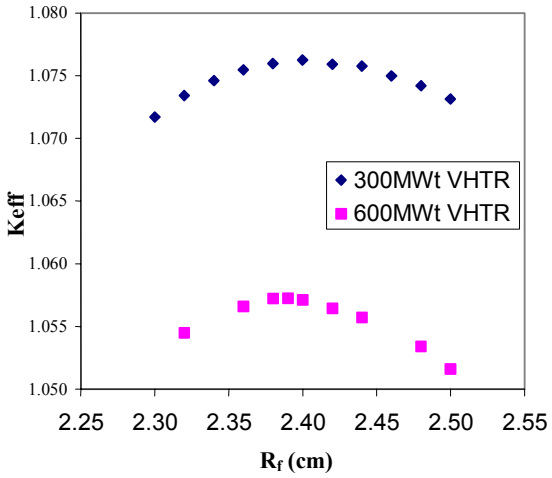

Figure 86. MICROX/PEBBED k_{eff} versus fuel zone radius.

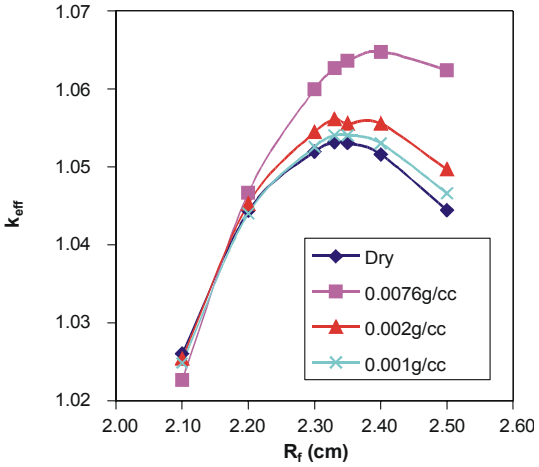

Figure 87. K_{eff} versus fuel zone radius (PEBBED model).

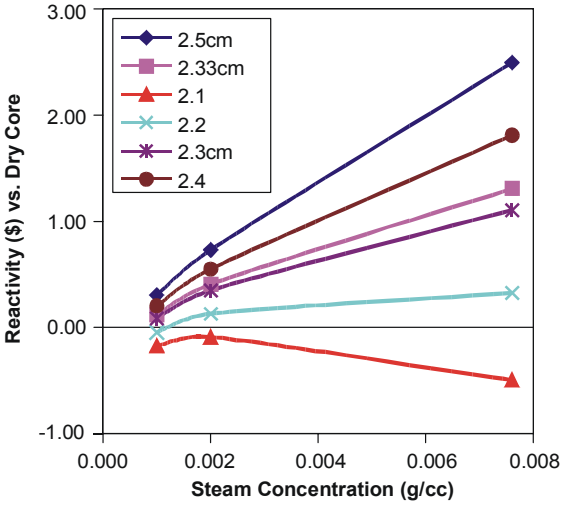

Figure 88. Reactivity insertion versus steam concentration.

Water ingress calculations were also performed with MICROX-generated cross sections. Figure 89 illustrates the effect for the 300 MWt and 600 MWt cores using both standard and optimized (dry) fuel. For both cases, the optimized fuel clearly indicates a decreased reactivity insertion compared to standard PBMR fuel.

The 600 MWt core indicates a slightly greater susceptibility to reactivity excursions compared to the 300 MWt cases. Peak reactivity insertions are listed in Table 20.

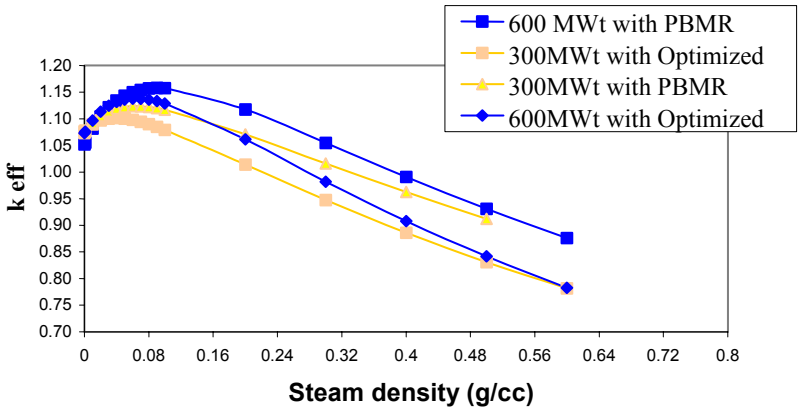

Figure 89. Core eigenvalue versus steam ingress.

Table 20. Peak water ingress reactivity insertion for various PBR configurations.

	Peak Insertion ($)	Water Density (g/cm^3)
300MWt –Standard Fuel	7.74	0.06
300MWt – Optimized Fuel	3.89	0.04
600MWt –Standard Fuel	16.34	0.09
600MWt – Optimized Fuel	9.49	0.06

The peak reactivity insertions from steam ingress for the optimized pebbles are roughly half as great as those for the standard pebbles. For the 600 MWt pebble-bed NGNP, the peak reactivity insertion is of the same magnitude as that for the prismatic NGNP, but slightly better (from Figure 28, one can calculate a peak reactivity insertion of about $11 at operating temperature, at a steam density of about 0.11 g/cm^3).

It is clear from these results and those presented in Sections 5.4.2 and 5.4.3 that the pebble design should be tailored to the reactor design. One generic pebble will not serve well for all pebble-bed reactors.

5.4.5. Temperature Coefficient of Reactivity

Any insertion of reactivity will result in an increase in power and core temperature (assuming that coolant flow is held constant). Such power excursions are inherently self-limiting because of the strong negative temperature coefficient of the graphite-moderated fuel.

Figure 90 illustrates the effect of temperature on the core multiplication factor. The data were generated using various graphite scattering kernels available in the COMBINE code. Figure 91 compares four operating conditions for cores with pebbles of different fuel region radii. Recall that the optimized pebble has a fuel radius of 2.33 cm and the standard pebble has a fuel radius of 2.5 cm. The thick dark curve shows the nominal NGNP with a core-wide average pebble temperature of 1100 K. The light blue curve corresponds to this temperature but with steam ingress of 0.0076g/cm^3, indicating a reactivity insertion of $1.39 for the optimized pebble and $2.66 for the standard PBMR pebble. (This steam density corresponds to the replacement of half the helium atoms by water molecules.) The pink curve corresponds to a dry core at 1200 K, a 100-degree increase above the nominal case. The red curve shows the combined reactivity effect of a 100 K

increase in core-wide average temperature and the steam ingress. The core-optimized pebble is \$0.43 *less* reactive than the nominal core while the core fueled with the standard PBMR pebble is \$0.63 *more* reactive. Fission product energy is deposited almost instantaneously, while the time scale for reactivity insertion is the transit time of coolant through the core, so thermal feedback will occur faster than the reactivity insertion. Clearly, an NGNP core can be designed that is largely immune to water ingress events.

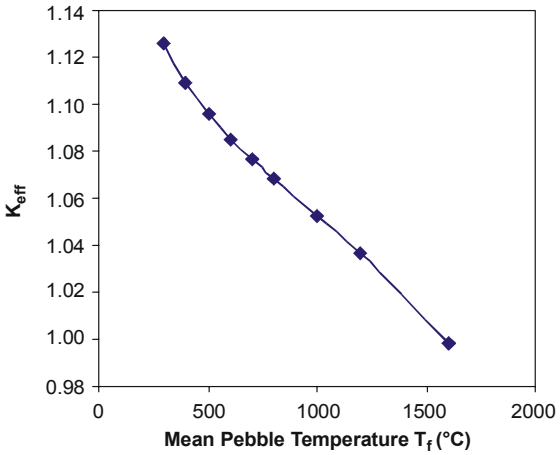

Figure 90. K-effective versus fuel temperature.

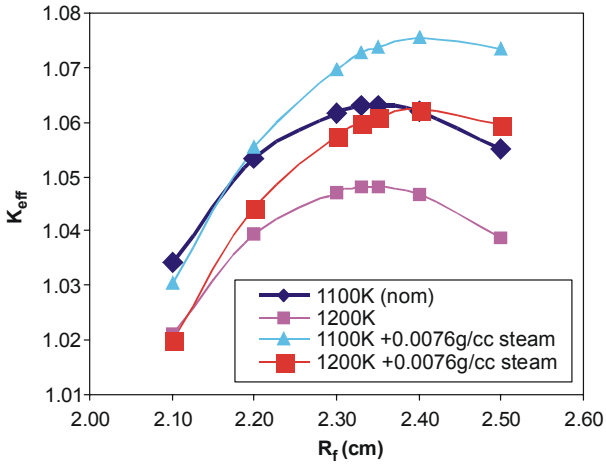

Figure 91. K-effective versus fuel zone radius.

All of the foregoing analyses were performed with a fuel enrichment of 8%. The results may be different if enrichment is allowed to vary. An extended optimization study that includes enrichment as a variable was beyond the scope of the current study, and should be undertaken in future work. (The automated optimization algorithm in PEBBED had not been developed when this part of the work was done.) The PEBBED studies also assume recirculation of the pebbles until they reach the maximum allowed burnup. Top layer fueling with fresh and recirculated pebbles is assumed random. Additional optimization of the core could be possible if specific circulation schemes are assumed with deliberate placing of pebbles in preferred zones.

These preliminary results indicate that pebble fuel can be made much more resistant to water ingress events. The NGNP core fueled with the optimized pebble, while still exhibiting a significant reactivity insertion for a sufficiently high steam density, is superior to the nominal German design in this regard. The higher moderating ratio of properly designed pebble fuel results in a significantly lower core excess reactivity that decreases the effect of water ingress. Furthermore, Figure 88 indicates that for certain pebble designs (relinquishing some of the fuel efficiency enhancement achieved with the fully optimally moderated pebbles), steam ingress reactivity will be negative under all circumstances; a feature not attainable in batch reload high-temperature gas reactor designs. Finally, as shown in Figure 91, temperature feedback can be expected to mitigate the steam ingress reactivity insertion for the dry optimized pebble.

5.4.6. Core Geometry Sensitivity Studies

The core design process in this project involved a search for core and reflector dimensions that provide the requested power output and coolant temperatures while retaining passive safety. Calculations were performed for power levels of 300, 450, 600 and 700 MWt. The 268 MWt PBMR with its central reflector of pebbles was used as the starting point for the 300 MWt pebble-bed version of the NGNP. The old-style PBMR central reflector, composed of graphite pebbles,

was replaced with a solid block reflector for the pebble-bed version of the NGNP. The radius of the inner reflector was varied to yield the highest core multiplication factor (Figure 92).

A neutronically optimal (40cm) inner reflector may not yield a core that is passively safe, i.e., one in which the fuel temperature remains under 1600 °C in the event of a LPCC event. PEBBED estimates peak fuel temperatures under such conditions using a one-dimensional transient conduction-radiation heat transfer module. This affords a rapid assessment of the natural cooling ability of a given design. If the peak LPCC temperature exceeds 1600 °C, the reflector or core dimensions are adjusted. If not, the computed power distribution is fed to a more sophisticated MELCOR[29] model for confirmation of the fuel temperature behavior. MELCOR is an integrated systems level code developed to analyze severe accidents. It has been used extensively to analyze LWR severe accidents and has been modified by the INEEL to use helium as the working fluid and to model graphite oxidation.

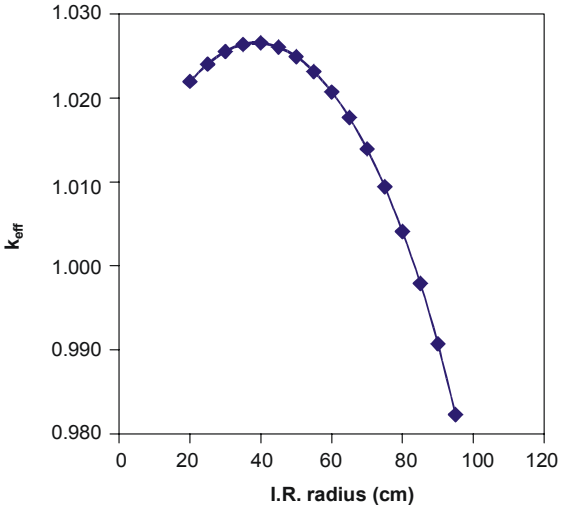

Figure 92. Inner reflector radius versus eigenvalue.

A manual search on core geometry was employed to obtain a core that satisfied basic requirements. The core eigenvalue was required to be at least 1.04 to leave enough excess reactivity for power control and fission products not modeled in PEBBED. The low-pressure conduction cooldown fuel temperature was limited to 1600 °C. Other parameters such a operating fuel temperature and pressure vessel fluence were minimized whenever possible. As a manual search, this method cannot guarantee the optimal design. Tables 21 and 22 list the results of the search for candidate 300 MWt and 600 MWt pebble-bed NGNPs.

5.4.7. Reflector Performance

Like the GT-MHR and the prismatic NGNP, the PBMR design has an annular core. The original PBMR design used a central reflector made of graphite pebbles, which were to flow downwards like the fuel pebbles. However, the large volume of coolant that would have flowed through the reflector pebbles essentially unheated would have reduced the plant thermodynamic efficiency, so the latest PBMR design employs a solid central reflector. The outer reflector for both editions of the PBMR design is solid. PBMR expects to replace the reflectors after 18-24 years, but hopes even longer reflector lives can be achieved.[43]

The lifetime of graphite in a reactor environment is dependent on the specific type of graphite used. For any specific type of graphite, the radiation effects that limit its life in a reactor are primarily dimensional change and thermal conductivity degradation.[44] Other radiation effects, including stored energy and radiation-induced creep, are not likely to be important in the NGNP.

Table 21. Manual Search for 300MWt Pebble-Bed VHTR

Height(cm)	950	Power Density		Operating Fuel Temperature		Peak ΔT	Pebble Power	Max	Max OR
	k-eff	Mean W/cm^3	Peak W/cm^3	Mean °C	Peak °C	Across pebble C°	Peak W	LPCC Tf °C	G1 Flux n/cm^2-s
IR(cm)	Outer Reflector Radius (cm) =175 cm								
80	1.0651	4.1	6.626	832	988	50	994	1372	2.20E+10
90	1.0524	4.4	6.994	833	989	55	1101	1323	2.40E+10
100	1.0358	4.8	7.507	835	990	61	1242	1277	2.70E+10
110	1.0140	5.33	8.229	837	993	69	1435	1231	3.10E+10
120	0.9840	6.07	9.261	841	999	81	1712	1186	3.60E+10
IR(cm)	Outer Reflector Radius (cm) = 195 cm								
120	1.0651	3.54	5.642	826	988	56.8	1130	1139	1.90E+10
130	1.0517	3.82	6.005	827	988	61.9	1247	1109	2.10E+00
140	1.0347	4.19	6.496	829	989	68.5	1401	1083	2.40E+10
150	1.0123	4.67	7.17	931	990	77.5	1614	1055	2.80E+10
160	0.9821	5.34	8.12	835	995	90.9	1919	1030	3.30E+10
IR(cm)	Outer Reflector Radius (cm) = 215 cm								
120	1.0657	3.12	4.891	824	986	50	994	782	1.70E+10
130	1.0510	3.38	5.238	825	987	55	1101	757	1.90E+10
140	1.0337	3.71	5.702	827	988	61	1242	734	2.20E+10
150	1.0112	4.16	6.328	829	989	69	1435	716	2.50E+10
160	0.9808	4.77	7.204	832	991	81	1712	712	3.00E+10

Table 22. Manual Search for 600MWt Pebble-Bed VHTR

Height(m)	950	Power Density		Operating Fuel Temperature		Peak ΔT	Pebble Power	Max	Max OR
	keff	Mean	Peak	Mean	Peak	across pebble	Peak	LPCC Tf	G1 Flux
		W/cm^3	W/cm^3	°C	°C	C°	W	°C	n/cm^2-s
IR(cm)		Outer Reflector Radius = 200 cm							
100	1.0375	7.51	12.315	866	1039	126	2550	1583	4.10E+10
110	1.0449	7.21	11.777	862	1038	119	2395	999	3.90E+10
115	1.0375	7.51	12.315	866	1039	126	2550	1583	4.10E+10
120	1.0294	7.85	12.637	865	1043	131	2667	961	4.30E+10
130	1.0095	8.7	13.809	869	1052	148	3035	923	5.00E+10
140	0.9828	9.85	15.455	875	1066	172	3556	887	5.80E+10
		Outer Reflector Radius = 225cm							
110	1.0543	5.51	8.824	856	1031	93	2163	1470	**2.80E+10**
120	1.0623	5.55	9.116	854	1032	90	1793	1518	2.90E+10
130	1.0508	5.96	9.644	856	1033	98	1958	1477	3.20E+10
140	1.0367	6.48	10.341	858	1034	107	2171	1437	3.60E+10
150	1.0190	8.51	11.269	862	1038	120	2452	1399	4.10E+10
IR(cm)		Outer Reflector Radius = 230 cm							
140	1.0397	6.51	10.048	838	1004	107	2156	1335	3.80E+10
150	1.0551	5.95	9.28	838	1003	97.1	1927	1370	3.40E+10
IR(cm)		Outer Reflector Radius = 250 cm							
120	1.0831	4.18	7.015	847	1028	67	1305	1669	2.10E+10
130	1.0755	4.41	7.275	848	1028	71	1393	1621	2.30E+10
140	1.0665	4.69	7.618	849	1028	76	1500	1576	2.50E+10
150	1.0559	5.03	8.061	851	1029	82	1633	1530	2.70E+10

Because the pebble-bed version of the NGNP will not be shut down regularly for refueling like the prismatic NGNP, it is important to extend the graphite life as long as possible. The removable reflector components in the prismatic NGNP can be replaced when the reactor is shut down for refueling, but the pebble-bed version of the NGNP would have to be shut down specifically for reflector replacement. A rigorous assessment of the reflector life was beyond the scope of this design project. However, we assume that the reflector components in the 300 MWt pebble-bed NGNP can be made to last as long as those in the PBMR – i.e., at least 18 years. In the 600 MWt pebble-bed NGNP, the core is slightly larger than in the 300 MWt version, so the neutron flux in the reflector will be approximately twice as high in the 600 MWt version as in the 300 MWt version. Thus, the reflector lifetimes will be about half as long – about 9 years. (The time required to empty the core and replace the reflector could be a problem.)

The pressure-vessel fast neutron fluences could be reduced by increasing the thickness of the outer reflector. A new idea for further reducing the pressure vessel fluence, without increasing the reflector thickness, was recently proposed; this idea is eligible for protection as intellectual property, so no additional details are given here. Figure 93 is a plot of fast neutron fluence versus radius at the axial location of the peak fast fluence near the inner surface of the pressure vessel for the 600 MWt pebble-bed NGNP. The values at radii greater than 271.375 cm are extrapolated. It is seen that the flux falls below 1.6×10^9 neutrons/cm^2-s, which corresponds to a 60-year fast fluence of 3×10^{18} n/cm^2, at a radius of about 290 cm. This radius corresponds to a pressure-vessel outside diameter of only 6.8 m, which is a good approximation of the value that would be found from a sequence of PEBBED runs. This diameter is considerably less than the 8 m value in the prismatic NGNP.

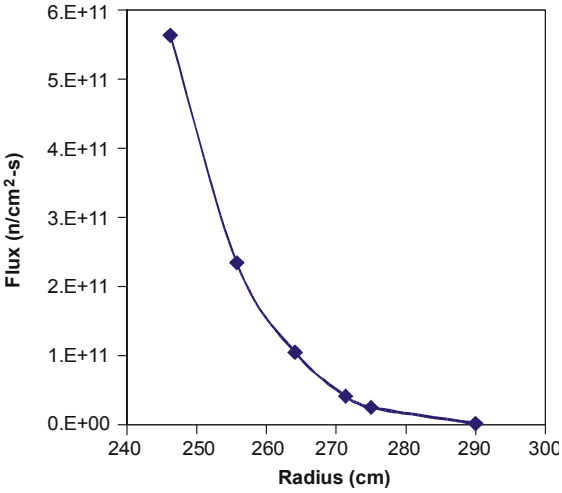

Figure 93. Estimated fast neutron flux near outer reflector inner boundary (r=275 cm) in the 600 MWt pebble-bed NGNP. The last calculated data point is at 271.375 cm, the midpoint of the outermost mesh cell.

Increasing the reflector thickness would also reduce the peak fuel temperature during a LPCC event. Graphite is a very good thermal conductor with high heat capacity, and the graphite reflectors serve as large heat sinks for residual core heat in the case of accidents. Increasing the mass of the reflector would increase the effectiveness of the heat sink and reduce the fuel temperature rise. Such tactics offer the potential to achieve passive safety in pebble-bed NGNP designs of even higher power. However, each trial adjustment will require a new revision of the MELCOR model, which will be the largest part of our continuing design studies.

5.4.8. Fuel Utilization

Table 23 contains fuel utilization data for the three aforementioned cases. The discharge burnups of the NGNP models were adjusted to yield the same core multiplication factor as that computed for the PBMR. Because the pumping power required in a pebble bed can be significant, the fuel utilization (mass of initial heavy metal per MWd) is based on the net power output (thermal power minus pumping power). The 300 MWt pebble-bed NGNP clearly exhibits superior neutronics performance. As a result, this design uses 14% fewer fresh fuel particles per MWd than the

PBMR. Even with the higher required pumping power, the fuel utilization of the 600 MW pebble-bed VHTR is still 5% better than that of the PBMR.

Table 23. Fuel utilization of PBMR and optimal pebble-bed versions of the NGNP.

	PBMR		NGNP-300		NGNP-600	
K_{eff}	1.073		1.073		1.073	
Discharge Burnup (MWd/kg_{hm})	80.1		94		87.2	
Enrichment	8%		8%		8%	
HM loading (g)	9.086		7.96		7.96	
Number of particles per pebble	15,000		13,271		13,271	
Pebble Injection Rate (peb/day)	372		401		865	
Number of passes per pebble	10		10		10	
Residence Time (days)	875		1160		623	
Discharge Concentration (g/day)						
U-235	53	-215	32	-223	83	-468
U-238	2,913	-163	2,744	-192	5,962	-368
Pu-239	20	20	18	18	39	39
Pu-240	12	12	13	13	27	27
Pu-241	10	10	9	9	19	19
Pu-242	7	7	10	10	18	18
HM Mass Daily Throughput (g/day)	3,345		3,192		6,884	
HM Mass Daily Throughput per MWd	12.5		10.6		11.5	
Particles/MWd	21,015		18,118		20,007	

5.5. Genetic Algorithm Design of the Pebble-Bed NGNP

As mentioned previously, a manual search for a candidate design cannot be guaranteed to yield the optimal design. A much more sophisticated approach must be used. Recently, such an optimization feature was added to PEBBED to perform design studies. The new tool was developed with funding from a DOE Nuclear Energy Research Initiative grant.[42] Preliminary results of its application to the VHTR are provided here.

5.5.1. Genetic Algorithm Optimization

The advanced optimization component now available in PEBBED is based upon a *genetic algorithm*.[45] A genetic algorithm is an exceptionally efficient method for sampling a large variable domain to obtain an optimal solution. Initially, a finite 'population' of individual cases is generated by randomly sampling the variables in multi-dimensional solution space. For the pebble-bed NGNP, these variables (genes) may include reflector width, core width, and height. A *fitness* function is specified that is a function of one or more key traits. For the VHTR runs, the specified traits include core multiplication factor, maximum accident fuel temperature, and outer reflector radius. A PEBBED analysis is performed on each case and the resulting fitness of each is computed from the traits.

The best individuals (as measured by their fitness) are allowed to propagate to the next 'generation' while the less fit individuals are discarded. The original population size is recovered by mixing the genes of the survivors to form new individuals in a process called *crossover*. Finally, there is a low

probability that any gene will be changed to a randomly selected new value. This *mutation* process helps to insure diversity in the solution set so that local optima can be replaced by the global optimum. After a number of generations, a core design yielding the best overall fitness is produced and submitted for further confirmation and analysis.

5.5.2. Genes, Traits, and Fitness

PEBBED allows the user to specify the variables over which the search is to be performed. For the NGNP study, these variables included the inner reflector radius, the fuel annulus width, and the core height. For the 600 MWt core, the inner reflector was allowed to vary from 1 to 100 cm; the fuel annulus was allowed to vary from 120 to 170 cm, and the height was allowed to vary from 750 to 1000 cm. The user then specifies the core characteristics or *traits* that determine fitness. For this study, traits included equilibrium core eigenvalue, maximum low-pressure conduction cooldown fuel temperature, outer reflector radius, and ratio of required pumping power to total thermal power. The way in which these traits are factored into the overall fitness is specified by the user in a 4-point interpolation scheme. As an example, the maximum accident fuel temperature fitness is illustrated in Figure 94.

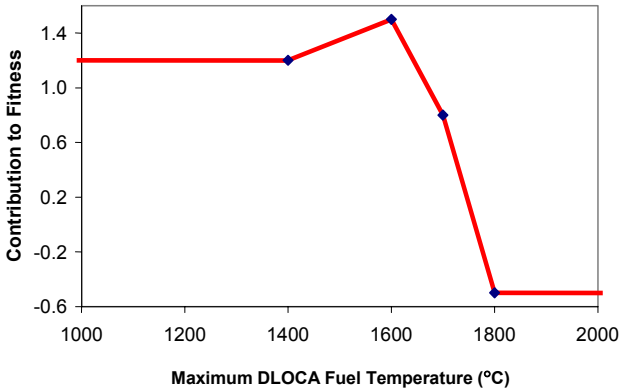

Figure 94. Maximum accident fuel temperature fitness contribution.

5.5.3. Search for Optimized Designs

The contribution of the maximum accident fuel temperature to the overall fitness is determined from the curve based upon the temperature computed by PEBBED. This curve favors temperatures between 1400 °C and 1600 °C, with a severe fitness penalty for temperature over 1700 °C. The other traits have their own user-specified fitness trajectories.

For this study, a population of 30 individuals was used, from which the six best individuals propagated to the next generation. The overall best individual was obtained after about seven generations. Table 24 shows the best individuals obtained for pebble-bed NGNP cores of 600 and 700 MWt. The 600 MWt optimized pebbles were used for each case and burned to 94 MWd/ kg (10% FIMA). The coolant inlet temperature for each was held at 600 °C, and the coolant flow rate was adjusted to yield an outlet temperature of 1000 °C. The 600 MWt core obtained from the manual search is included for comparison.

The fitness specification for the 700MW design was modified to provide a little margin in the peak accident fuel temperature (see Figure 95). The

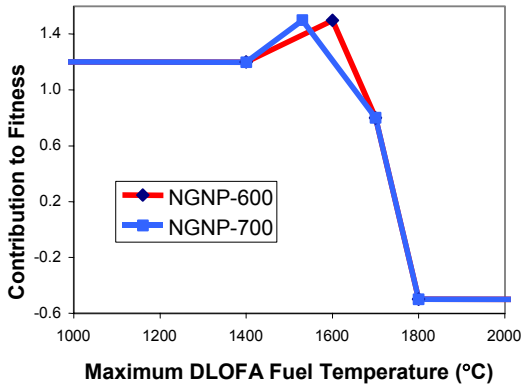

Figure 95. Maximum accident fuel temperature fitness contribution - 600 vs. 700 MW runs.

fitness peak was shifted to 1530 °C, and the algorithm drove the design to this value. To achieve the lower temperature, the fuel annulus was made taller and somewhat thinner. This also resulted in a significant increase in pumping power.

Table 24. Summary of Genetic Algorithm Search for Optimal Pebble-Bed NGNP

	VHTPBR-600 (Manual Search)	VHTPBR-600	VHTPBR-700
Inner reflector radius (cm)	110	90	96
Fuel annulus radius (cm)	225	223	230
Outer reflector radius (cm)	301	299	306
Height (cm)	900	805	1074
K_{eff}	1.073	1.070	1.075
Maximum low-pressure conduction cooldown fuel temperature (°C)	1455	1599	1530
Pumping power (MW)	26	20	39
Maximum operating fuel temperature (°C)	1038	1047	1026
Mean core power density (W/cm^3)	5.5	5.7	4.8
Peak core power density (W/cm^3)	9.0	9.0	8.3

5.6. Licensing Issues

Some licensing issues can be addressed solely using neutronics-based considerations. These include concerns about pebble bed densification, or "slumping" (such as may arise during an earthquake), random formation of hot spots owing to the random clustering of high-reactivity pebbles in high neutron flux zones, air and water ingress scenarios, and proliferation resistance. These matters have been addressed partly either in this or in other studies. They are discussed in turn below.

5.6.1. Pebble-bed Slumping

It is usually observed in cylindrical vats of spheres that the packing fraction is about 61%, except near solid walls. (The packing fraction is zero at the wall, and it fluctuates spatially over about five sphere diameters before approaching the asymptotic value in the interior.) But the packing fraction may increase above the usual value if the spheres are shaken, as by an earthquake. In separate work,[46] we have examined the effects on k-effective of such shifts in packing fraction. We found that the increase in reactivity could be severe in the absence of thermal feedback, but that thermal feedback effects may be expected to keep reactivity insertions within safe bounds.

5.6.2. Hot Spots

In pebble-bed reactors, pebbles are dropped in at the top, and a mound develops below each drop point. The pebbles roll off the mounds until they reach stable positions, and then they move downward in an essentially axial direction. However, some radial wandering is expected, and the stable position on the top from which any pebble begins its downward course is somewhat randomly determined. These stochastic processes generate concern about the possibility that "hot spots" may develop, where clusters of highly reactive pebbles may form in regions of high thermal neutron flux, so that excessive heat generation might occur locally.

To explore the possibility and consequences of such hot spot formation, we used the feature of PEBBED by which arbitrary recirculation schemes may be imposed. Several scenarios were proposed wherein pebbles were made to pass through regions of high thermal flux while they were highly reactive, and then moved to regions of lower thermal flux when they had reached a burnup level that made them less reactive. Table 25 presents the results of the PEBBED thermal analysis of these scenarios during LPCC events.

Table 25. Results of the pebble-bed reactor hot spot analyses.

Case	Peak power density (g/cm^3)	Peak HPCC fuel temperature (°C)	Probability of Configuration Occurrence (per yr)	Peak fuel temperature (°C)	Peak k-eff
Nominal NGNP	8.0	1583	~1	1037	1.0673
Out-In	5.6	1521	$<<10^{-231}$	1049	1.0618
In-Out-1	9.0	1680	$<<10^{-231}$	1334	1.0735
In-Out -2	9.2	1725	$<<10^{-231}$	1307	1.0777
In-Out -3	8.8	1727	$<<10^{-231}$	1256	1.0810
In-Out -4	8.5	1722	$<<10^{-231}$	1211	1.0805
Pebble channeling	6.0	1597	$<<10^{-231}$	1039	1.0657
Fully random	6.2	1600	$<<10^{-231}$	1039	1.0672
WARM1-20	6.4	1607	$<<10^{-231}$	1053	1.0698
WARM1-30	6.7	1614	$<<10^{-231}$	1070	1.0691
WARM1-40	7.0	1622	$<<10^{-231}$	1093	1.0685
WARM1-50	7.3	1630	$<<10^{-231}$	1120	1.0678
Out-In	5.6	1521	$<<10^{-231}$	1049	1.0618

Except for the nominal case, the PEBBED model for which these runs were performed was a pebble-bed reactor without a central reflector, which produces higher power peaking than an annular core. The nominal case is the 300 MWt pebble-bed NGNP. The remaining cases feature an inner fuel zone and an outer fuel zone into which pebbles may be dropped. In the "out-in" cases, the pebbles are loaded into and kept in the outer fuel zone for 8 passes then transferred to the inner zone for 2 passes; the "in-out" cases assume that the pebbles are loaded into the inner zone and kept for x passes before being transferred to the outer. The "pebble-channeling" case assumes that the pebbles remain in their original channels throughout their life, and the "fully random" case assumes fully random recirculation. The WARM1-X is the case where x percent of fresh pebbles are loaded into the central channel and then redistributed randomly thereafter. The remaining (100-x)% of fresh pebbles are distributed randomly over the remainder of the core top. The central channel constitutes 10% of the total pebble flow area in the core in all of these calculations.

Only in the "in-out" cases does the peak LPCC fuel temperature significantly exceed the limit of 1600 °C. Probabilities for these events have not yet been calculated rigorously, but some general conclusions may be drawn. One would not try to make reactive pebbles concentrate in regions of high thermal neutron flux, so the most likely way in which such concentration would develop is if no attempt is made to prevent it – ie., random placement of pebbles. Therefore, 10% of the fresh pebbles should ordinarily fall into the sensitive "hot" zone. The pebbles make about 10 passes each during their life, so about 10% of all the pebbles are fresh. Hence, if all of the fresh pebbles fell onto the hot-zone 10% of the surface area, they would cover that part of the surface. As each pebble fell onto the hot zone, it would reduce the remaining available area for the remaining pebbles. In the NGNP designs, there are about 2300 pebbles per layer in the core. So about 230 particular pebbles must fall onto a particular 10% of the surface area in each layer. Ignoring

competition from the recirculated pebbles, one may estimate that the probability that even one layer will be so arranged is less than 10^{-232}. The pebble injection rate is a few hundred per day, so that several days are required for enough pebbles to be injected to make a complete layer. About 60 layers per year are laid down. Therefore, the probability per year that even one layer will have its fresh pebbles concentrated in the "hot zone" is about $6x10^{-231}$. For successive layers to be arranged similarly is even more improbable. Such estimates indicate that hot spots will not be a problem in pebble-bed reactors.

Izenson[47] developed a rigorous method for analyzing the probability of hot-spot formation in pebble-bed reactors and applied his method to the 200 MWt HTR-Modul reactor design. His concluding statement is, "Preliminary hot spot analysis of the 200 MWt MHTGR indicates that severe hot spot[s] during operation are unlikely. Furthermore, since local power density is quite small during a depressurization transient, the probability of peak accident temperatures significantly exceeding expectation is extremely small." Our analyses indicate that his conclusions will hold for reactors of higher power.

In fact, the motion of the pebbles confers a unique benefit not shared by nuclear reactors with static cores. Although the pebbles move slowly downward, the locations of radial and axial temperature and power density peaks are essentially constant once the core reaches an asymptotic state. Pebbles flow through these hot spots and then move on to cooler areas. Figure 96 is a plot of the pebble center point temperature in the 600 MWt NGNP, which was generated using the manual search. The curves correspond to the different passes the average pebble makes through the core and the number at the left end of each curve is the burnup accumulated before the start of the pass. For example, a pebble spends about 40% of its total core life above a temperature of 800 °C and a burnup above 54 MWd/kg. The residence time for pebbles in this design is about 625 days.

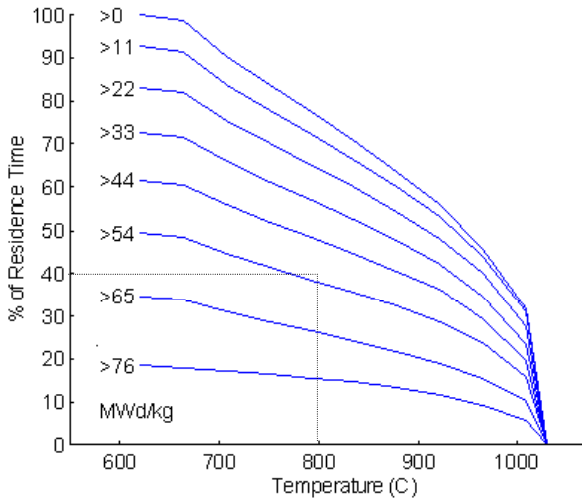

Figure 96. Percent of residence time that the average pebble is above temperature.

The probability of fuel failure increases with temperature and burnup. The top curve indicates that a pebble is above 1000 °C for only about 1/3 of its core life. The bottom curve indicates that the pebble is above 1000 °C *and* 76 MWd/kg for only about 7 % of its residence time. The integrated stress on fuel particles is substantially lower than that of batch-loaded cores, in which certain fuel elements reside at hot spots throughout a fuel cycle. In the pebble bed, thermal and irradiation–induced stresses are shared almost equally among all pebbles, thus reducing the likelihood of fuel failure.

5.6.3. Air and Water Ingress

Water ingress has been discussed in Section 5.4.3. Air ingress was not treated in this study, but the phenomenon is discussed for pebble-bed reactors in Reference 39. In the design reported in that reference, incoming oxygen was consumed by the lower reflector and did not reach the core. However, the proposed high-pressure nitrogen injection system (cf. Section 5.8) will prevent any oxygen from entering the pressure vessel in the first place.

5.6.4. Nuclear Weapons Proliferation

Finally, the pebble-bed reactor has been shown to be a poor choice for nuclear weapons proliferation. We have published several papers on the subject, including Reference 48.

In summary, the issues that are generally raised to challenge the licensing of a pebble-bed reactor all appear to be quite tractable.

5.7. Point Design Description

The core designs obtained from the manual and automated search methods discussed previously are described here. Both pebble-bed versions of the NGNP designs use an optimized pebble as discussed above.

Table 26 presents design specifications for the 300 MWt, 600 MWt, and 700 MWt versions of the pebble-bed NGNP and repeats the PBMR specifications from Table 20.

Table 26. Summary of features of PBMR and optimal pebble-bed versions of the NGNP.

	PBMR	NGNP-300	NGNP-600 (manual)	NGNP-600 (Gen. Alg.)	NGNP- 700 (Gen. Alg.)
Power (MW)	268	300	600	600	700
Inlet temperature (^{o}C)	503	600	600	600	600
Outlet temperature (^{o}C)	908	1000	1000	100	1001
Coolant flow rate (kg/s)	126	144	288	288	336
Active core volume (m^3)	81.8	85.7	108.9	105.5	146.6
Inner reflector radius (cm)	~ 87	40	110	90	96
Core radius (cm)	175	175	225	223	230
Outer reflector thickness (cm)	75	76	76	76	76
Active core height (m)	8.4	9.4	9.0	8.05	10.74
Pressure vessel outside diameter (m)	6.02	6.02	7.02	7.06	7.1
Mean pebble temperature (^{o}C)	806	857	864	865	870
Peak pebble temperature (^{o}C)	1041	1023	1038	1047	1026
Peak ΔT across pebble (^{o}C)	59	58	87	93	85
Peak pebble power (W)	1379	1272	1912	2112	1951
Mean core power density(W/cm^3)	3.3	3.5	5.5	5.7	4.8
Peak core power density (W/cm^3)	6.8	7.7	9.0	9.0	8.3
60 year fast fluence near RPV (n/cm^2)	$4.5x10^{19}$	$3.0x10^{19}$	$2.8x10^{19}$	$1.5x10^{10}$	$1.3x10^{10}$
Reactivity ($) for steam ingress of $0.001/cm^3$	0.30	0.42	0.13	0.14	0.13
Required pumping power (MW)	3	6	26	20	39
Peak LPCC temperature from PEBBED (^{o}C)	1370	1521	1455	1599	1581
Peak LPCC temperature from MELCOR (^{o}C)	1390	1473	N/A	N/A	N/A

The 300 MWt pebble-bed NGNP differs little from the PBMR, being only slightly scaled up in power and delivering hotter outlet coolant to meet the requirements for hydrogen production. The 600 MWt pebble-bed NGNP required considerable adjustment to meet the requirements for passive safety. The key to achieving this objective was to provide a very short thermal conduction path length from the core interior to the graphite-reflector heat sink. Then, even though the power density in the core was almost doubled, the decay heat generated in the core after an accident is able to escape into the heat sink. The cores of the 300 MWt and 600 MWt designs are comparable

in volume (including height). Therefore, energy is being extracted from the pebbles in the 600 MWt reactor at roughly twice the rate at which it is extracted from the pebbles in the 300 MWt reactor. The discharge burnup is higher for the 300 MWt core, so more energy is extracted from the pebbles before they are discharged. This reduces the fresh pebble injection rate for this design.

Both versions of the NGNP are shown to possess the required passive safety characteristic, as indicated by the peak accident coolant temperature. So does the 700 MWt version, which was found by the automated optimization algorithm in PEBBED. However, the 600 MWt and 700 MWt configurations have not yet been subjected to verification by MELCOR analysis. All cases yielded peak pressure-vessel fast neutron fluences greater than the GT-MHR limit of $3x10^{18}$ n/cm^2 in 60 years. However, increases in reflector thickness to provide additional shielding for the pressure vessel will further reduce the peak fuel temperature in accidents, while providing additional graphite volume as a heat storage reservoir in accidents.

The 300 MWt and 600 MWt pebble-bed versions of the NGNP designs presented in Table 26 are not optimized except in their use of a partially optimized pebble. The 700 MWt design has been optimized to obtain the best combination of eigenvalue, accident fuel temperature, outer reflector radius, and pumping power. In future work, further refinements of the core design, the reflector dimensions, and perhaps the design of the pebble itself, will be made. Also, there needs to be further evaluation of the allowable steady state fuel temperatures and the possibility of hot streaks in the pebble bed core.

Many factors are involved in the decision between two 300 MWt modules and a single 600 MWt module for the pebble-bed version of the NGNP. For example, pressure vessel cost is lower for the single 600 MWt version, but fuel utilization is better for the design using two 300 MWt modules. At present, the information required to choose between them is not all available. Therefore, point designs are provided for both versions.

Indeed, it has become apparent from studies conducted here that passive safety is primarily met by restricting the core radial extent, and that higher power levels can be achieved by increasing the core height (and also by reducing the core inlet temperature). We have chosen to limit the size of the pressure vessel to that initially proposed for the GT-MHR, and to retain the initial core inlet temperature of 600 °C. That is, we attempted to fit the passively safe PBR of the greatest possible power into the pressure vessel of the GT-MHR. It is clear to us that by relaxing the conditions on vessel size (especially height) and inlet temperature, we could achieve even higher powers while maintaining passive safety. Eventually, pumping power will become excessive; this is probably the limiting factor on increasing the power of a pebble-bed NGNP.

The annular core is reflected by a cylindrical inner reflector, an annular outer reflector, and upper and lower reflectors. The detailed design of these reflectors was beyond the scope of the project. However, a general design description of the inner and outer reflectors was developed. In the prismatic NGNP, the reflector is built from hexagonal blocks like the fuel blocks, but containing no fuel. In the pebble-bed version of the NGNP, the idea of reflectors made of pebbles has been discarded for the sake of thermodynamic efficiency, and also because of the presence of mixing zones where the core and reflectors meet. Therefore, the reflectors will be solid, but they will not be made of the same hexagonal blocks used in the prismatic reactor. The inner and outer reflectors will be made in several layers of annular segments. The segments in each layer will subtend the same arc, and the successive layers will be shifted so that the boundaries between segments in one layer will not line up with the boundaries between segments in another layer. This shift will prevent neutron streaming at these boundaries. Use of several layers will permit replacement of

only those parts of the reflector that need to be replaced. Also inside the pressure vessel, the automatically scramming control rods are emplaced (cf. Section 5.8).

The pebble recirculation system is similar to that in the PBMR, except that a new pebble checking system will be used that has recently been announced by Hawari et al. at North Carolina State University.[49] This system permits pebble burnup to be measured shortly after the pebbles emerge from the core, instead of after a cooldown period of several days. Thus, the ex-core pebble inventory is greatly reduced.

The balance-of-plant components are similar to those in the prismatic NGNP, except that the version of the pebble-bed NGNP based on two 300 MWt modules will require two ducts between the modules and the power conversion unit, and a power conversion unit design modified accordingly. The high-pressure nitrogen tank and safety valve are incorporated into the design for protection against air ingress (cf. Section 5.8).

5.8. Safety Studies

The peak temperature values presented in Table 26 were computed by the simple thermal module in PEBBED and, in the 300 MWt design, by a sophisticated model for the code MELCOR. In this subsection, the MELCOR model is described and results are presented, and some design features are identified that provide inherent safety to the pebble-bed version of the NGNP. Passive safety is the term used to describe the condition where no active system or operator intervention is required to prevent reactor damage or release of radionuclides from the reactor into the environment in the event of accidents. Passive safety is provided in the pebble-bed version of the NGNP by the high heat-absorbing capacity of the graphite reflectors and by choosing the core and reflector dimensions appropriately; these properties and design choices are intended to ensure that fuel temperatures are not reached at which damage and consequent radionuclide release would occur.

5.8.1. Thermo-Hydraulic Analyses

Accident safety in the 300 MWt pebble-bed version of the NGNP was assessed with MELCOR, as mentioned above. The basic modeling parameters for the reactor concept modeled are listed in Table 27. The 300MWt core used in the MELCOR study has a height of 9.4 m, 0.9 m higher than the 300 MWt core described in Section 5.4.4. The active core volume and number of pebbles are proportionately larger. For this core, PEBBED computes the maximum fuel temperature during a LPCC event to be 1480 °C.

Table 27. Summary of basic modeling parameters for the 300 MWt pebble-bed version of the NGNP.

	VHTGR-300
Thermal Power (MW)	300.00
Core coolant inlet temperature (°C)	600.00
Core coolant outlet temperature (°C)	1000.00
Radius of inner reflector (m)	0.40
Outer radius of inner flow zone (m)	1.06
Outer radius of middle flow zone (m)	1.44
Outer radius of outer flow zone (m)	1.75
Outer radius of radial reflector	2.50
Outer radius of inlet coolant channel (m)	2.80
Outer radius of core barrel (m)	2.83
Outer radius of gas annulus (m)	2.90
Outer radius of reactor pressure vessel (m)	3.00
Inner radius of reactor cavity cooling system (m)	4.27
Number of pebbles in reactor	462304.00
Active height of core	9.40
Active core volume (m^3)	90.44
Core mean power density (MW/m^3)	3.32
Core mass flow rate (kg/sec)	161.00
Height of zone 1 (m)	1.00
Height of zones 2 to 8 (m)	1.20
Maximum fuel temperature LPCC (°C)	1473.00

Schematic diagrams of the control volumes and the heat structures used to model the pebble-bed version of the NGNP are presented in Figures 97 and 98, respectively. As shown in Figure 97, the active core of the reactor was divided into three radial zones and eight axial zones for a total of 24 core control volumes. The top layer, comprising Volumes 25, 26, and 27, represents the plenum between the top layer of pebbles and the top reflector. The core control volumes are annular and centered about the core centerline. The coolant inlet channel at the top of the reactor is represented by Control Volume 100. For nominal operating conditions the coolant enters the bottom of the reactor at 600 °C and flows up an annular flow channel (yellow control volumes) located between the reactor side reflector and the reactor core barrel. The coolant then flows radially along the top of the reactor (CV 100), exiting into a plenum above the core represented by CV025, CV026, and CV027. From the plenum the coolant flows down through the core and exits the bottom of the core at 1000 °C. The coolant then flows to the power conversion unit located in the vault. Control volumes representing the helium bypass flow annulus (300-series volumes) and the reactor cavity air (400- and 600-series volumes) are shown as gray and red in Figure 97.

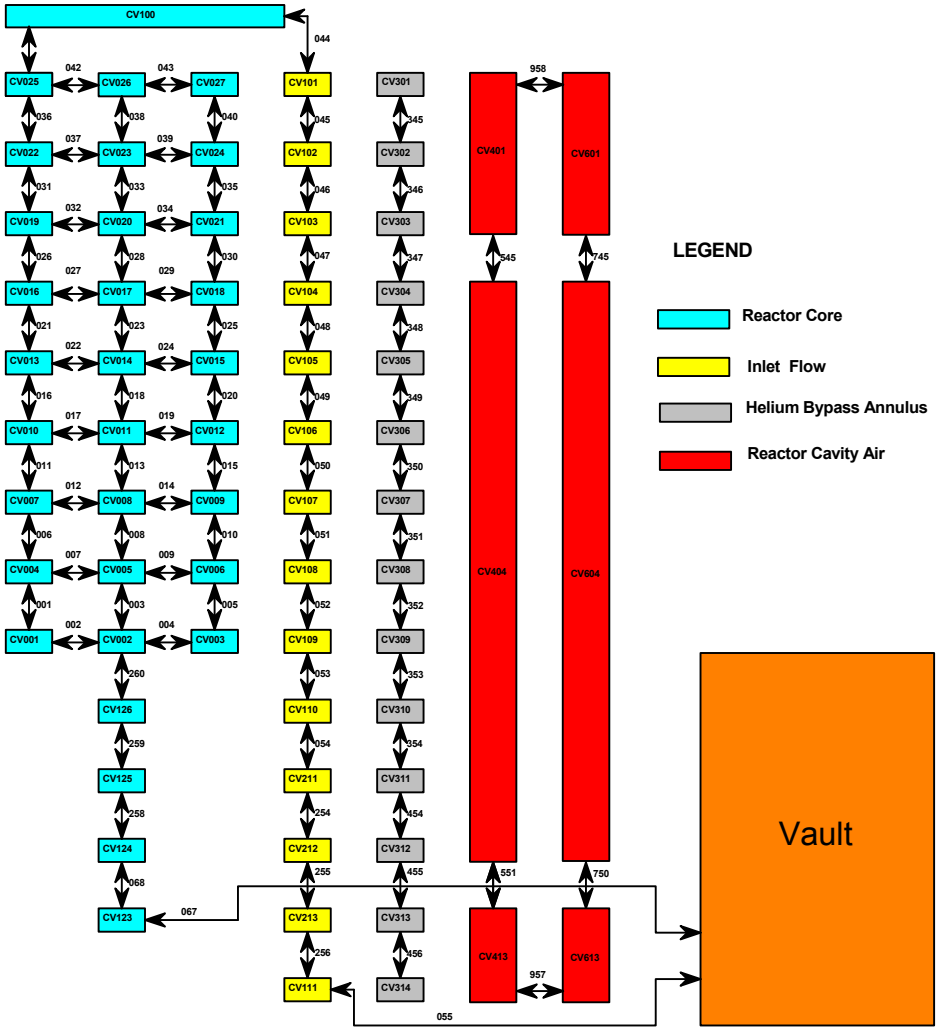

Figure 97. 300 and 600 MWt NGNP control volume diagram.

The main heat structures used in the MELCOR model are shown in Figure 98, with the exception of the solid center reflector, which is not shown. These heat structures are used to model the conduction and radiation heat transport in the reactor fuel, heat transport from the fuel through the

reflectors, and finally, heat transport through the reactor primary vessel wall out to the RCCS cooling panels[22] (400-series heat structures). The numbers presented in parentheses correspond to the control volumes to which the heat structures are connected (see Figure 97). The RCCS cooling panels are assumed attached to the vault wall facing the reactor pressure vessel (RPV).

The RCCS is a passive heat removal system that relies upon both radiation and natural convection heat transfer to remove the decay heat from the reactor in the event of a loss-of-coolant accident. The natural convection flow in the region between the RPV and cooling panels is induced by buoyancy forces in the air as a result of the temperature difference between the RPV and the cooling panels[22]. It is assumed for the MELCOR results presented in this report that the cooling panels have enough heat removal capability to maintain the panel surface temperature at approximately 27 °C. Although this assumption results in non-conservative RPV maximum temperatures, it has been reported in other documents that the RCCS has little impact on the maximum core temperature because of the large heat capacity provided by the graphite core and reflectors[3].

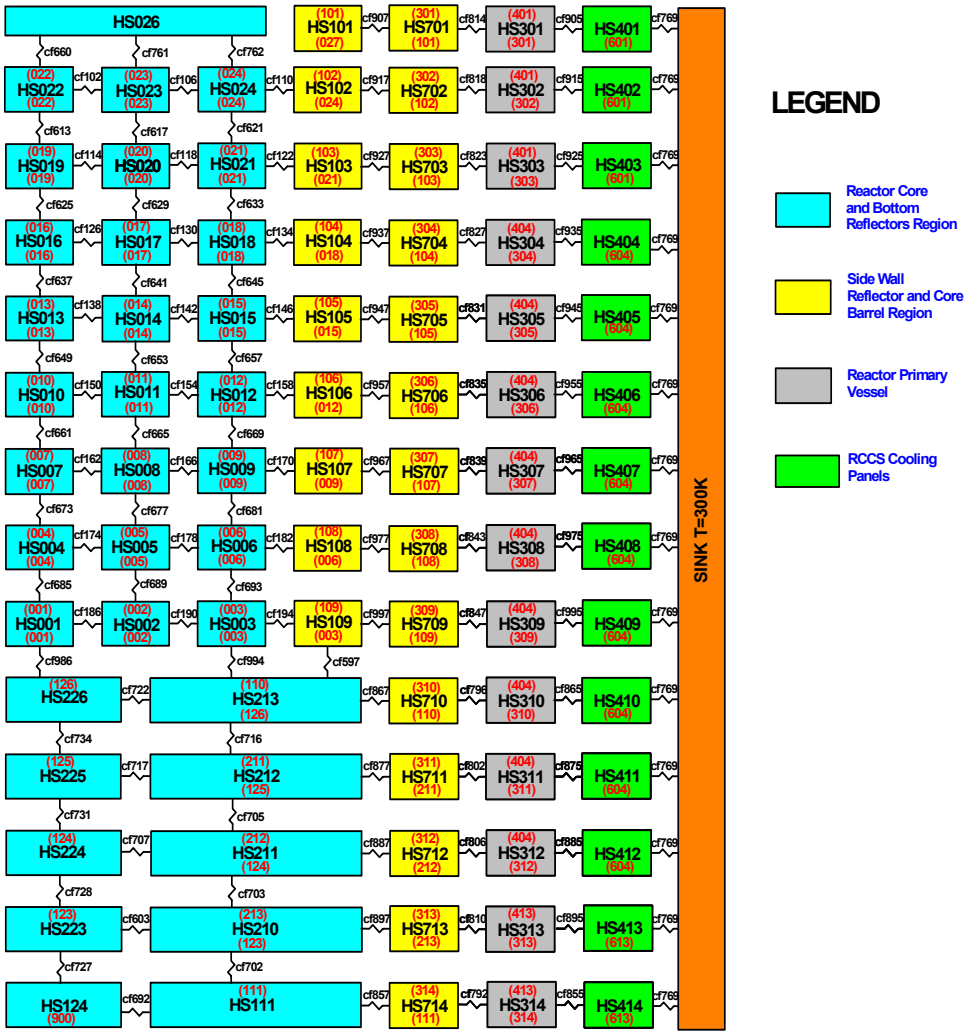

Figure 98. 300 and 600 MWt NGNP heat structure diagram.

The heat transfer from the pebbles is dominated by convection during nominal operation of the reactor. However, during an accident when the flow in the core decreases to near zero, the heat

generated by the pebbles is removed by conduction and radiation through the pebbles to the graphite reflector. The pebbles in the core are modeled as spherical heat structures, one heat structure per control volume. The heat being transferred from this single structure is then multiplied by the number of pebbles in the control volume to obtain the overall heat transfer from all the pebbles in the volume. A user subroutine is applied to model the conduction heat transfer between heat structures according to the following equation:

$$q = \frac{2\pi hk\left(T_2 - T_1\right)}{\ln\left(\frac{r_2}{r_1}\right)} \quad ,$$

where k is the effective thermal conductivity of the pebble bed, h is the height of the area normal to the direction of heat flow, and q is the heat transfer rate between structures. The effective thermal conductivity of the pebble bed used in this model is the same as reported in Reference 50. The nuclear heating data for all the cases analyzed were obtained from the PEBBED code described above.

To demonstrate that the pebble-bed versions of the NGNP are passively safe reactors, it must be shown that the maximum core temperature will remain below 1600 °C for all accidents. Two accidents, which have been identified as being the most challenging in terms of generating maximum core temperatures, were analyzed, namely, a HPCC and a LPCC event. These two accidents are also referred to as a high-pressure conduction cooldown event and a low-pressure conduction cooldown event, respectively. The system pressure in the loop remains high for the HPCC event because no coolant is lost from the loop.

The HPCC event is simulated by assuming that the circulator in the primary loop loses power and at the same time the reactor is scrammed. Even if a scram were not to occur, the fuel's large negative temperature coefficient of reactivity would cause the reactor to shut down. The loss of the circulator causes the downward forced flow through core to stop, after which a natural-circulation flow up through the core is established by buoyancy forces. In this simulation it was assumed that the natural circulating flow occurs through the entire primary loop. However, in order to keep excessively hot helium out of the power conversion vessel, natural circulation may be restricted to the pressure vessel; if so, we may need to look at this case again.

The results corresponding to this accident are presented in Figures 99 and 100 for the 300 MWt reactor. The mass flow rate in the primary loop is shown in Figure 99. The accident is initiated at 1000 s. The first 1000 s is used by MELCOR to establish steady state conditions prior to the initiation of the transient. As shown in the figure, prior to 1000 s the mass flow through the core is -161 kg/s, which is the required mass flow to maintain a 400 °C temperature rise through the core. The negative flow rate corresponds to downward flow through the core. At 1000 s, the power to the circulator is turned off, causing the flow through the core to decrease to zero, then to reverse as a positive natural circulating flow is established in the core. The natural circulating flow rate is 5 kg/s initially, and it gradually decreases to 0.6 kg/s by 120 h.

The maximum core temperature corresponding to this accident is shown in Figure 100. As seen in the figure, the maximum pebble temperature for this accident (in heat structure HS-019) is 1080 °C, occurring at 3 h into the transient. The location of HS-019 is shown in Figure 98. The remaining two curves presented in Figure 100 are the pebble temperatures in the middle (HS-020) and outer (HS-021) zones corresponding to the same height as HS-019. As seen, the natural convection flow rate through the core is enough to remove the core decay heat to the outside

pressure vessel wall, thus keeping the core maximum temperature well below 1600 °C. Based on these results, the HPCC event for the 600 MWt design was not run since there is little reason to expect that the temperature in the core will approach 1600 °C for the 600 MWt HPCC event.

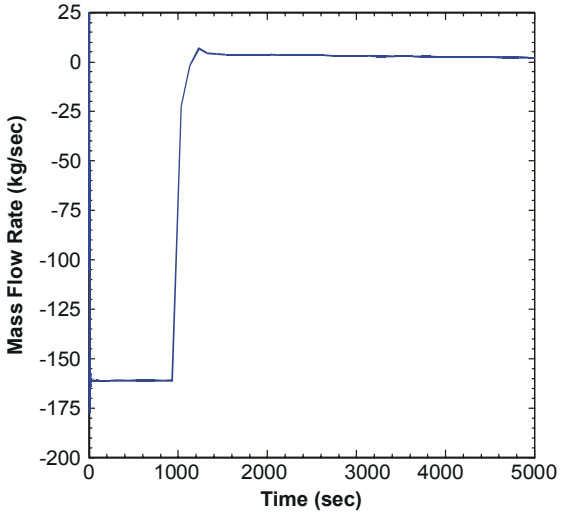

Figure 99. Primary Loop Mass Flow Rate during a HPCC event in a 300 MWt pebble-bed NGNP.

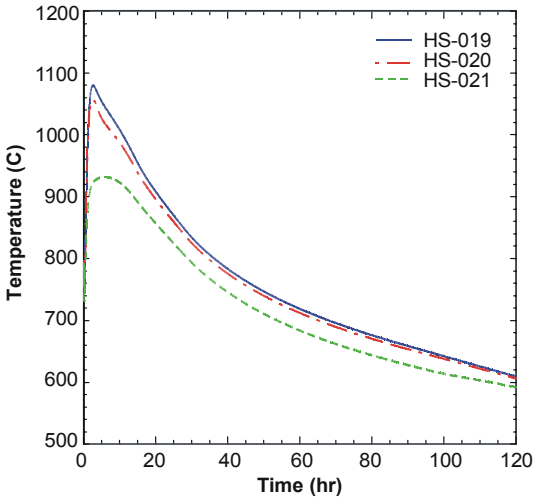

Figure 100. Maximum core temperature during a HPCC event in a 300 MWt pebble-bed NGNP.

The next accident considered is the 300 MWt LPCC event. The LPCC event is initiated by a guillotine break of the cross duct connecting the reactor with the power conversion unit in the vault. In the model, the LPCC event was initiated at 1000 s by opening four valves (used to simulate the break) connecting the hot and cold legs to the containment. The circulator was tripped at 1000 s and the reactor was scrammed at the same time. The simultaneous double-ended rupture of the hot and cold legs causes a rapid depressurization of the primary coolant system from approximately 7.0 MPa down to atmospheric pressure. After the depressurization phase of the LPCC event, the mass flow rate of helium through the core from natural convection is essentially zero out to 50 hours, at which time the transient was terminated because the maximum core temperature had peaked. As in the 300 MWt HPCC event, the initial mass flow down through the core was -161 kg/sec.

The maximum predicted core temperature for this case is presented in Figure 101. As shown in Figure 101, the maximum pebble temperature for this accident (in HS-013) is 1473 °C, occurring at 27 h into the transient. The location of HS-013 is shown in Figure 98. The remaining two curves presented in Figure 101 are the pebble temperatures in the middle (HS-014) and outer (HS-15) zones corresponding to the same height as HS-013. The 300 MWt pebble-bed version

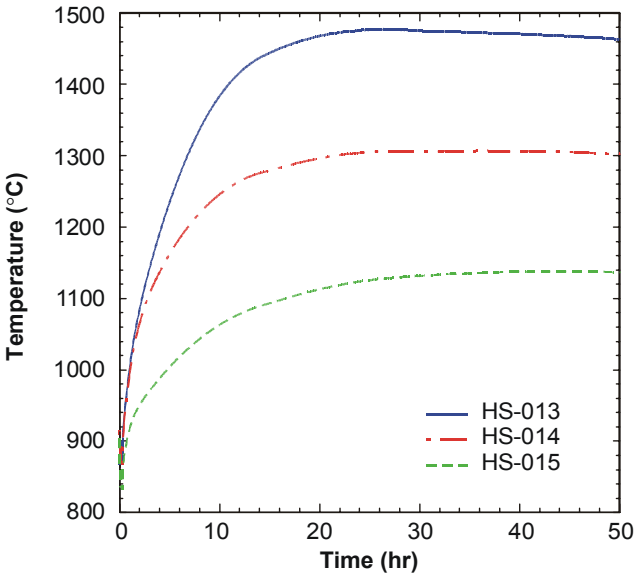

Figure 101. Maximum core temperature during a LPCC event in a 300 MWt pebble bed NGNP.

of the NGNP meets the passive-safety criterion of not exceeding a maximum fuel temperature of 1600 °C for the worst-case NGNP accident scenario.

5.8.2. Passive Safety Systems

The INEEL has applied for patents for two automatically actuated scramming control rod concepts applicable to the PBRs. In one of these concepts, the scram rods are suspended by the flowing helium coolant through a U-shaped tube that converts the downward flow into an upward pressure on the rods. When the coolant flow stops, the scram rods fall into the core. The other concept applies electromagnets to suspend the scram rods. When the temperature in the core increases, the electrical resistance in the electromagnet circuits increases, so that insufficient current flows in the circuits to provide the magnetic field strength needed to suspend the rods, which then fall into the reflectors. One or both of these two safety systems could be installed in a pebble-bed version of the NGNP.

For protection against air ingress events, the vault in which the reactor(s) and the power conversion system are installed is sealed, and a large tank filled with high-pressure nitrogen is connected to the vault. When a break in the primary coolant system is detected, a valve that is the subject of an invention disclosure releases the nitrogen from the tank into the vault, so that essentially any gas flowing into the core from the vault will be nitrogen instead of air.

5.9. Summary and Conclusions

An effort was undertaken to design a system based on the pebble-bed concept that would satisfy the requirements specified for the NGNP. These requirements are a coolant outlet temperature of 1000 °C, passive safety, and a total power of at least 600 MWt. The pebble-bed design team further added the constraints that the peak fast neutron fluence in the pressure vessel would not exceed that specified for the competing prismatic NGNP concept and that, as in the prismatic version, the coolant inlet temperature would be 600 °C, although we now believe that it is desirable to consider lower inlet temperatures.

A passively safe PBR module design of 600 MWt had not been previously reported, so two parallel designs were developed. One of these employs two PBR modules of 300 MWt each, supplying helium at 1000 °C to a single power conversion unit similar to that used for the prismatic NGNP, except that it will have two pairs of ducts for transferring the helium to and from the reactor modules. The other was nominally a single module of 600 MWt.

The design based on two modules of 300 MWt was shown both by PEBBED and MELCOR to be passively safe, which was expected because a module of 300 MWt has only slightly more power than the PBMR, which has received considerable safety analysis. The capital cost of such a system would be about twice as great as the capital cost of a single unit of 600 MWt, because the pressure vessels for a 300 MWt module and a 600 MWt module are almost the same size. However, the fuel utilization for the system based on 300 MWt modules is considerably better, so that its fuel cost will be lower. A detailed economic comparison of the two systems was beyond the scope of the study, so no recommendation is made at this time in favor of one or the other.

The design based on one module of 600 MWt was shown by PEBBED to satisfy the requirements for passive safety, but because of time and budget limitations, the MELCOR analysis of the 600 MWt pebble-bed NGNP was not completed. This work will be continued in FY-04.

References

1. *A Technology Roadmap for Generation IV Nuclear Energy Systems*, GIF–002-00, Generation IV International Form, (Dec. 2002).
2. Toward a More Secure and Cleaner Energy Future for America, National Hydrogen Energy Roadmap, November 2002, U.S. Department of Energy.
3. "Gas Turbine-Modular Helium Reactor (GT-MHR) Conceptual Design Description Report", Revision 1, Report 910720, GA Project No. 7658, General Atomics, San Diego, CA, July 1996.
4. Goodjohn, A. J., "Summary of Gas-Cooled Reactor Programs", *Energy*, Vol. 16, No. ½, pp.79-106, 1991.
5. Frewer, H. and Keller, W. "The Modular High-Temperature Reactor", *Nuclear Science and Engineering*, Vol. 90, p411-426, 1985.
6. Bäumer, R. AVR-Experimental High-Temperature Reactor VDI-Verlag GmbH, Düsseldorf, 1990.
7. Van Heek, A. I., "ACACIA, A Small Scale Nuclear Power Plant with Cogeneration Capabilities," *Proceedings of the American Society of Mechanical Engineers (ASME) Turbo Conference*, June 2002.
8. "MCNP4B: Monte Carlo N-Particle Transport Code System," contributed by Los Alamos National Laboratory, Los Alamos, New Mexico, April 1997 and distributed as package CCC-660 by Oak Ridge National Laboratory.
9. MCNP4C Monte Carlo N-Particle Transport Code System", contributed by Los Alamos National Laboratory, Los Alamos, New Mexico, February 29, 2000 and distributed as package CCC-700 by Oak Ridge National Laboratory.
10. A. G. Croff, "ORIGEN2 – A Revised and Updated Version of the Oak Ridge Isotope Generation and Depletion Code," ORNL-5621, Oak Ridge National Laboratory, July 1980.
11. R. S. Babcock, D. E. Wessol, C. A. Wemple, S. C. Mason, " The MOCUP Interface: A Coupled Monte Carlo/Depletion System", EG&G Idaho, Inc., Idaho National Engineering Laboratory, presented at the 1994 Topical Meeting on Advances in Reactor Physics, Vol. III, Knoxville, TN, April 11-15, 1994.
12. R. E. MacFarlane and D. W. Muir, "The NJOY Nuclear Data Processing System Version 91," LA-12740-M, October 1994.
13. L. R. Greenwood and R. K. Smither, "SPECTER: Neutron damage Calculations for Materials Irradiations," ANL/FPP/TM-197, Argonne National Laboratory, 1985.
14. Mingle, J.O., "The Influence of Control Rod Management upon the Xenon Stability of HTGR-Type Cores," General Atomics Report GA-P-1100-19, October 15, 1968.
15. "450MW(t) MHTGR Core Nuclear Design", General Atomics report DOE-HTGR-90237, Revision 1, September 1993
16. Merrill, M.H., "Nuclear Design Methods and Experimental Data in use at Gulf General Atomic," GA-LTR-2, July 1973.
17. Derstine, D.L., "DIF3D: A Code to Solve One-, Two-, and Three-Dimensional Finite-Difference Diffusion Theory Problems," ANL-82-64, Argonne National Laboratory, 1982.
18. "GT-MHR Power Increase Study," GA-C21974, General Atomics Staff, March 1995.
19. Kapernick, R., "POKE User's Manual," CEGA-002928, Rev. N/C, General Atomics, November 1993.
20. Sherman, R., "3D Rodded Burnup Results for the GT-MHR," DCR-910832, Rev.0, General Atomics, July 1995.
21. The RELAP5-3D Code Development Team, RELAP5-3D Code Manual, Idaho National Engineering and Environmental Laboratory, INEEL-EXT-98-00834, Revision 2.1, April 2003.
22. Bechtel National, Inc., "450 MWt Reactor Cavity Cooling System Design Description" DOE-HTGR-90016, Revision 0, November 1993.

23. *TAC2D - A General Purpose Two-Dimensional Heat Transfer Computer Code*, GA Report GA-A14032, July 1976.
24. *Preliminary Safety Information Document for the Standard MHTGR*, DOE Report HTGR-86-024, September 1986.
25. Gilbert Melese and Robert Katz, Thermal and Flow Design of Helium-Cooled Reactors, American Nuclear Society, 1984, pp. 48-52.
26. "AVR – Experimental High-Temperature Reactor: 21 Years of Successful Operation for a Future Energy Technology," Association of German Engineers (VDI) – The Society for Energy Technologies (Publ.) – VDI Verlag GmbH, Düsseldorf, 1990.
27. Zhong Daxin and Qin Zhenya, "Overview of the 10 MW High Temperature Gas-Cooled Reactor," Proc. Seminar on HTGR Application and Development, Beijing, China, March 19-21, 2001, pp. 194-206.
28. G. H. Lohnert and H. Reutler, "The modular HTR – a new design of high-temperature pebble-bed reactor," Nucl. Energy **22**, No. 3, 1983, pp. 197-200.
29. R. O. Gauntt, R. K. Cole, S. A. Hodge, S. B. Rodriguez, R. L. Sanders, R. C. Smith, D. S. Stuart, R. M. Summers, and M. F. Young, "MELCOR Computer Code Manuals," NUREG/CR-6119, Vol. 1, Rev. 1, SAND97-2397-2398 (1997).
30. Guido Baccaligni, et al., "Very High Temperature Reactor (VHTR) – Survey of Materials Research and Development Needs to Support Early Deployment," INEEL/EXT-03-00141, January 31, 2003.
31. W. K. Terry, H. D. Gougar, and A. M. Ougouag, "Direct Deterministic Method for Neutronics Analysis and Computation of Asymptotic Burnup Distribution in a Recirculating Pebble-Bed Reactor," Annals of Nucl. Energy **29**, 2002, pp. 1345-1364.
32. A. M. Ougouag, W. K. Terry and H. D. Gougar, "Examination of the Potential for Diversion or Clandestine Dual Use of a Pebble-Bed Reactor to Produce Plutonium," Proceedings of HTR 2002, 1st International Topical Meeting on High Temperature Reactor Technology (HTR), Petten, Netherlands, April 22-24, 2002.
33. A. M. Ougouag and H. D. Gougar, "Preliminary Assessment of the Ease of Detection of Attempts at Dual Use of a Pebble-Bed Reactor," Transactions of the Winter 2001 Annual Meeting of ANS, Reno, NV, Trans. ANS **85**, pp. 115-117, Nov. 2001 (Invited).
34. H. D. Gougar and A. M. Ougouag, "The Modular Pebble Bed Reactor as Power/Heat Supply for Remote Industrial Operations," CIM-Vancouver 2002, Canadian Institute of Mining, Metallurgy, and Petroleum Annual Conference – Vancouver, B.C., April 28-May 01, 2002.
35. E. Teuchert, U. Hansen, and K. A. Haas, "V.S.O.P. - Computer Code System for Reactor Physics and Fuel Cycle Simulation," KFA-IRE Report Jül-1649, 1980.
36. R. A. Grimesey, D. W. Nigg, and R. L. Curtis, "COMBINE/PC - A Portable ENDF/B Version 5 Neutron Spectrum and Cross-Section Generation Program," EGG-2589, Revision 1, Idaho National Engineering Laboratory, February 1991.
37. "MICROX-2, Code System to Create Broad-Group Cross Sections with Resonance Interference and Self-Shielding from Fine-Group and Pointwise Cross Sections," PSR-374, Oak Ridge National Laboratory, January 1999.
38. B. J. Merrill, R. L. Moore, S. T. Polkinghorne, and D. A. Petti, Fusion Engineering and Design, **51-52,** 555-563 (2000).
39. W. K. Terry (editor), "Modular Pebble-Bed Reactor Project, Laboratory-Directed Research and Development Program FY 2001 Annual Report," INEEL/EXT-2001-1623, Idaho National Engineering and Environmental Laboratory, December 2001.
40. D. R. Nicholls, "Status of the pebble bed modular reactor," Nucl. Energy **39**, No. 4, 2000, pp. 231-236.
41. Paul R. Kasten, Performance of German Fuels for Modular High-Temperature Gas-Cooled Reactors, Oak Ridge National Laboratory, 1992.
42. Abderrafi M. Ougouag, "Development of Advanced Methods for Pebble-Bed Reactor Neutronics: Design, Analysis, and Fuel Cycle Optimization," NERI Project No. 2002-195.
43. Frederik Reitsma, PBMR (Pty.) Ltd, personal e-mail, June 24, 2003.

44. "Irradiation damage in graphite due to fast neutrons in fission and fusion systems," IAEA-TECDOC—1154, International Atomic Energy Agency, Vienna (Austria), 2002.
45. David E. Goldberg, *Genetic Algorithms in Search, Optimization, and Machine Learning,* Addison-Wesley, 1989.
46. A. M. Ougouag and W. K. Terry, "A Preliminary Study of the Effect of Shifts in Packing Fraction on k-effective in Pebble-Bed Reactors," American Nuclear Society Mathematics & Computation Division Conference, Salt Lake City, Utah, September 9-13, 2001.
47. Michael G. Izenson, "Effects of Fuel Particle and Reactor Core Design on Modular HTGR Source Terms," PhD Thesis, Department of Nuclear Engineering, MIT, 1986.
48. A. M. Ougouag, W. K. Terry and H. D. Gougar, "Examination of the Potential for Diversion or Clandestine Dual Use of a Pebble-Bed Reactor to Produce Plutonium," Proceedings of HTR 2002, 1st International Topical Meeting on High temperature Reactor Technology (HTR), Petten, The Netherlands, April 22-24, 2002.
49. A. I. Hawari, Bingjng Su, and J. Chen, and Z. Zhao, "Investigation of On-Line Burnup Monitoring of Pebble-Bed Reactor Fuel Using Passive Gamma-Ray and Neutron Detection Methods." Transactions of the Winter 2001 Annual Meeting of ANS, Reno, NV, Trans. ANS **85**, pp. 98-99, Nov. 2001. See also ongoing NERI project.
50. "Heat Transport and Afterheat Removal for Gas Cooled Reactors Under Accident Conditions," IAEA-TECDOC-1163, IAEA, Vienna, 2000.